KINETICS/KINEMATICS OF INTACT AND ARTHRITIC KNEE CARTILAGES AND A NOVEL APPROACH TO ENHANCE WEAR CHARACTERISTICS OF UHMWPE TIBIAL INSERTS FOR PROSTHETIC KNEE

Thesis

Submitted in partial fulfilment of the requirement for the degree of

DOCTOR OF PHILOSOPHY

by

VAISHAKH R

(Reg. No. 187028ME017)

DEPARTMENT OF MECHANICAL ENGINEERING

NATIONAL INSTITUTE OF TECHNOLOGY KARNATAKA

SURATHKAL, MANGALORE – 575025

MARCH, 2023

KINETICS/KINEMATICS OF INTACT AND ARTHRITIC KNEE CARTILAGES AND A NOVEL APPROACH TO ENHANCE WEAR CHARACTERISTICS OF UHMWPE TIBIAL INSERTS FOR PROSTHETIC KNEE

Thesis

Submitted in partial fulfilment of the requirement for the degree of

DOCTOR OF PHILOSOPHY

by

VAISHAKH R

(Reg. No. 187028ME017)

Under the guidance of

Dr POORNESH KUMAR KOORATA

Assistant Professor

DEPARTMENT OF MECHANICAL ENGINEERING

NATIONAL INSTITUTE OF TECHNOLOGY KARNATAKA

SURATHKAL, MANGALORE – 575025

MARCH, 2023

DECLARATION

I hereby declare that the Research Thesis entitled **"KINETICS/KINEMATICS OF INTACT AND ARTHRITIC KNEE CARTILAGES AND A NOVEL APPROACH TO ENHANCE WEAR CHARACTERISTICS OF UHMWPE TIBIAL INSERTS FOR PROSTHETIC KNEE"** which is being submitted to the **National Institute of Technology Karnataka, Surathkal** in partial fulfillment of the requirements for the award of the degree of **Doctor of Philosophy** in **Mechanical Engineering** is a *bonafide report of the research work carried out by me*. The material contained in this Research Theis has not been submitted to any University or Institution for the award of any degree.

Register Number: **187028ME017**

Name of the Research Scholar: **VAISHAKH R**

Signature of the Research Scholar:

Department of Mechanical Engineering

Place: NITK, Surathkal

Date: 31-03-2023

CERTIFICATE

This is to certify that the Research Thesis entitled **"KINETICS/KINEMATICS OF INTACT AND ARTHRITIC KNEE CARTILAGES AND A NOVEL APPROACH TO ENHANCE WEAR CHARACTERISTICS OF UHMWPE TIBIAL INSERTS FOR PROSTHETIC KNEE"** submitted by **Mr. VAISHAKH R (Register Number: 187028ME017)** as the record of the research work carried out by him, *is accepted as the Research Thesis submission* in partial fulfilment of the requirements for the award of the degree of **Doctor of Philosophy**.

Research Guide

Dr. Poornesh Kumar Koorata
Assistant Professor
Department of Mechanical Engineering

5/4/2023

Chairman-DRPC
Department of Mechanical Engineering
National Institute of Technology Karnataka
Surathkal, Mangalore - 575025

ACKNOWLEDGEMENT

A guru is someone who genuinely cares for their disciples without any selfish motives. He cares far more about the disciple than parents, who typically overlook the highest good in their haste to provide their kids with material comfort. I am grateful to my research supervisor **Dr. Poornesh Kumar Koorata,** for giving me this excellent chance to pursue a Ph.D. I broadened my vision of information, comprehension, and interpretation by devoting the necessary time to conversations and discussions.

I am incredibly grateful to our honourable director (additional-charge) **Prof. Prasad Krishna**, for creating an attitude towards research for students. I sincerely thank our HOD **Prof. Ravikiran Kadoli,** for providing all facilities needed during research work. I am also thankful to my Research Progress Assessment Committee (RPAC) members **Dr. Jeyaraj P** and **Dr. Ramesh H,** for their counsel and recommendations during my presentation. I also thank the secretary of DRPC, **Dr. Vasudeva Madav,** for helping in the smooth conduct of the presentations. I want to thank former HOD **Prof. Narendranath** for his words of motivation during my research. My special thanks to **Prof. M N Sathyanarayan,** chairman of CRF-NITK, for permitting my research work to utilize the facilities in CRF. I am thankful to all the Deans of NITK for providing facilities at NITK Surathkal.

I want to thank **Dr. Yogeesh D Kamat**, specialist consultant in knee & hip orthopaedic surgery at KMC Hospital, Mangalore, for giving valuable suggestions about my work. Also, I would like to express my gratitude to Dr. Sharada Rai, Professor and Head, Department of Pathology, KMC-Mangalore, for helping with my research. I thank **Gee M**, Microtrol Sterilisation Services Pvt. Ltd., Bangalore, for their support and encouragement in conducting research.

I am grateful to the members of our research group **Umesh Shinde, Vikas Kumar, Sachin Kumar Varshney,** and **Pranav Padavu,** for their unwavering support throughout my PhD studies. I want to thank **K Nishan** and **Pradeep** Machine Shop-NITK for their support. Additionally, I would like to thank **Kiran** from the technical staff of NITK-CRF for their efforts to help my research work. I want to thank all the

other teaching and non-teaching staff, security, health care centre, hostels, and physical education and sports department.

I prostrate myself at the feet of my parents, **Shri. M S Raju** and **Smt**. **Latha Raju**, for providing the resources I needed to realise my goals and for always encouraging me to do so. I am grateful to my younger sister **Smt. Vaishnavi R** for taking care of my parents during my stay in NITK. I am incredibly thankful to my father-in-law **Shri. Dinesan P V** and mother-in-law **Smt. Pushpa Dinesan** for believing in me and encouraging me to pursue my passion. I especially thank my loving wife **Smt. Jyothi Dinesan** for understanding, motivating and supporting me during my Ph.D. work. I would also like to thank all my relatives, teachers and friends.

I am blessed to pursue my education in National Institute of Technology Karnataka, Surathkal, which gave me immense exposure towards research and way of thinking and believing. Finally, I want to thank all those who helped me directly or indirectly at various stages of this research work.

VAISHAKH R

NITK, SURATHKAL - 575 025

ABSTRACT

Osteoarthritis is a severe and progressive disorder that affects the knee joint due to cartilage degradation from daily rigours activities. Articular cartilage is more susceptible to knee arthritis compared with other soft tissues. Hence, understanding degradation phenomena are more critical and require understanding the tissue's stress fields. Experimental methods have limitations, such as inaccessible cadaveric knees and obtaining in-vivo data from intact and arthritic knees is difficult and imprecise. Hence the numerical method is the most effective technique for understanding the cartilage's mechanical behaviours under different conditions. The cartilage constituents make the cartilage geometrically and mechanically heterogeneous. A 3D finite element knee joint model is used to compute the articular cartilage response during multiple activities. Various material models are available to model the heterogeneity of articular cartilage. Multiple constitutive models are compared for the prediction of mechanical response. In addition, the influence of the inhomogeneous distribution of collagen fiber in cartilage is investigated for intact and arthritic knee kinematics cases.

In reality, the cartilage structure is heterogeneous, and the computational study shows the importance of heterogeneity in the mechanical response of the knee joint. Conventionally the knee implant-bearing material (UHMWPE) is homogeneous. Incorporating the heterogeneous characteristics in the bearing material may help enhance the implant's mechanical characteristics. The proposed model generates property-modulated characteristics in the bearing material using gamma irradiation, and the heterogeneous characteristics are incorporated into the knee implant. UHMWPE's tribological and chemical characteristics are analysed experimentally, and the wear rate and volume are calculated. The wear rate decreases as the radiation dose increase to a particular level and then increases as the dose increases further. Compared with the conventional technique, a reduction in wear rate for the material is observed for the proposed technique. Also, the hardness of the UHMWPE is measured, and its value increases as the irradiation dose increases.

Keywords: *Knee joint Articular cartilage; Material heterogeneity; Collagen fiber orientation; Gait cycle; Osteoarthritis; Knee implant; UHMWPE*

TABLE OF CONTENTS

TABLE OF CONTENTS **i**

LIST OF FIGURES **vii**

LIST OF TABLES **xi**

NOMENCLATURE **xiii**

1. INTRODUCTION **1**

1.1 Background of study 1

1.2 Motivation 2

1.3 Knee joint structure 4

1.4 Articular cartilage 5

1.5 Prosthetic knee 6

1.6 Assumptions and limitations of study 7

1.7 Organisation of thesis 8

1.8 Closure 9

2. LITERATURE SURVEY **11**

2.1 Introduction 11

2.2 Computational study of soft tissues 11

2.2.1 Materials used to model articular cartilage 11

2.2.2 Collagen fiber structure and its influence on tissue response 14

2.3 Prosthetic knee 15

2.3.1 Prosthetic knee design and its influence in the mechanical characteristic 16

2.3.2 The evolution of UHMWPE and its application in prosthetic knee 17

2.4 Polyethylene wear in total knee arthroplasty (TKA) 19

2.4.1 Crosslinking of UHMWPE to HXLPE 19
2.4.2 1st generation highly cross-linked polyethylene 20
2.4.3 2nd generation highly cross-linked polyethylene 21
2.5 Commercially available tibial insert of TKA implant 22
2.6 Summary and motivation from the literature survey 24
2.7 Research objectives 25
2.8 Closure 25
3. KNEE RESPONSES USING GRADED CARTILAGE MATERIAL 27
3.1 Introduction 27
3.2 Geometry and finite element model 27
3.3 Methodology 28
3.4 Material models 29
3.5 Results and discussions 30
3.5.1 Comparison of contact pressure and stress on cartilage 30
3.5.2 Significance of mechanical responses in knee mechanism 32
3.6 Conclusions 33
3.7 Closure 34
4. RESPONSE OF SOFT TISSUES DURING GAIT CYCLE 35
4.1 Introduction 35
4.2 Methodology 35
4.3 Material models 37
4.4 Results and Discussions 38
4.4.1 Soft tissue responses during the gait cycle 38
4.5 Conclusion 41
4.6 Closure 42

5. COMPUTATIONAL STUDY ON CARTILAGE MATERIAL HETEROGENEITY **43**

5.1 Introduction 43

5.2 Geometry and finite element model 43

5.3 Interface, constraints, loading and boundary conditions 44

5.4 Material models 45

5.5 Results and discussions 48

5.5.1 Comparison of different material models for homogeneous and heterogeneous cases 48

5.5.2 Significance of cartilage heterogeneity in mechanical response 52

5.6 Conclusions 54

5.7 Closure 55

6. CARTILAGE CONSTITUENT'S INFLUENCE ON KNEE KINETICS/KINEMATICS **57**

6.1 Introduction 57

6.2 Methodology 57

6.3 Finite element model 57

6.4 Gait input data 59

6.5 Contact and boundary conditions 60

6.6 Material models 60

6.7 Results and discussions 65

6.7.1 The tissue response during walking and running cycle 65

6.7.2 Comparison of walking and running cycle 68

6.7.3 Importance of collagen fiber orientation in knee kinematics 68

6.7.4 Significance of Lagrange strain in knee articulation between cartilages 71

6.7.5 Tissue responses on knee kinematics 72

6.8 Conclusions 74

6.9 Closure 74

7. MODELING OF PROSTHETIC KNEE 75

7.1 Introduction 75

7.2 Computational model of knee prosthesis 75

7.3 Loading and boundary conditions 76

7.4 Material models 77

7.5 Contact pressure distribution and Lagrange strain measurement 78

7.6 Wear Calculation 80

7.7 Discussions 81

7.8 Conclusions 82

7.9 Closure 82

8. EXPERIMENTAL STUDY OF PROSTHETIC KNEE-BEARING MATERIAL (UHMWPE) 83

8.1 Introduction 83

8.2 Radiation crosslinking (γ ray) 83

8.3 Methodology 85

8.3.1 Materials and sample preparation 85

8.3.2 Preparation of cross-linked UHMWPE 85

8.3.3 Calculation of thickness for lead block 86

8.4 Mechanical characterisation 87

8.4.1 Wear and friction measurement 87

8.4.2 Hardness measurement 92

8.4.3 Storage and loss modulus 95

8.5 Chemical characterisation 98

8.5.1 FTIR analysis 98

8.5.2 Cross-link density and molecular weight 100

8.5.3 Oxidation index 101
8.6 Conclusions 102
8.7 Closure 102
9 CONCLUSIONS 103
9.1 Future scope 105
REFERENCES 107
PUBLICATIONS 131

LIST OF FIGURES

Figure 1.1	Schematic representation of knee joint structure adapted from (Drake et al. 2019)	4
Figure 1.2	A Schematic representation of depth wise structure of articular cartilage	6
Figure 2.1	Schematic of the chemical structure of polyethylene	18
Figure 2.2	Comparison of wear rates of HDPE and UHMWPE in a multi-directional hip simulator adapted from (Edidin and Kurtz 2000)	19
Figure 3.1	Finite element model of tibio-femoral joint showing all components	28
Figure 3.2	Comparison of contact pressure and Mises stress generated on the surface of gradient material	31
Figure 4.1	The rotation of the femur over the tibia from heel strike to toe-off of a knee during gait	35
Figure 4.2	(a) Gait input force date for during the stance phase (b) Knee joint rotation data during the stance phase (Orozco et al. 2018)	36
Figure 4.3	Maximum contact pressure distribution soft tissues during the stance phase of a gait cycle	38
Figure 4.4	Effective Lagrange strain on soft tissues during the stance phase of a gait cycle	39
Figure 4.5	(a) Contact pressure distribution in soft tissues (b) Effective Lagrange strain (c) Maximum shear stress (d) Effective stress (e) Total displacement	41
Figure 5.1	(a) The posterior view of 3D finite element knee joint model (b) enlarged view of tibial cartilage (c) bodyweight of 1000N acting	44
Figure 5.2	Distribution of contact pressure on (a) the tibial lateral surface; (b) the femoral surface	49

Figure 5.3	The contours for equivalent stress generation on (a) the tibial lateral surface (b) the femoral surface	49
Figure 5.4	The normal stress distribution on (a) the tibial surface; (b) the femoral surface	50
Figure 5.5	The cartilage deformation (a) U1 (anterior-posterior) (b) U2 (proximal-distal) at full extension position	50
Figure 6.1	Schematic of workflow (a) the stance phase of the walking gait (b) running gait (c) sagittal view of femoral cartilage with the orientation of collagen fibers (d) finite element model of the knee joint	58
Figure 6.2	Input gait data for the analysis (a) the components of forces acting during stance phase of walking cycle (b) the rotation angle during walking cycle (c) the forces as acting during the running cycle (d) the rotation during running cycle	59
Figure 6.3	Femoral cartilage models based on distinct collagen fiber orientation (a-d) intact cartilage model (e-g) osteoarthritic models, the fiber orientation in the depth-wise direction is shown in the boxes	63
Figure 6.4	Contours of mechanical responses of femoral cartilage on the surface of intact model-1 during the stance phase of walking (60% gait cycle)	66
Figure 6.5	Contours of mechanical responses of femoral cartilage on the surface of intact model-1 during the stance phase of running (40% gait cycle)	67
Figure 6.6	The comparison of mechanical responses of cartilage for different models (a) the contact pressure (b) maximum principal elastic stress (c) maximum principal Lagrange strain (d) maximum fluid pressure generated	69
Figure 6.7	The comparison of mechanical characteristics of cartilage for different models (a) the contact pressure (b) maximum	70

	principal elastic stress (c) maximum principal Lagrange strain (d) maximum fluid pressure	
Figure 6.8	The effective Lagrange strain in the sagittal plane sectional view of the articulating region	71
Figure 7.1	(a) The 3D finite element model of the TKA (b) circular design femoral component (c) elliptical design femoral component	76
Figure 7.2	The input gait data for the analysis (a) the rotation angle in all 3 dof (b) the components of forces	77
Figure 7.3	Contours of maximum contact pressure and Max Lagrange strain generated on UHMWPE tibial insert	78
Figure 7.4	The mechanical responses of UHMWPE tibial inserts (a) the contact pressure (b-d) Effective stress, principal stress and shear stress (e) Lagrange strain (f) the articulating area of contact	79
Figure 7.5	The maximum femoral component translation for circular and elliptical design	81
Figure 8.1	Crosslinking of UHMWPE samples using gamma irradiation	84
Figure 8.2	Samples prepared from ram extruded UHMWPE by CNC machining	85
Figure 8.3	Irradiation of UHMWPE samples through lead block with hole patterns	86
Figure 8.4	The gamma-irradiated UHMWPE sample mounted on a reciprocating tribometer	87
Figure 8.5	The comparison of coefficient of friction for lower and higher irradiation dose (a) lower irradiation dose 30 kGy (b) higher lower irradiation dose 150 kGy	88
Figure 8.6	Profile of the wear track on the sample for 1x105 cycles obtained from profilometer	89

Figure 8.7	The wear volume plotted against the number of cycles obtained from the samples irradiated (a) low dose, (b) moderate dose and (c) high dose	90
Figure 8.8	The wear rate/wear factor of UHMWPE obtained for different radiation dose levels (a) low dose, (b) moderate dose and (c) high dose	91
Figure 8.9	The wear rate/wear factor of UHMWPE obtained for different radiation dose levels at 1x105 cycles	91
Figure 8.10	The hardness of UHMWPE is measured using the indentation test	92
Figure 8.11	The digital microscopic view (10 x) of the indentation under 5N load on the UHMWPE surface	93
Figure 8.12	The Rockwell hardness values on the surface of different samples at different irradiation dose levels (a) low dose, (b) moderate dose and (c) high dose	94
Figure 8.13	The comparison of indentation depth with respect to the irradiation dose (a) 5N indentation load, (b) 20N indentation load, and (c) 50N indentation load	95
Figure 8.14	The DMA analysis of UHMWPE thin film using a dynamic hybrid rheometer	96
Figure 8.15	(a-c) The storage modulus of samples at 30, 100 and 150 kGy (d-f) the loss modulus of samples at 30, 100 and 150 kGy	97
Figure 8.16	The FTIR spectrum for all the UHMWPE samples at different irradiation (a) 30 kGy dose (b) 100 kGy dose (c) 150 kGy dose	99
Figure 8.17	The crosslink density and molecular weight between crosslinks against the irradiation dose	100
Figure 8.18	The oxidation index calculated from the FTIR spectrum for all the UHMWPE samples at a different irradiation dose	102

LIST OF TABLES

Table 2.1	Molecular weight of different polyethylene	17
Table 2.2	Comparison of physical properties of high-density polyethylene and ultra-high molecular weight polyethylene (Hussain et al. 2020b)	18
Table 2.3	Physical properties for standard non-irradiated and crosslinked/remelted/annealed (GUR 1050) at increasing gamma radiation doses. (Baker et al. 2003)	21
Table 2.4	Comparison of manufacturing techniques of different commercially available cross-linked polyethylene tibial inserts (Brown et al. 2017; Lachiewicz and Geyer 2011)	23
Table 3.1	Material parameter for different material models of the knee components such as bone, ligaments, meniscus and cartilage	29
Table 3.2	Comparison of contact pressure on the cartilage of the current study with results from the literature	32
Table 3.3	The material constants for the constitutive material model for ligament	37
Table 3. 4	Literature based comparison of the values of the total contact pressure for the basic knee model with intact geometry on the soft tissues.	41
Table 5.1	The material parameters for modelling homogeneous and heterogeneous articular cartilage	45
Table 5.2	The material parameters for the components of the knee joint other than cartilage	48
Table 5.3	The estimated over-prediction of mechanical measures in percentage for a homogeneous model relative to its heterogeneous alternative	51

Table 5.4	Comparison of mechanical response on femoral/tibial cartilage (maximum principal stress/contact pressure) for different material models from literature	54
Table 6.1	Material constants for FRPHE intact and arthritic cartilage models (intact model-1 and OA model-1)	64
Table 6.1	Comparison of mechanical response on femoral/tibial cartilage throughout the gait cycle (intact walking) of the present work with respect to the literature	73
Table 7.1	The material constants for the components of the TKA implant	77
Table 7.2	The wear depth produced on the tibial insert during the gait cycle	80
Table 7.2	Comparison of wear rate/factor of the UHMWPE tibial insert obtained from the present study with respect to the literatures	81
Table 8.1	Prominent FTIR bands of UHMWPE and its oxidised species	98

NOMENCLATURE

Symbols

$\bar{B}$	The left Cauchy-green deformation tensor
C_1, C_2	Mooney-Rivlin material constants
d	Penetration depth [μm]
D_1	Neo-Hookean material constant
e	Void-ratio
e_1, e_2, e_3	Orthonormal vectors representing the local element coordinate system for the fibers
E	Modulus of elasticity [MPa]
E'	Storage modulus [MPa]
F	Deformation gradient
F_n	Normal force [N]
G	Modulus of rigidity or shear modulus [MPa]
I_x	Initial intensity
I_o	Intensity after path length
I_1, I_2	First and second invariant corresponding to the left Cauchy-Green deformation tensor
I_n	Strain component
I_{ox}	Oxidation index
$\bar{I}_1$	First invariants of the left Cauchy-green deformation tensor
J	Jacobian of the deformation
k	Permeability [mm^4/Ns]
k_0	Isotropic hydraulic permeability [mm^4/Ns]
K	Bulk modulus [MPa]
K_w	Wear factor [mm^3/Nm]

$k(J)$	Strain dependent permeability [mm^4/Ns]
K_s	Permeability of soft tissues by Holmes-Mow [mm^4/Ns]
l_n	Fiber stretch
M	Exponential strain-dependent co-efficient
M_c	Molecular weight between crosslinks [g/mol]
n_z	Solid volume fraction
N	The fiber orientation in the reference configuration represented by θ and φ
P	Contact pressure [MPa]
R	Gas constant [J/molK]
S	Sliding distance [m]
T	Absolute temperature [K]
V	Wear volume [mm^3]
x	Shield thickness [mm]
z	Volume fraction variable varies from 0 to 1 from cartilage surface to subchondral bone

Greek Letters

a	Coefficient of exponential argument
a_1	Power-law exponent
b	Power of exponential argument (fiber non linearity)
ρ	Mass density [kg/m^3]
γ	Gamma ray
ϵ	Strain
ξ	Represents a measure of fiber modulus [MPa]

Θ, φ	Spherical angle for fiber orientation in local coordinate system [deg]
μ	Shear modulus [MPa]
σ	Cauchy stress tensor
ν	Poisson's ratio
ν_d	Cross-link density [mol/mm^3]
Ψ	Strain energy density function [J/m^3]

Abbreviations

ACL	Anterior Cruciate Ligaments
DOF	Degree of Freedom
ECM	Extracellular Matrix
GUR	Granular UHMWPE Ruhrchemie
HDPE	High Density Polyethylene
HR	Rockwell Hardness Number
HXLPE	Highly Crosslinked Polyethylene
LCL	Lateral Collateral Ligaments
MCL	Medial Collateral Ligaments
PE	Polyethylene
PCL	Posterior Cruciate Ligaments
RP	Reference Point
THA	Total Hip Arthroplasty
TKA	Total Knee Arthroplasty
TKR	Total Knee Replacement
UHMWPE	Ultrahigh Molecular Weight Polyethylene

CHAPTER 1

INTRODUCTION

1.1 Background of study

The knee is the largest joint in the musculoskeletal system of the human body and supports whole body weight and expedites locomotion. The joint includes tibiofemoral and patella-femoral articulations. The articular cartilage is the load-bearing component of knee joints (Mononen et al. 2011). Osteoarthritis (OA) is a significant public health concern due to knee joint pain during walking, climbing, and kneeling. OA is a chronic progressive musculoskeletal disorder characterised by articular cartilage degradation in knee joints. Also, the recent increase in knee replacement operations among younger patients is direful (Adouni and Shirazi-Adl 2014). Thus, understanding degradation phenomena requires knowledge of the stress fields within the tissue. The numerical method is a better way to understand the behaviour of cartilage (Shirazi and Shirazi-Adl 2009). Since experimental measures have limitations like the accuracy of in-vivo tests, measurements at lower spatial scales, synchronous measurements of joint level kinematics or kinetics, difficulty in measuring variables such as stress, fluid flow, and contact pressure within the cartilage (Sibole and Erdemir 2012). Finite element simulation is widely adopted to investigate knee joint biomechanics at the cell, tissue, and joint levels (Anderson et al. 2008). Also, accurate simulations can provide detailed information on knee response under various situations.

The critical challenge in simulating articular cartilage is the complexity of its structure, compounded by the heterogeneous distribution of collagen fibers throughout its cross-section. A graded material design mimics the complex cartilage structure and can impart unique advantages that can be used to improve the durability of implants. However, multiple material models have been used to investigate the mechanical behaviour and damage mechanism of articular cartilage. Further, the impact of collagen fiber orientation significantly influences the mechanical response of articular

cartilages for the healthy and arthritic knee during multiple gait activities. Daily physical activities like walking, jogging, and running lead to significant compressive loads on the knee cartilage. The load on the knee joint is different for each of these activities 1BW, 1.5BW, 2BW, and 4BW, respectively (Meng et al. 2017).

In the extreme phase of osteoarthritis, knee replacement surgery might be the only choice. Total Knee Replacement (TKR) or Total Knee Arthroplasty (TKA) involves the surgically removing of worn-out cartilage and bone particles from the knee area and substituting them with artificial joints made of metal alloys and high-grade polymers. In most cases, total knee replacement surgery is suggested for the patient who undergoes severe knee pain or stiffness, knee pain even during sitting or lying down, chronic swelling and knee deformities, among other reasons.

Aseptic loosening, joint infection, and instability are the leading cause of failure after TKR, and polyethylene wear is the primary reason for revision surgery. Implant design, surgical technique, polyethylene manufacturing and patient factors influence the rate and volume of polyethylene wear (Beck et al. 2012). Ultra-high molecular weight polyethylene (UHMWPE) is a common polymer used in total knee prosthetics due to its higher wear resistance, ductility, chemical inertness, and biocompatibility (Hussain et al. 2020a). However, the deterioration of the implant's bearing surfaces contributes to the accumulation of particle debris inside the knee. These particles cause periprosthetic Osteolysis, which increases patient discomfort and, in extreme cases, may necessitate revision surgery (Kandahari et al. 2016; Kurtz et al. 2011). In addition, the degradation of UHMWPE over time gradually reduces the lifespan of knee prosthetics. Therefore, it is essential to enhance the wear resistance of UHMWPE for it to be used as an implant material.

1.2 Motivation

Computational models of the biomechanics of the whole joint have the potential to be incredibly effective clinical tools. They allow researchers and clinicians to examine the significance of particular tissue structures in normal and pathological joint movements. Joints are extraordinarily complex mechanical systems characterised by their nontrivial

geometry and intrinsically coupled behaviour. Numerical tools can provide insights into both local tissue deformation and global joint kinematics with normal physiology by illustrating the role of each constituent tissue structure in maintaining functionality. Physiological influences related to age, sex, usage, injury, and illness alter actual joint mobility, and this variation may significantly contribute to a cascade of tissue deterioration, resulting in an escalation of decreased joint performance. Therefore, it is essential to comprehend the normal working conditions of joints in order to develop computational frameworks that can make accurate predictions regarding the causes of acute damage, such as ligament rupture, and degenerative illnesses, such as osteoarthritis.

It is alarming that the rate of TKR performed in India is increasing annually. According to Frost and Sullivan survey, almost 70,000 knee joint replacement surgeries (TKR) were performed in India in the year 2011 (Pachore et al. 2013), and currently, it is estimated that 1,20,000 TKR are performed yearly in India (Chawla 2019). Likewise, it is said that the reason for the beginning of this reason is said to be expanding the life span of Indians. Presently, India's 65 and above population is likely to be about 177 million, whereas India had 100 million people in this age group in 2010. Similarly, the number of total knee arthroplasty (TKA) performed in the United States has increased dramatically over the past ten years to more than 615,000 in 2008 (Losina et al. 2012). Projections estimate that demand will continue to grow to more than 3 million annually by 2030.

The volume of revision TKA increased to more than 75,000 during ten years in 2007 and has been projected to increase further by 600% by 2030 (Kurtz et al. 2007). Whereas it is expected that increased primary knee volume would increase revision volume, the cause and rate of failure cannot be ignored. Aseptic loosening was the predominant mechanism of failure (31.2%), followed by instability (18.7%), infection (16.2%), polyethylene wear (10.0%), and malalignment (6.6%) are the main reasons for TKR revision (Schroer et al. 2013). Many researches are going on knee implants to improve the performance and life by reducing the revision rate of TKR.

1.3 Knee joint structure

The knee joint is comprised of three bones and a variety of soft tissues. The bones are the femur, the tibia, and the patella. The femur and tibia, which are the essential bones of the upper and lower leg individually, are shown in Figure 1.1. The patella bone is located in front of the tibia-femoral articulation and is connected via quadriceps tendons. The knee joint consists of pair of articulation, femoral-patellar and tibio-femoral, among which the tibio-femoral is the most complex and consists of many soft tissues like cartilage, meniscus and ligaments.

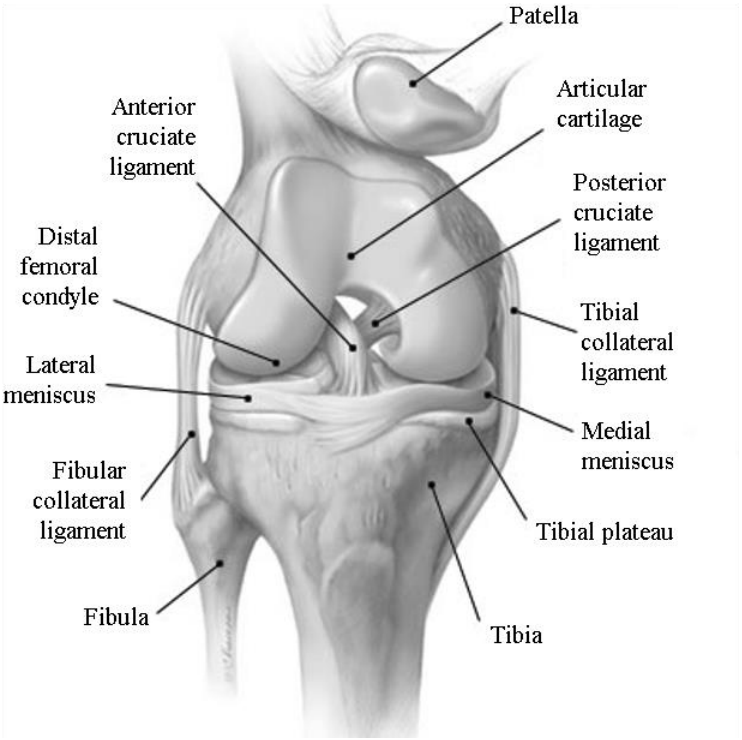

Figure 1.1 Schematic representation of knee joint structure adapted from (Drake et al. 2019)

Each bone has a layer of articular cartilage covering its articulating surfaces (femoral cartilage and tibial cartilage). In the gap between femoral and tibial cartilage, a couple of menisci (lateral and medial meniscus) wrap over the condyles. These are encompassed by a liquid-filled capsule, guaranteeing that the soft tissues are soaked in synovial fluid. The cartilage and menisci transmit the huge load experienced by the joint, while the synovial fluid lubricates up the articulating surfaces to bring down

friction and reduce wear. The femur bone is attached to the tibia through the medial and lateral collateral ligaments (MCL and LCL) and the anterior and posterior cruciate ligaments (ACL and PCL). These four ligaments ensure the structural stability of bones: femur and tibia and also control the relative positioning of the two bones during knee flexion.

1.4 Articular cartilage

Articular cartilage plays a vital role in the knee joint while transferring loads from the underlying bone; it acts as a frictionless bearing and prevents high-stress concentrations by distributing loads uniformly. The study of articular cartilage is essential in the diagnosis of osteoarthritis patients, kinematics of intact and prosthetic knees, knee implants, biomaterials etc. Cartilage is a multi-phase material comprised of a dense extracellular matrix (ECM) with a random distribution of chondrocyte cells, which maintains the ECM and is primarily composed of collagen fibers, proteoglycan and water(Sophia Fox et al. 2009). The collagen fiber network in the articular cartilage provides tensile strength and stiffness to the composite tissue; Figure 1.2 shows the schematic representation of cartilage structure with collagen fibers. Jointly these components help to maintain water in ECM, which is critical in maintaining its mechanical properties like sudden impact strength, high compressive strength etc.

The structure of articular cartilage is mainly divided into three zones: superficial, transverse and deep zone, which is given in Figure 1.2. The thin, superficial (tangential) zone protects deeper layers from shear stresses and makes up approximately 10% to 20% of articular cartilage thickness. The collagen fibers of this zone are packed tightly and aligned parallel to the articular surface. This zone is in contact with synovial fluid. It is responsible for most cartilage tensile properties, which enable it to resist the sheer, tensile, and compressive forces imposed by articulation. Immediately deep to the superficial zone is the middle (transitional) zone, which provides a functional bridge between the superficial and deep zones. The middle/transverse zone represents 40% to 60% of the total cartilage volume and contains proteoglycans and thicker collagen fibrils. In this layer, the collagen is

organized obliquely and functionally; the middle zone is the first line of resistance to compressive forces. The deep zone is responsible for providing the most significant opposition to compressive forces, given that collagen fibrils are arranged perpendicular to the articular surface. The deep zone represents approximately 30% of the articular cartilage volume (Sophia Fox et al. 2009).

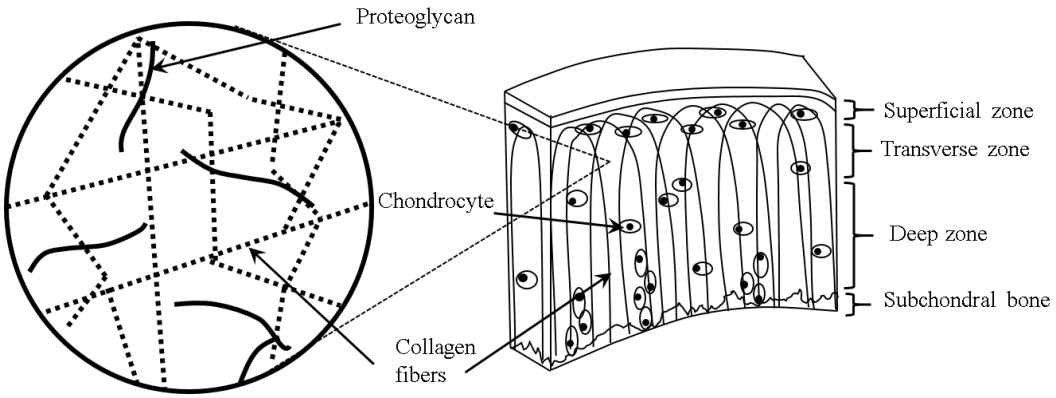

Figure 1.2 A Schematic representation of depth wise structure of articular cartilage

To understand in detail about osteoarthritis conditions, extensive experimental and computational studies have been performed on the knee joint in vivo and in vitro cases. Among computational studies, Finite Element (FE) modelling of the knee joint is widely used to identify changes in tissue-level mechanical stresses and strains and describe how these parameters might relate to joint and cartilage pathologies. The exactness of the FE show can be approved by how it can simulate reality, and it can depend on different factors such as the geometry of the articulating surfaces, material models and properties, joint loads, and boundary conditions (Besier et al. 2005).

1.5 Prosthetic knee

Total knee replacement (TKR) or Total knee arthroplasty (TKA) has been widely used to relieve osteoarthritis pain. It has been established as a successful treatment for advanced degenerative joint disease. The TKR involves removing the articulating surfaces of the affected knee joint and replacing them with artificial components made of biomaterials. Knee implants are metal alloys, ceramic materials, or strong plastic parts. A typical knee implant has a femoral component and tibial tray made of metals

such as titanium-based alloys, stainless steels and cobalt-chromium (Co-Cr) alloys, a high-density polyethylene insert, and a polyethylene button. The femoral component and tibial tray are made of cobalt-chromium alloy and polymer insert by ultrahigh molecular weight polyethylene (UHMWPE).

The metal femoral component curves around the end of the femur so that it can rotate smoothly against the bone as the knee bends and straightens. The tibial component is typically a flat metal platform with a cushion of strong, durable plastic called polyethylene. For additional stability, the metal portion of the element may have a stem that inserts into the centre of the tibia bone. Components are designed so that metal always borders with plastic, providing smoother movement and less wear of the implant. One of the prosthetic knee's main aims is patient walking properly; however, literature shows that some patients remain walking abnormally following TKR. The altered gait patterns do not necessarily mean that the TKR has failed, but it may impact the patient's functional capacity daily. For example, more pain, joint stiffness, not able to walk, instability, longer leg, and loose of the implanted knee have been reported by patients.

1.6 Assumptions and limitations of study

The computational study has some limitations in terms of model generation, input data, and assumptions. The knee kinematics is very complex, and hard to simulate the exact motion; the tibia stresses are a combination of loading (compression and tensile) and shear and the input data in this investigation are applied in terms of forces and rotation. Other soft tissues (patella, patellar tendon, joint capsule, and skin) are excluded from the model due to the complexity of the analysis. A significant limitation in the computational analysis is the load acting on the knee joint from other components, such as the patella, tendons, fibula, and skin, is ignored. Only the tibial and femoral bones force act on the cartilage during a gait cycle. Material properties of tissues are entirely based on literature and are not specimen specific. Also, the gait input data chosen for the present investigation is subject-specific, and the results may vary from subject to subject. For the experimental study, the availability of in-vivo knee

simulators is limited in India, and the wear characteristics are measured using the ball-on-disc tribometer method.

1.7 Organisation of thesis

This thesis contains eight chapters, and a brief description of the contents of each chapter is given below

Chapter 1 briefly explains the introduction to the knee joint, the importance of articular cartilage structure in knee mechanism, the limitations and motivation of the computational study of knee joint analysis, and the motivation of the present investigation to enhance the durability of the current knee implants.

Chapter 2 includes a comprehensive literature overview of the computational methods of articular cartilage mechanics in knee joint analysis and the various methodologies utilised to improve the design and durability of knee implants from the past to the present. Literature identified research gaps aided in formulating the current study's objectives.

Chapter 3 illustrates the numerical simulation to obtain knee joint contact pressure distribution while loading using a graded implant material for the cartilage.

Chapter 4 discusses the investigation of the influence of soft tissues in the knee joint on the load transfer mechanism during the gait cycle

Chapter 5 discusses the computational analysis of the impact of material heterogeneity on the calculation of mechanical responses of articular cartilage and their behaviour under different material models.

Chapter 6 shows the numerical investigation of the influence of articular cartilage's constituent structure during various activities for the intact and arthritic joints.

Chapter 7 describes the modelling of knee prostheses and the enhancement of mechanical properties through design modifications relative to conventional knee prostheses.

Chapter 8 describes a novel experimental technique for incorporating material heterogeneity in knee implant material (UHMWPE-bearing material) to improve wear and other mechanical properties.

Chapter 9 concludes the overall representation of the research work. It also explains the scope for future work.

1.8 Closure

This chapter narrated the general introduction to knee biomechanics and its structure of constituents. It explained the basic concepts of the problem statement considered in this present work. This chapter also presented the details of the organisation of the thesis. The next chapter depicts the literature review, scope and objectives of the present study.

CHAPTER 2

LITERATURE SURVEY

2.1 Introduction

Much research has been carried out in the field of orthopaedic biomechanics and the study of articular cartilage for a better understanding of osteoarthritis patients in the past few decades. The literature shows the mechanical response of knee joints with different constitutive models for the cartilage and multiple collagen fiber-oriented cartilage models for the intact and arthritic knee kinematics during the walking and running gait cycle. For knee prosthesis durability, UHMWPE tibial insert wear is the primary concern after 10 to 15 years of implant surgery. In recent years, a substantial study has been conducted to enhance the mechanical and tribological properties to provide patients with durable implants.

2.2 Computational study of soft tissues

Cartilage is essential to the mechanical operation of a knee joint in which it is present. The mechanical function of articular cartilage is not only governed by its structural compositions and material qualities but also by the joint's contact circumstances. This section briefly presents some background information on the mechanical structure and function of articular cartilage.

2.2.1 Materials used to model articular cartilage

Articular cartilage is a biphasic, heterogeneous and isotropic soft tissue and various material models are used for determining the mechanical behaviour of articular cartilage (Mononen et al. 2011). Sometimes cartilage is considered an isotropic, homogeneous and linear elastic material for saving high computational cost and time (Peña et al. 2007). Sometimes cartilage is considered an isotropic, homogeneous and linear elastic material for saving high computational cost and time (Peña et al. 2007).

The material models such as isotropic elastic (IE), isotropic poroelastic (IPE), transversely isotropic poroelastic/ transversely isotropic elastic (TIPE/TIE), and fibril-reinforced poroviscoelastic/poroelastic (FRPVE/FRPE) are commonly used to simulate the mechanical response of articular cartilages (Faisal et al. 2019; Halonen et al. 2016a, 2017; Julkunen et al. 2008; Kazemi et al. 2013; Meng et al. 2014; Naghibi Beidokhti et al. 2016; Orozco et al. 2018; Shirazi et al. 2008; Shirazi and Shirazi-Adl 2009; Tanska et al. 2015; Venäläinen et al. 2016).

The isotropic elastic model predicts the instantaneous cartilage response faster compared with its alternative models (Donahue et al. 2002; Li et al. 2019; Trad et al. 2018; Zhang et al. 2019). Essentially these models give a qualitative understanding of the response. Also, this model accurately predicted instantaneous cartilage response and proved that there were no significant changes in cartilage contact response after loading, which was demonstrated in an article (Donzelli et al. 1999). Young's modulus was chosen as 15 MPa, and Poisson's ratio was selected as 0.475, based on an experimental study by (Shepherd and Seedhom 1999); these values have been chosen because it has modelled that cartilage shows the instantaneous response to loading corresponding to Young's modulus 5-15 MPa and 0.5 Poisson's ratio (Blankevoort and Huiskes 1991) (Mommersteeg et al. 1996). However, linear elastic models have limitations; it is not selected for large deformations, which is why cartilage is considered hyperelastic material. According to different complexities, several hyperelastic models are available, like Mooney-Rivlin and Neo-Hookean. The simplest model is Neo-Hookean and suitable for large deformations; it is a particular case of the Mooney-Rivlin model and is widely used in the literature (Anderson et al. 2008).

Finally, some previous work used depth-dependent material properties (Shirazi and Shirazi-Adl 2009), (Shirazi et al. 2008), (Adouni et al. 2012a). They used depth-dependent isotropic hyperelastic for the non-fibrillar solid matrix of cartilage with a modulus of elasticity varying from 10 MPa at the superficial zone to 18 MPa at the deep zone with a Poisson's ratio of 0.49. The variation in structure and composition through the depth from articulating surfaces causes an increase in fixed charge density

from the superficial zone to the deep zone. Hence, the compressive modulus of cartilage increases from top to bottom. It has been reported that the compressive modulus of cartilage increases with depth from articulating surface to the deep zone and ranges from .079 MPa in the superficial zone to 2.69 MPa in the deep zone (Schinagl et al. 1997a).

Nevertheless, in reality, articular cartilages comprise a porous matrix saturated with water (68% - 88% of cartilage weight). The response of cartilage tissue is influenced by fluid pressure (Ateshian et al. 1998; Klets et al. 2016). Hence the biphasic characteristics of cartilage are generally studied with IPE models. In IPE models, the fluid flow in cartilage is modelled with Darcy's law related to permeability(k) (Suh and Disilvestro 1999). In a few studies, researchers modelled cartilage and meniscus as isotropic poroelastic material to study fluid-solid interaction behaviour. The Young's modulus (E) they have taken as 0.7 MPa, Poisson's ration (ν) of 0.1 and permeability (k) of 2.1710 x 10^{-15} m^4/Ns (Zhang et al. 1999).

Apart from biphasic characteristics, the articular cartilage constitutes a non-fibril matrix and collagen fibril network. FRPE model may suit well to simulate the response of such a structure (Orozco et al. 2018). Also, it is reported that FRPE model is good at representing the static and dynamic response of articular cartilage compared to other models and validated experimentally through creep and stress-relaxation tests (Korhonen et al. 2003). Therefore FRPE models have been used in recent studies to analyse knee joint reaction forces and cartilage stresses. The main drawback of the model is, for a single run, it would take days or even weeks (Essinger et al. 1989). The material orientation is assigned such that it mimics the contribution of collagen fibril orientation (arcade-like structure). However, this model is computationally not cost-effective and lacks relevance in clinical applications.

TIE models are also widely used in modelling articular cartilage (Bolcos et al. 2018; Klets et al. 2018; Liukkonen et al. 2017b). From recent studies, the TIE model can predict intact articular cartilage uniaxial compression responses with higher accuracy (Deneweth et al. 2013). The highly heterogeneous nature of the superficial zone can

simulate well with such models(Clark 1991; Jeffery et al. 1991) the most influential compartment on articular cartilage to mechanical response (Mizrahi et al. 1986).

2.2.2 Collagen fiber structure and its influence on tissue response

Daily physical activities like walking, jogging, and running lead to significant compressive loads on the knee cartilage, causing knee osteoarthritis (OA), especially in older people (Halloran et al. 2012; Nuckols et al. 2020; Thordarson 1997; Yao et al. 2019). The articular cartilage constituents such as collagen fibers, proteoglycan matrix, and interstitial fluid collectively withstand the body weight (BW) during activities like walking, running, stair climbing, and kneeling. The load on the knee joint is different for each of these activities 1BW, 1.5BW, 2BW, and 4BW, respectively (Meng et al. 2017; Park et al. 2003; Peters et al. 2018a). The collagen network of articular cartilage protects chondrocytes, withstands high tensile force, and protects cartilage from rupture. Also, it provides mechanical rigidity, which helps to maintain the solid matrix's structure. This network attaches the cartilage to the subchondral bone and provides attachment for proteoglycans (Panula et al. 1998). In the loading and unloading stages, the osmotic pressure increases in the articular cartilage, significantly increasing the interstitial fluid pressure. The body force is distributed throughout the cartilage during the loading stage and increases the shearing force on the articulating surface. Hence collagen fibers are subjected to complex loading conditions due to the interstitial fluid pressure and shearing force (Cohen et al. 1998; Kazemi et al. 2012; Sophia Fox et al. 2009). OA leads to degradation in cartilage structure in terms of fibrillation and proteoglycan depletion, hindering the mechanical characteristics of the cartilage (Is et al. 2005; Messier 1994; Peters et al. 2018b; Saxby and Lloyd 2017). To better understand cartilage degradation associated with OA, it would be convenient to characterize the collagen fiber orientations and their responses in a complex loading environment under different gait activities.

The collagen fibers in cartilage provide mechanical rigidity, which helps to maintain the solid matrix's structure. Also, the fibers are distributed heterogeneously throughout the cartilage, with their structure similar to an arcade-like design from the articulating surface to the subchondral bone (Klika et al. 2016; Wilson et al. 2004). The fibrils are

horizontally oriented parallel to the articular surface in the superficial zone. However, they become more randomly oriented in the transitional zone and turn perpendicular to the bone-cartilage interface in the deep zone to firmly anchor the tissue to the subchondral bone (Clark 1990; Halonen et al. 2013; Korhonen and Herzog 2008). The zonal thickness of SZ, TZ, and DZ is about 12%, 32%, and 56% of the cartilage's total thickness, respectively (Kazemi et al. 2013). The fiber orientation in the respective zones is represented with split-line patterns, the most widespread technique used in the literature (Below et al. 2002; Bursać et al. 1999; Halloran et al. 2012; Mononen et al. 2012).

The superficial layer is the most affected arthritic part compared to other layers, and fibrillation occurs on this surface (Gannon et al. 2015; Guilak et al. 1994; Ruggiero et al. 2015). The fiber network is known to be organized differently in healthy and arthritic cartilage. The collagen fiber orientation significantly influences the tissue response and the contact mechanism for OA cartilage (Clark 1990; Lin et al. 2020; Meng et al. 2017; Shirazi et al. 2008). In addition, it is reported that the tissue response is highly sensitive to fiber reorientation and loading direction (Moger et al. 2009). Fiber reorientation is the major mechanism when loading perpendicular to collagen fiber orientation; however, when loading parallel to the fiber direction, a reduction in collagen fibers crimp and fiber reorientation occurs (Sellaro et al. 2007). Hence it is necessary to understand the behaviour of cartilage response with respect to the collagen fiber orientation. Even though literature is available on the tissue responses for arthritic cartilage cases, the relation between collagen fiber orientation/loading direction and tissue response is not adequately studied (David et al. 2015a; Halonen et al. 2016a; Mononen et al. 2015; Yao et al. 2019).

2.3 Prosthetic knee

For severe knee osteoarthritis, total knee replacement (TKR) is a standard surgical procedure that reduces knee discomfort and restores mobility (Bei et al. 2004; Smith et al. 2016). Ultra-high molecular weight polyethylene (UHMWPE) and cobalt-chromium alloy (Co-Cr) are the most popular biomaterials used in knee prosthetics for decades. Recent developments have been in the design of customized implants based

on patient-specific data obtained from MRI scans and subsequent image processing techniques. In addition, several computer studies are being undertaken to analyse the implant's wear and thus develop a durable component.

2.3.1 Prosthetic knee design and its influence in the mechanical characteristics

In India, around 1,20,000 TKRs are projected to be conducted annually (Kurtz 2009). TKR operations are increasingly being done on people of younger ages. Traditionally, the advice is to postpone TKR as much as possible; however, the emphasis is now on enhancing functional ability and, therefore, standard of living, regardless of the patient's age (Enab 2014). This shift of thinking is partly due to the availability of higher-quality, longer-lasting implants and the increased public acceptability of TKR. Youngers who engage in more excellent physical activity where high flexion is culturally expected are more concerned about excessive knee flexion after TKA. Hence they are more likely to overload the prosthetic joint. As a result, they are at a higher risk of premature wear and failure. Revision surgery is necessary if the original TKR wears out or fails to work correctly. As a result, it is critical to enhancing the life of mechanical joint replacements, especially in younger patients (Clary et al. 2013).

Clinical performance has been enhanced due to advancements in TKA prosthesis design, including a more excellent range of movement and a longer implant lifespan. However, TKA kinematics influences the joint's functioning and durability. There are several TKR implants in the market, each with its design reason. Different implant designs strive to improve patient comfort by offering kinematics that is as similar to normal as possible. Implanted knee kinematics are modified by conformity, loading circumstances, ligament integrity, and muscle function. Knee conformity due to the curvature of the Co-Cr femoral component over the UHMWPE tibial insert is the most crucial (Kazemi et al. 2013; Kurtz 2009). The femoral component curvature is hypothesised to influence knee kinematics and patient comfort. The wear on the tibial insert is influenced by relative sliding between the metal components due to the shift in maximum knee flexion caused by the femur's anterior-posterior placement on the tibia. Also, the wear of the UHMWPE tibial insert is hypothesized to be linked to the curvature of the Co-Cr femoral component. Conventionally the wear of the tibial insert

is measured using a knee joint simulator for multiple millions of cycles passed over the UHMWPE insert. When compared to testing using a knee simulator, pin-on-disc wear tests reveal similar results of TKA while saving money and time (Fisher et al. 2004). Consequently, it is vital to evaluate the mechanical responses of the implant, including contact pressure, stresses, and wear, in relation to design modifications. Therefore investigation of the influence of this curvature of the femoral component on the mechanical response of the bearing component is essential.

2.3.2 The evolution of UHMWPE and its application in prosthetic knee

High-density polyethylene (HDPE) was used in implants before the discovery of UHMWPE, and compared to HDPE, UHMWPE has higher ultimate strength and impact strength. Perhaps more relevant from a clinical perspective, UHMWPE is significantly more abrasion and wear-resistant than HDPE. UHMWPE, low-density polyethylene (LDPE) and high-density polyethylene (HDPE) come from a family of polymers with a deceptively simple chemical composition, consisting of only hydrogen and carbon. Polyethylene is a polymer formed from ethylene (C_2H_4) shown in Figure 2.1. The generic chemical formula for polyethylene is - $(C_2H_4)_n$- where n is the degree of polymerization. The resins commonly used for manufacturing UHMWPE are GUR 1020, GUR 1050 and 1900 H (powder form). For UHMWPE, the molecular chain consists of 1 lakh to 2.5 lakh ethylene repeat units, but for high-density polyethylene (HDPE), the molecular chain has 700 to 1800 ethylene repeat units. Table 2.1 shows the molecular weight of different polyethylene used in implants.

Table 2.1 Molecular weight of different polyethylene

Polyethylene	Molecular Weight (g/mol)
Low density polyethylene (LDPE)	50,000
High density polyethylene (HDPE)	2,00,000
Ultra high molecular weight polyethylene (UHMWPE)	60,00,000

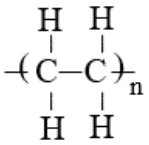

Figure 2.1 Schematic of the chemical structure of polyethylene

The comparison of the physical properties of high-density polyethylene and ultra-high molecular weight polyethylene is given in Table 2.2. The following wear data for UHMWPE and HDPE were collected using a contemporary, multidirectional hip simulator (Edidin and Kurtz 2000). Based on hip simulator data, shown in Figure 2.2, the volumetric wear rate for HDPE is 4.3 times greater than that of UHMWPE. For the past 50 years, ultra-high molecular weight polyethylene (UHMWPE) has been used in orthopaedics as a bearing material in artificial joints. Wear and damage of the UHMWPE components have historically been one of the factors limiting implant longevity. In the past 15 years, highly cross-linked UHMWPE biomaterials have shown dramatic reductions in wear and improved long-term survivorship in total hip replacements worldwide (Kurtz 2016).

Table 2.2 Comparison of physical properties of high-density polyethylene and ultra-high molecular weight polyethylene (Hussain et al. 2020b)

Property	HDPE	UHMWPE
Molecular weight (10^6 g/mol)	0.05 – 0.25	3.5 – 7.5
Poisson's ratio	0.40	0.46
Modulus of elasticity (GPa)	0.4 – 4.0	0.5 – 0.8
Tensile yield strength (MPa)	26 – 33	21- 28
Tensile ultimate strength (MPa)	22-31	39-48
Tensile ultimate elongation (%)	10 – 1200	350 – 525
Wear rate ($mm^3/10^6$ cycles)	380-400	8-100

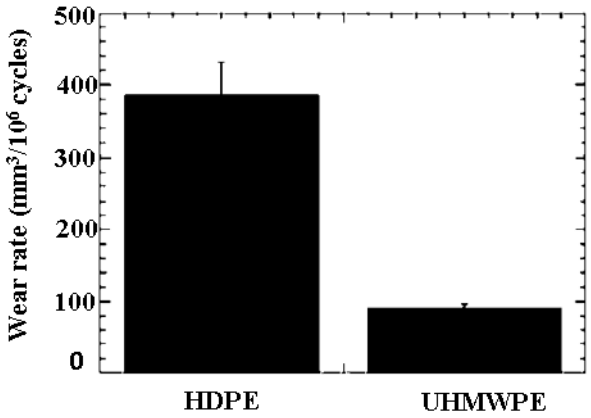

Figure 2.2 Comparison of wear rates of HDPE and UHMWPE in a multi-directional hip simulator adapted from (Edidin and Kurtz 2000)

2.4 Polyethylene wear in total knee arthroplasty (TKA)

2.4.1 Crosslinking of UHMWPE to HXLPE

Crosslinking of UHMWPE significantly improves wear performance which can be achieved through saline or chemical methods using peroxides and irradiation. Irradiation crosslinking is the most common and effective method for sterilizing and crosslinking UHMWPE. Radiation Cross-linking of virgin UHMWPE is performed by gamma irradiation or electron beam whereby hydrogen atoms are removed from the polyethylene chain, creating free radicals, which recombine by linking with free radicals of neighbouring PE molecule chains. This new network of cross-linked polyethylene chains dramatically increases the wear resistance but also increases the stiffness of the polyethylene and makes it more brittle (Heisel et al. 2004). However, not all free radicals created by irradiation recombine to form cross-links. These residual free radicals are highly reactive and responsible for the polyethene's early oxidation (ageing).

From the earliest phases of virgin UHMWPE to the current highly cross-linked polyethylene (HXLPE), the polymer experienced a progressive shift in wear resistance and mechanical performance. The introduction of HXLPE to the market was more than three decades ago, and the numbers have increased significantly. Researchers are

trying various approaches, such as irradiation, surface modifications, and reinforcements, to improve the implant's durability (Kurtz et al. 1999; Muratoglu et al. 2001; Wang et al. 2017). Radiation cross-linking is a vital technique to enhance the UHMWPE's wear resistance (Baena et al. 2015; Dhar Badgayan et al. 2020). Studies suggested in vitro (McKellop et al. 1999; Muratoglu et al. 2003) and in vivo cross-linking of UHMWPE have been effectively utilised to reduce wear (Digas et al. 2007). The cross-linking of UHMWPE is accomplished through ionising radiation (gamma or electron beam) (Charlesby and A 1952). Irradiation of UHMWPE generates free radicals by radiolytically cleaving C-H and C-C bonds in polyethylene, the majority of which recombine to form cross-links in the amorphous region of the polymer. The uncombined free radicals generated get trapped in the amorphous area, and the oxidation of those residual free radicals causes the degradation of mechanical properties (Oral et al. 2008). Radiation cross-linking followed by heat treatments and antioxidant additives are used to overcome oxidation stability and bearing performance.

2.4.2 1st generation highly cross-linked polyethylene

1st generation of highly cross-linked polyethylene (HXLPE) was introduced in 1990 instead of conventional polyethylene with annealing or remelting thermal treatments (Takada et al. 2017). The wear resistance of UHMWPE is significantly enhanced by cross-linking. Wear of UHMWPE occurs by plastic deformation of the polymer, with molecular alignment in the direction of motion, resulting in the creation of tiny, parallel fibrils. As a result, the wear surface may become stronger in the direction of sliding while weakening in the transverse direction (Wang et al. 1998). Under the conditions of multi-directional motion, such as those of the hip and knee joints, fibrous wear debris detaches from the worn surfaces, as documented in several publications (Tipper et al. 2000). Since crosslinking creates carbon-carbon connections between neighbouring chains, it has been hypothesised that it would have been effective in reducing the production of surface fibrils and making polyethylene more resistant to wear (Moratoglu 2009).

Table 2.3 Physical properties for standard non-irradiated and crosslinked/ remelted/ annealed (GUR 1050) at increasing gamma radiation doses. (Baker et al. 2003)

Properties	Non irradiated UHMWPE	Irradiated 50 kGy	Irradiated 100 kGy	Irradiated 200 kGy
Crystallinity (%)	50.1 ± 0.5	45.6 ± 0.7	46.3 ± 0.8	47.1 ± 0.4
Elastic modulus (MPa)	495 ± 56	412 ± 50	386 ± 23	266 ± 30
Yield stress (MPa)	20.2 ± 1.0	19.9 ± 0.8	18.9 ± 0.7	20.2 ± 1.0
True stress at break (MPa)	315.5 ± 31.6	237.6 ± 12.3	185.7 ± 7.5	126.0 ± 14.0

Most authors agree that the crosslinking density increases linearly up to radiation dose in order of 100 kGy (kilo grey) or 10 Mrad (mega rad) (Muratoglu et al. 1999). However, the tensile and fracture toughness continues to reduce at a radiation dose higher than 100 kGy (Baker et al. 2003). Therefore, most of the 1st generation of highly cross-linked polyethylene that appeared in experimental were irradiated to doses between 50 and 105 kGy in the early 2000s. Similarly, acetabular cups machined from a polyethylene gamma-irradiated in air at doses ranging from 33 to 1000 kGy demonstrated an 87% wear reduction with increase in the radiation dose from 33 to 95 kGy, when tested for 5 million cycles in a hip simulator; similarly, the wear decreased to undetectable levels at a radiation dose greater than 200 kGy. Observing the trade-off between the reduction in tensile properties and the increase in wear resistance as the radiation dose was increased, the authors of the same study concluded that 100 kGy is the optimal dose to reduce wear below the threshold for clinically significant effects while preserving sufficient tensile properties. The properties are listed in Table 2.3.

2.4.3 2nd generation highly cross-linked polyethylene

Second-generation annealed HXLPE (X3, Stryker Orthopaedics) has been developed to improve further 1st generation annealed HXLPE to achieve oxidative resistance and maintain low wear and mechanical strength. Cross-linking for the specimens of the X3

material was performed in three cycles using a sequential irradiating and annealing process (total radiation dose was 90 kGy). This process increases the amount of cross-linking. Simulator testing found 60% lower wear than for first-generation annealed material. An alternative approach to the second generation of highly cross-linked polyethylene involves the addition of an anti-oxidant stabiliser (Vitamin-E) to inhibit oxidative degradation without the need for thermal treatment of the irradiated polyethylene in order to maintain the original morphology, mechanical properties, and fatigue resistancetu (Bracco and Oral 2011) . Furthermore, recent studies developed in the orthopaedics community show that the optimum wear behaviour of UHMWPE is obtained using a minimum of 50 –150 kGy of gamma or electron beam radiation.

2.5 Commercially available tibial insert of TKA implant

Most TKA tibial and patellar polyethylene prostheses are cross-linked because all manufacturers use gamma (less than 50 kGy) irradiation. These products differ in the type of polyethylene resin used, the method of irradiation, and the amount of radiation. There are also significant differences in the thermal treatments after irradiation given in Table 2.4. In addition, each manufacturer has a different proprietary method of polyethylene fabrication, sterilization, and packaging. Thus, the clinical results of these TKA polyethylene liners cannot be grouped. The results may have significant differences in their in vivo wear, the prevalence of osteolysis, and complications.

One laboratory reported a significant decrease in wear, with 50 (54%), 75 (78%), and 100 kGy (95%), respectively (Akagi et al. 2006; Asano et al. 2007). There was no improvement in wear with higher doses of irradiation. However, the mechanical properties (toughness, as measured by small punch tests) were improved from 50 to 75 kGy only, then decreased with increasing irradiation doses. Some polyethylene is remelted (heated above the melting temperature), and some are annealed (heated to just below the melting temperature). With radiation doses at or near 100 kGy, remelted highly cross-linked polyethylene exhibits reduced mechanical and fatigue properties compared to conventional and annealed polyethylene. However, annealed highly cross-linked polyethylene has a higher level of free radicals. With increased oxidation

in vivo after implantation, long-term follow-up may reduce mechanical strength and increase wear.

Table 2.4 Comparison of manufacturing techniques of different commercially available cross-linked polyethylene tibial inserts (Brown et al. 2017; Lachiewicz and Geyer 2011)

Manufacturer	Product Name	Radiation Dose (kGy)	Fabrication	Resin
Biomet	E1 - Vanguard	100	Gamma, vitamin E doping/diffusion	GUR 1020
DePuy	XLK-Sigma	50	Gamma, remelted 155^{o} C	GUR 1020
DePuy	AOX	75 – 80	Gamma, PBHP blend	GUR 1020
Smith & Nephew	XLPE-Legion	75	Gamma, full remelt	GUR 1020
Stryker	X3-Triathlon	90 (30 x 3)	Sequential radiation, annealing below melt temperature x 3	GUR 1020
Zimmer	Prolong-NexGen	65	Electron-beam, remelted 150^{o} C	GUR 1050
Zimmer	Durasul-Natural Knee II	95	Electron-beam, remelted 150^{o} C	GUR 1050
Zimmer	Vivacit-E	100	Electron-beam, Vitamin E blend	GUR 1020

2.6 Summary and motivation from the literature survey

The above literature survey highlights: (i) the scope of further investigation in the field of cartilage tissue mechanics, (ii) the scope of the investigation extends further to

identify the critical differences among material models in predicting contact pressure and stress distributions, (iii) further development for the design of durable knee implants (iv) the scope of UHMWPE knee implant material requires its wear resistance to be enhanced.

1. Estimating the mechanical reactions of the knee joint during the load transmission mechanism using the finite element approach is essential due to the inaccuracy of in-vivo measurements.
2. Gradient material models are widely utilised in the literature, and it is necessary to acquire tissue responses as graded material instead of conventional homogeneous material models.
3. Although many studies were conducted on the articular cartilage behaviour with multiple constitutive models, the mechanical response of heterogeneous cartilage at maximum loading position in a gait is not adequately compared.
4. Even though literature is available on the tissue responses for arthritic cartilage cases, the relation between collagen fiber orientation/loading direction and tissue response is not adequately studied. And consequently, the findings may help develop a non-invasive diagnostic tool for assessing possible joint issues and surgery planning.
5. The TKR implant research is ongoing, and there is a need to improve the implant's design in terms of its durability.
6. The current knee implant lifespan is predicted to be between 10 and 15 years in-vivo, with the possibility of revision surgery after bearing material degradation. Therefore, a highly durable implant is required in knee orthopaedics.
7. Highly cross-linked UHMWPE material used in knee implants shows a progressive shift in wear resistance and mechanical performance from the earliest phases of virgin UHMWPE in the last decade. There is a need for the development of new techniques to improve the wear resistance of UHMWPE from conventional methods.

The following objectives are formulated based on the previous literature review and the identified research gaps.

2.7 Research objectives

1. A numerical study on contact pressure improvisation using graded implant material in articular cartilages.
2. To simulate the mechanical response of articulated cartilages and their behaviour on different material models.
3. To perform a numerical investigation on the influence of articular cartilage's constituents structure on knee kinetics/kinematics.
4. Modelling of polyethylene bearing for computational analysis against the mechanical responses for the prosthetic knee.
5. Enhance the wear characteristics of UHMWPE tibial insert material using gamma irradiation cross-linking for the prosthetic knee experimentally.

2.8 Closure

This chapter outlined the objectives of the present work, which were formulated based on a research gap identified through a comprehensive literature review of methodologies applied to inverse heat transfer problems. The subsequent chapter describes the approach utilised to solve the current work.

CHAPTER 3

KNEE RESPONSES USING GRADED CARTILAGE MATERIAL

3.1 Introduction

This chapter elaborates on the complete methodology to determine the mechanical response of knee joints using a graded cartilage implant material. The articular cartilage is known as the knee joint's load-bearing component. Due to knee joint pain, while walking, climbing, and kneeling, osteoarthritis (OA) is a significant public health concern. Additionally, the recent increase in knee replacement surgeries among younger patients is alarming (Adouni and Shirazi-Adl 2014). The effect of graded design compared to homogeneous cartilage material is investigated for contact pressure distribution in a human knee joint. Knee implants are assumed to be homogeneous material. In reality, the cartilages are not homogeneous, and to replicate the cartilages' heterogeneity, a graded design is proposed.

3.2 Geometry and finite element model

The geometry of the knee joint is taken from an open source project (open knee) for studying the knee joint and its effect on different loading conditions on underlying tissues. The specimen details along with its co-ordinate system used in this work as gender-female, age-70 years, weight- 77.1 kg, side- right knee, and height-5’6’’and the co-ordinates like the x-axis as anterior-posterior, y-axis as proximal-distal and z-axis as medial-lateral directions.

The graded design for articular cartilage is given in Figure 3.1, and the model is applied to both femur and tibial cartilage. The graded design replicates the realistic cartilage structure, which is the orientation of collagen fibres in cartilage from the articular surface to the bone. A dynamic implicit analysis of the knee joint is performed by simulation software- Abaqus 6.14 (Dassault Systems Simulia Corp., Providence, RI,

USA). The knee joint model contains four ligaments (anterior cruciate ligament, posterior cruciate ligament, medial collateral ligament and lateral collateral ligament), two cartilages (femur cartilage and tibial cartilage), two menisci (lateral and medial) and two bones (femur and tibia). Patella and patellar tendon are neglected to reduce the complexity of the model, as our primary focus is on the tibio-femoral joint.

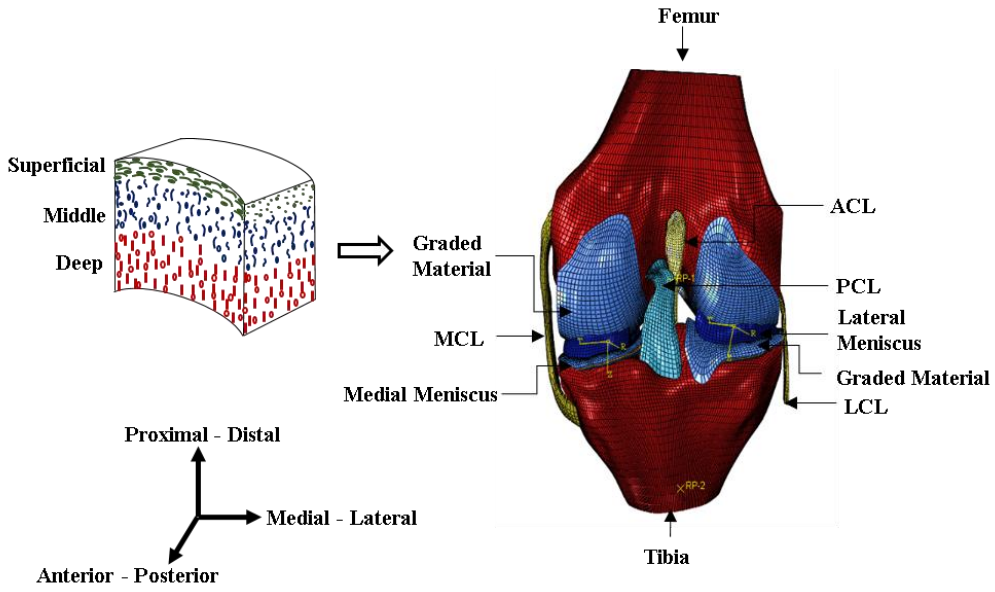

Figure 3.1 Finite element model of tibio-femoral joint showing all components

3.3 Methodology

The proposed graded material model is applied to the femoral and tibial cartilage. The displacement of the meniscus is constrained in such a way that it can mimic the horn arrangement of the meniscus as well as retain its position between cartilages. Nodes on the medial face of the lateral meniscus and the lateral face on the medial meniscus are constrained in the z-direction, along with the nodes on the interior edge of these faces are constrained in the x and z-direction. The cartilage and bones are tied together using rigid body constraints. The tibia is constrained in all rotational and translational DOF where the femur is free to advance in five degrees of freedom and restricted in knee flexion (rotational DOF) to simulate a gait load at full extension. Then, the femur is given by distal (compressive) displacement of 1mm rather than force (to avoid convergence issues) at the reference point (RP-2) from a time period of 0-1 second,

resulting in linear ramping. A dynamic implicit analysis was conducted using Abaqus version 6.14 to determine the micro-scale changes in the tissue.

3.4 Material models

A Nearly incompressible isotropic hyperelastic material model (Neo Hookean) represents the behaviour of all ligaments with strain energy function given by Equation. 3.1. In this work, bone is selected as a rigid body due to its higher stiffness (several orders of magnitude higher than soft tissues), modulus of elasticity and Poisson's ratio and the Neo Hookean material constants of Equation 3.1 are given by Table 3.1.

$$W = C_1(I_1 - 3) + (J - 1)^2/D_1 \tag{3.1}$$

$$C_1 = \frac{G}{2}, D_1 = \frac{2}{K}, G = \frac{E}{2(1+\nu)}, K = \frac{E}{3(1-2\nu)} \tag{3.2}$$

where I_1 corresponds to the first invariants of the left Cauchy-Green deformation tensor B, J is Jacobian = det (F), and F is the deformation gradient. C_1 and D_1 are material constants defined by the shear modulus (G) and bulk modulus (K), which depends on the modulus of elasticity (E) and Poisson's ratio (ν) given in Equation 3.2. C_1 represents the deviatoric part, and D_1 represents the volumetric part of the strain energy per unit volume while deforming.

Table 3.1 Material parameter for different material models of the knee components such as bone, ligaments, meniscus and cartilage

Knee components	Material models	Parameters	Values
Bone	Linear elastic (Donahue et al. 2002)	*E* (MPa) ν (-)	8000 0.3
Ligaments ACL	Isotropic hyperelastic	C_1 (MPa) D_1 $(MPa)^{-1}$	1.95 0.00683

	PCL	(Neo Hookean) (Peña et al. 2006)	C_1 (MPa)	3.25
			D_1 $(MPa)^{-1}$	0.0041
	MCL		C_1 (MPa)	1.44
			D_1 $(MPa)^{-1}$	0.00126
	LCL		C_1 (MPa)	1.44
			D_1 $(MPa)^{-1}$	0.00126
Meniscus		Transversely isotropic linear elastic (Łuczkiewicz et al. 2015)	E_θ (MPa)	120
			$Ez = Er$ (MPa)	20
			v_{rz} (MPa)	0.2
			$v_{r\theta} = v_{z\theta}$ (MPa)	0.3
			G_{rz} (MPa)	8.33
			$G_{r\theta} = G_{z\theta}$ (MPa)	57.7
Cartilage		Homogeneous material (Peña et al. 2006)	E (MPa)	15
			v (-)	0.46
		Graded material	E_s (MPa)	5
			E_t (MPa)	10
			E_d (MPa)	15
			v (-)	0.46

The meniscus is modelled as transversely isotropic linear elastic material with material constants circumferential, axial and radial elastic modulus, similarly Poisson's ratio and shear modulus in circumferential, axial and radial directions. For the case of the gradient material model, the elastic constants are chosen to increase Young's modulus from the superficial zone to the deep zone, and the values are given in Table 3.1.

3.5 Results and discussions

3.5.1 Comparison of contact pressure and stress on cartilage

Using the values of the material parameters from the literature (Table 3.1), contact pressure in the knee joint with graded and homogeneous cartilage was analysed.

Contact pressure on the tibial and femoral cartilage at the full extension position of a stance phase (standing/equilibrium position) is given in Figure 3.2 (a). The maximum contact pressure generated on gradient linear elastic tibial cartilage is 4.232 MPa which is less than homogeneous linear elastic tibial cartilage at 6.45 MPa

Similarly, for femur cartilage, the contact pressure generated is 4.483 MPa on homogeneous material and 3.00 MPa on graded material. Also, by comparing the femur and tibial cartilage, a significant contact pressure appeared in the medial part of the tibia cartilage and moderate contact pressure was observed on the lateral aspect of femur cartilage. The obtained results also show that both material contact pressure is more evenly distributed on the lateral and medial compartment of femur cartilage. In contrast, for tibial cartilage, pressure is more concentrated on the lateral compartment. Similar to contact pressure, Von-Mises stress also has a vital role in predicting knee pathologies accurately. The maximum Von Mises stress generated on tibial cartilage for graded material is 1.671 MPa, less than homogeneous material 2.274 MPa, as shown in Figure 3.2 (b).

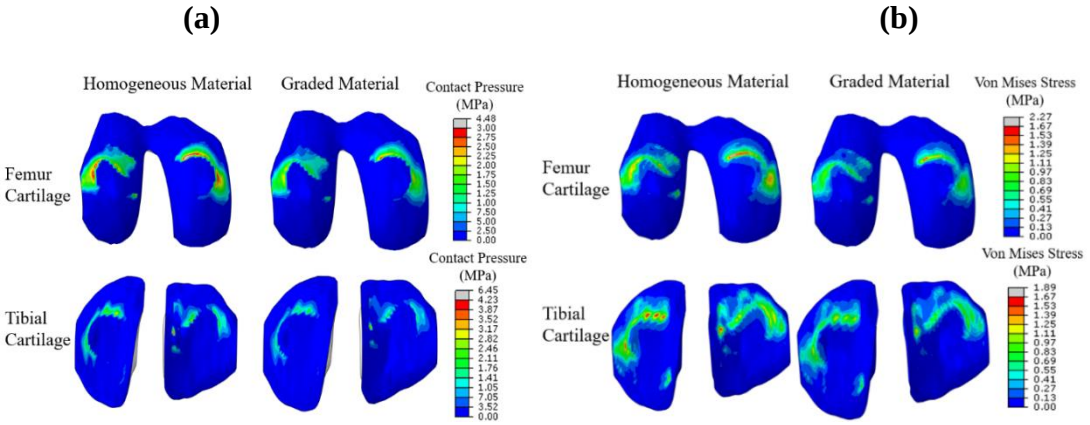

Figure 3.2 Comparison of contact pressure and Mises stress generated on the surface of gradient material

Also, for femur cartilage, the maximum Von-Mises stress generated for graded material is 1.671 MPa which is less than homogeneous material 1.897 MPa. The mises stress induced on the articulating surface of the cartilage is higher for the homogeneous elastic material model than the gradient material. Also, the maximum Von Mises stress for femur cartilage (2.274 MPa) generated is more elevated than tibial cartilage (1.897

MPa). The maximum contact pressure generated on the knee joint, in the range of 2.3 - 5.08 MPa during standing position (full extension) given by Table 3.2.

3.5.2 Significance of mechanical responses in knee mechanism

The intact knee joint supports the contact pressures, compression stresses and shear stresses over a large femoral and tibial cartilage area. The present study shows the effects of graded design articular cartilage over homogeneous cartilage in human knee joints, particularly in contact pressure distribution and compression stresses. By comparing femur and tibial cartilage, the contact pressure in tibia cartilage is higher than in femur cartilage. The main reason behind this is that the reaction force on tibia cartilage is higher than that of the femur as body force is acting in a downward direction. Hence there is a higher chance of degradation for tibial cartilage than for femur cartilage.

Table 3.2 Comparison of contact pressure on the cartilage of the current study with results from the literature

	Compression load (N)	Peak cartilage contact pressure (MPa)	Source
Experimental study	1000 N	3.6 MPa	(Morimoto et al. 2009)
	1800 N	5.08 MPa	(Marzo and Gurske-DePerio 2009)
	1000 N	5.0 MPa	(Allaire et al. 2008)
	1800 N	4.5 MPa	(Lee et al. 2006)
Computational study	1800 N	2.3 MPa	(Paletta et al. 1997)
	1800 N	3.0 MPa	(Halonen et al. 2016b)
	800 N	6.45 MPa	Current study

Also, this study investigated how cartilage material properties affect the contact pressure and stress generated on the articulating surface during loading (simulating

standing). However, the results imply that gradient material helps reduce the contact pressure and stress generation on the articular surface and helps predict outcomes more accurately. Therefore graded material design can be used as an alternative material for homogeneous cartilage components in artificial knee implants.

The maximum contact pressure generated on cartilage during loading from literature is given in Table 3.2. From the current study (graded material), the maximum contact pressure generated is 6.45 MPa for a 1000 N load, while other results show a lesser contact pressure corresponds to a higher load. There is no significant cause for the phenomenon, and this may be due to the limitations of the model, such as no standard constraints, different geometry (variation in the contact area), different analysis software packages etc.; however, the maximum contact pressure generated on the cartilage is in the range of 2 to 8 MPa for a knee at full extension position is confirmed.

Other limitations to the situation in Vitro is the nutrition of cartilage as per its deformation and 'weeping lubrication' which is a severe limitation of an artificial design and a challenge for future development. The weeping lubrication in the knee joint is not considered in the simulation. Hence the predicted values obtained through simulation are not accurate when compared with actual values. If such properties are included (weeping lubrication around joint), the results would marginally change; however, they should not change any conclusions concerning the gradient material model. These critical findings will be utilised to optimise the required mechanical characteristics of the articular cartilage and eventually accomplish successful cartilage transplantation in a clinical scenario.

3.6 Conclusions

The proposed gradient material can be used as an implant material for osteoarthritis patients. Also, these discoveries and proposals are applicable in biomechanical models to investigate treatments (surgical or traditionalist) related to knee osteoarthritis. Hence, the outcome of our finite element simulation can be extrapolated into the in-vivo scenarios.

3.7 Closure

Using finite element analysis, this chapter describes the contact pressure and Mises stress created during the maximal loading position of the knee joint during a gait cycle. The obtained values are compared to those of conventionally homogenous materials. The results are validated by comparing the result of experimental and computational investigations published in other scholarly works.

CHAPTER 4

RESPONSE OF SOFT TISSUES DURING GAIT CYCLE

4.1 Introduction

This chapter discusses the extension of work from the previous chapter. The influence of soft tissues in the knee joint on the load transfer mechanism during the gait cycle is analysed. The knee kinetics (forces and rotation) during the stance phase of a gait in all degrees of freedom are incorporated into the model. The contact pressure, effective Lagrange strain, maximum shear stress, effective stress and total displacement generated on all the soft tissues are compared. The results might help develop comprehensive computational tools to help us better understand knee injury and disease causes.

4.2 Methodology

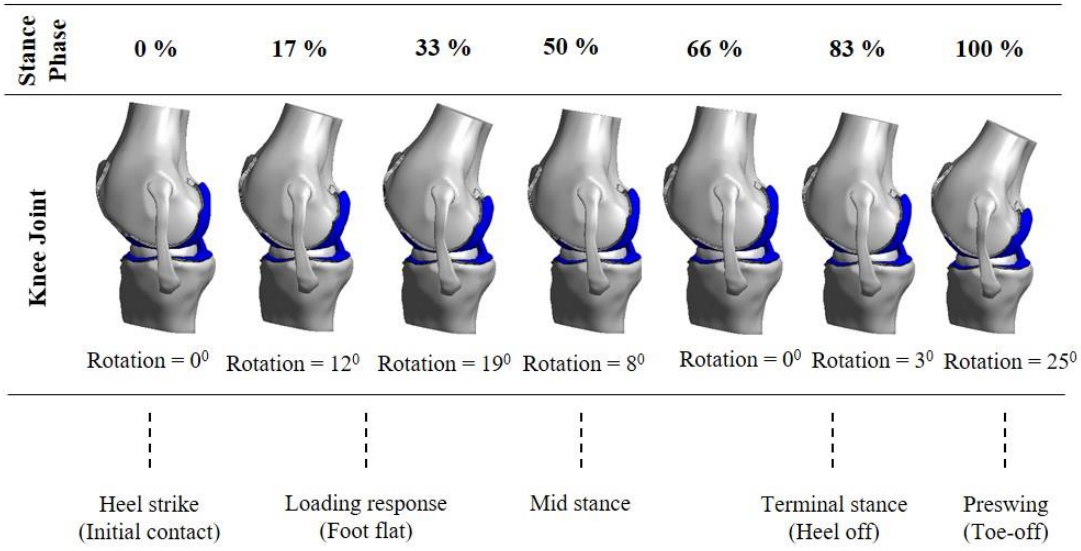

Figure 4.1 The rotation of the femur over the tibia from heel strike to toe-off of a knee during gait.

The influence of complex constitutive soft tissue knee joint kinetics is investigated with a three-dimensional, subject-specific FE model. The stresses and deformations of tissues are investigated by inputting the normal knee kinetics, that is, the rotation and loading cycle during the gait cycle (walking). Figure 4.1 shows the rotation of the femur over the tibia from heel strike to toe-off during a gait. The stance phase of gait was represented in an implicit FE framework to accurately capture all time-dependent and inertial factors. The model incorporated primary tissues and bone components seen in healthy knee joints and soft tissues such as ligaments, meniscus, and articular cartilage. The soft tissues were compared at various stance positions in order to identify their influence on knee kinetics.

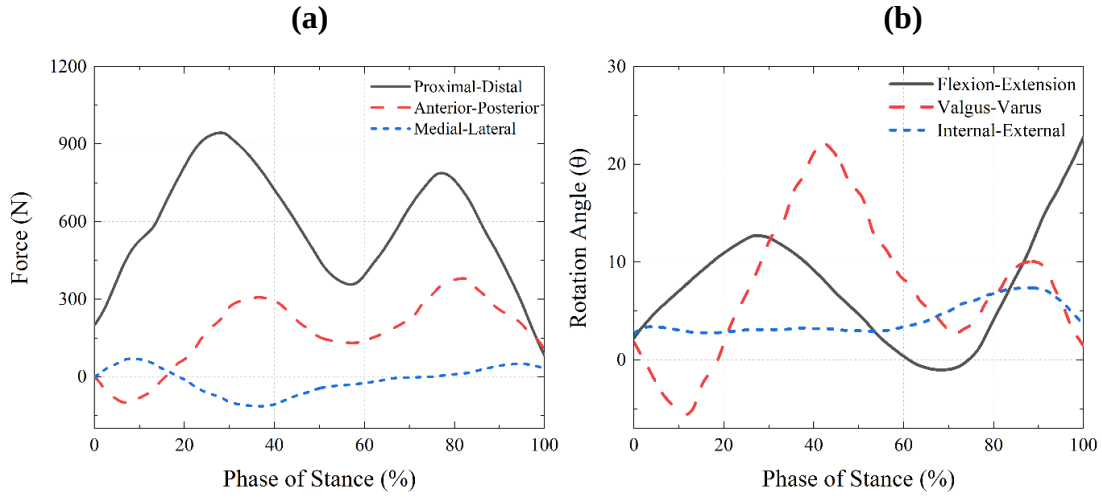

Figure 4.2 (a) Gait input force date for during the stance phase (b) Knee joint rotation data during the stance phase (Orozco et al. 2018).

The interaction between the soft tissues at the articulating surface is assigned as frictionless contacts, such as the interactions between cartilages and menisci, the outer surfaces of ligaments and cartilages, and the ACL and PCL. A rigid cylindrical joint is used to input forces and rotation in all degrees of freedom into the mechanism. The forces and rotation generated on the knee during the stance phase of a gait cycle when a person is subject to walking are given in Figure 4.2. Femur-ImgLnk1 joint for Flexion-Extension rotation and Medial-Lateral force, similarly ImgLnk1-ImgLnk2 joint for Valgus-Varus rotation and Anterior-Posterior force and ImgLnk2-Tibia joint

for Internal-External rotation and Distal-Proximal force selected for the model. The gait input, patellofemoral soft tissues characteristics, and boundary conditions for the knee model were identical to previous research (Orozco et al. 2018).

4.3 Material models

The femur and tibial cartilage are modelled as a Hyperelastic material model with Mooney-Rivlin constants given by Equation 4.1. The Mooney-Rivlin material constants C1= 0.856 MPa, C2=0 and Bulk modulus, K= 8 MPa.

$$W = C_1(\bar{I}_1 - 3) + C_2(\bar{I}_2 - 3) + \frac{K}{2}(J-1)^2 \quad (4.1)$$

The ligaments are modelled as a Hyperelastic transversely isotropic Mooney-Rivlin material model given by Equation 4.2. The material constants for the constitutive model for ligaments are shown in Table 3.3.

$$W = C_1(\bar{I}_1 - 3) + C_2(\bar{I}_2 - 3) + \frac{K}{2}ln(J)^2 + F(\lambda) \quad (4.2)$$

The menisci modelled as Fung orthotropic Hyperelastic material. The material constants defined by the model, such as in-plane direction elastic modulus $E_p = 125\,MPa$, transverse directions elastic modulus, $E_t = 27.5\,MPa$, in-plane direction Poisson's ratio, $\nu_p = 0.1\,(-)$, transverse direction Poisson's ratio, $\nu_t = 0.33(-)$, in-plane direction shear modulus, $G_p = 2\,MPa$, transverse direction shear modulus, $G_t = 12.2\,MPa$, bulk modulus $K = 10MPa$.

Table 3. 3 The material constants for the constitutive material model for ligament

Ligaments	C1 (MPa)	C2 (MPa)	C3 (MPa)	C4 (MPa)	C5 (MPa)	K (MPa)	λ_m (-)
ACL	1.95	0	0.0139	116.22	535.039	73.2	1.046
PCL	3.25	0	0.119	87.178	431.063	122	1.035
MCL	1.44	0	0.57	48	467.1	397	1.063
LCL	1.44	0	0.57	48	467.1	397	1.063

C1 and C2 = Mooney-Rivlin material constants, C3, C4, and C5 = fiber material constants, K = Bulk modulus, λ_m= stretch factor

Linear springs used to model horn arrangement connect each node on the meniscal horn faces to a node on the tibia that nearly intersects the normal of the horn face stretched from the estimated face centroid. The spring constants for the horn attachments were determined using the stated Young's modulus.

4.4 Results and Discussions

4.4.1 Soft tissue responses during the gait cycle

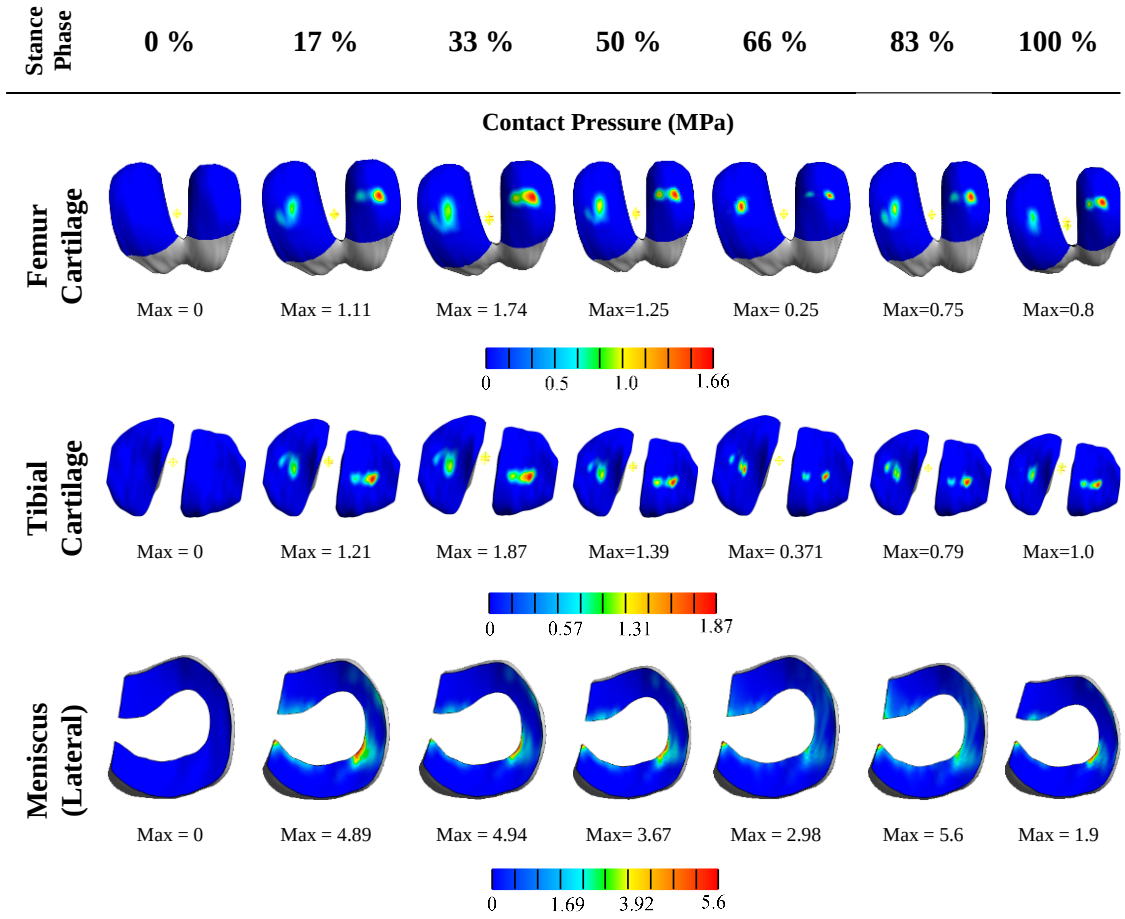

Figure 4.3 Maximum contact pressure distribution soft tissues during the stance phase of a gait cycle.

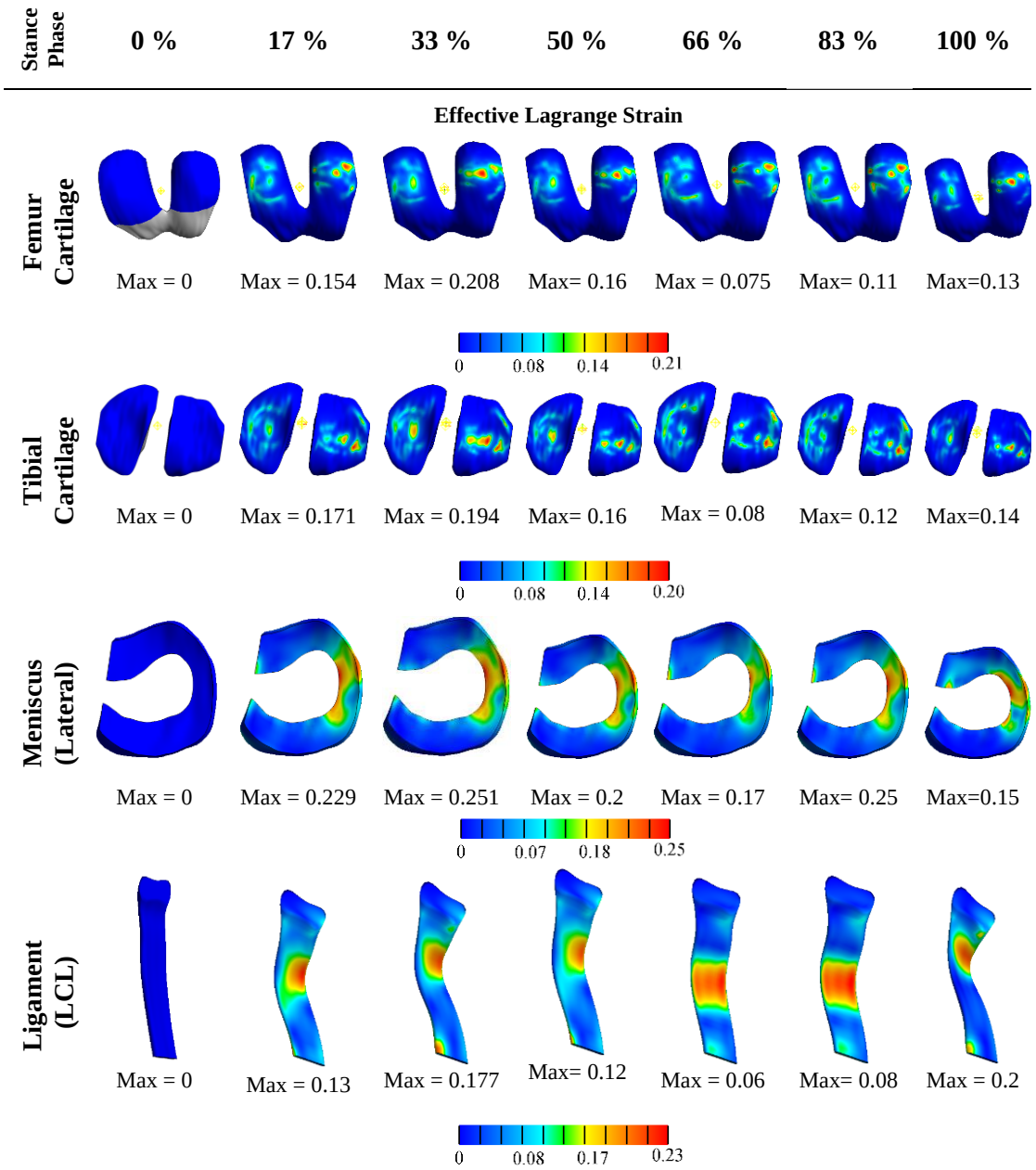

Figure 4.4 Effective Lagrange strain on soft tissues during the stance phase of a gait cycle

Contact pressure distribution and effective Lagrange strain on femur cartilage, tibial cartilage and lateral meniscus during different phases of a stance are given in Figures 4.3 and 4.4. Upon closer observation, the meniscus shows a higher contact pressure value of 5.6 MPa than the femur and tibial cartilage. The articular cartilage on the medial side showed more significant contact pressure than the lateral side and a

maximum of 1.87 MPa, marked at one-third of the stance phase. The equivalent Lagrange strain has an essential role in predicting knee pathologies. Figure 4.5 shows that the meniscus experienced significantly higher Lagrange stain than other tissues.

The contact pressure, effective Lagrange strain, maximum shear stress, effective stress and total displacement generated on different soft tissues are plotted and compared in Figure 4.5 (a-e). The ligament shows an overall lower Lagrange stain, and the meniscus shows a higher stain, as observed in Figure 4.5 (b). Also, the peak contact pressure was observed in all tissues between 20% - 40% of the stance phase.

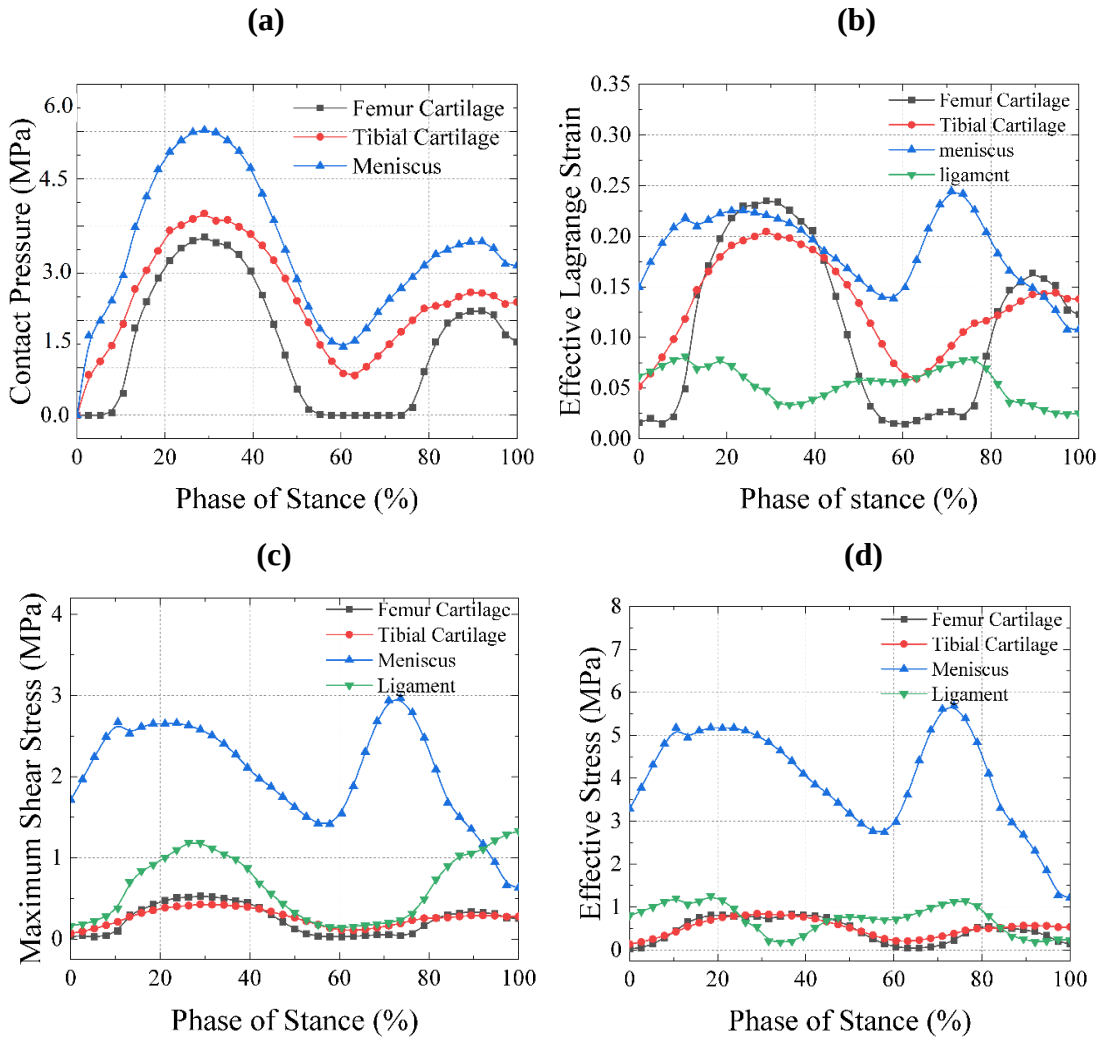

(e)

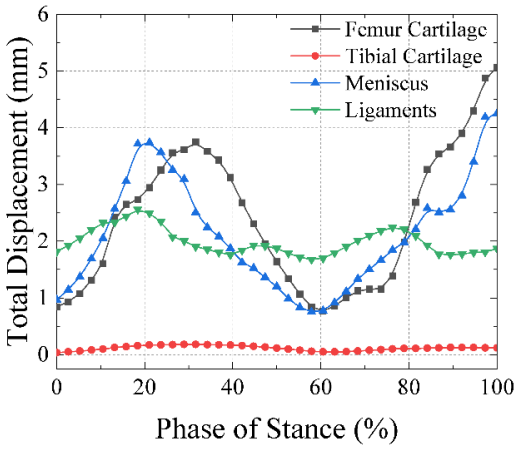

Figure 4.5 (a) Contact pressure distribution in soft tissues (b) Effective Lagrange strain (c) Maximum shear stress (d) Effective stress (e) Total displacement

Table 3. 4 Literature based comparison of the values of the total contact pressure for the basic knee model with intact geometry on the soft tissues.

	Femoral cartilage [MPa]	**Tibial cartilage [MPa]**	**Meniscus [MPa]**
Present study	3.50	3.20	5.60
(Shirazi et al. 2008)	1.29	-	-
(Bao et al. 2013)	-	3.09	-
(Walker and Erkman 1975)	-	-	3.20
(Allaire et al. 2008)	-	-	5.20
(Bolcos et al. 2018)	-	4.1	-

Also, our FE simulation's peak contact pressure at maximum axial compressive load (distal force curve) 5.6 MPa agrees well with previous findings in the literature (Morimoto et al. 2009; Wang et al. 2014). Femur cartilage shows a lower shear and effective stress among all tissues. It is also noted that the meniscus has a 4 to 5 times more effective shear stress than other tissues given by Figure 4.5 (c) and 4.5 (d). Hence the present study shows that the meniscus significantly influences knee kinetics rather than other soft tissues. Also, our FE simulation's peak contact pressure at maximum

axial compressive load (distal force curve) 5.6 MPa agrees well with previous findings in the literature (Morimoto et al. 2009; Wang et al. 2014).

4.5 Conclusion

In summary, we have demonstrated that the soft tissues' contact pressures, stresses, strains and displacement are sensitive to knee kinetics. The meniscus has a more significant influence on knee kinetics than other tissues. At peak compressive force, the maximum stress on the meniscus tissue is 4 to 5 times higher than cartilage and ligament. Also, tibial cartilage has a higher impact on the knee mechanism than femur cartilage; hence it supports more load than femur cartilage. However, during the early stages of the cycle, the effective Lagrange strain of femur cartilage is greater than that of tibial cartilage and then declines. These values could aid in developing comprehensive computational tools to assist us in better understanding the causes of knee injury and diseases.

4.6 Closure

This chapter examines the application of the finite element approach in determining the tissue responses in the knee joint during a gait cycle. The methodology helped to converge the results, showing an accurate method to predict the tissue responses computationally. In the next chapter, an attempt is made to numerically analyse cartilage heterogeneous properties' influence on the mechanical response for different constitutive models.

CHAPTER 5

COMPUTATIONAL STUDY ON CARTILAGE MATERIAL HETEROGENEITY

5.1 Introduction

This chapter discusses the influence of cartilage material and geometrical heterogeneity on the mechanical response under different constitutive models. Different material models are created with conventional homogeneous cases and heterogeneous cases. The variation of mechanical responses of articular cartilages is compared with different models.

5.2 Geometry and finite element model

An existing knee joint geometry (open knee) developed at Computational Bio modelling Core and Department of Biomedical Engineering, Cleveland Clinic from a female corpse (70 years & 77 kg) is used for the current study (Erdemir 2014; Erdemir and Sibole 2010). An expanded view of knee geometry is shown in Figure 5.1, and the 3D knee substructure is imported into Abaqus CAE for analysis. The model contains four ligaments anterior and posterior cruciate ligaments (ACL and PCL) and medial and lateral collateral ligaments (MCL and LCL), two cartilages (femur and tibia cartilage), two menisci (lateral and medial meniscus) and two bones (femur and tibia).

The geometry coordinate system is synchronized with the Abaqus, such that the x-axis is anterior-posterior, where the anterior or posterior force component can apply. Similarly, the y-axis is the proximal-distal where the vertical ground reaction force can use, and the z-axis is the medial-lateral direction where medial or lateral joint force components can apply. The ground reaction force becomes the body weight (BW) when the body is in a full extension position during the stance phase of a gait cycle. The valgus or varus rotation is about the x-axis, internal or external rotation is about the y-axis, and the flexion or extension rotation is about the z-axis.

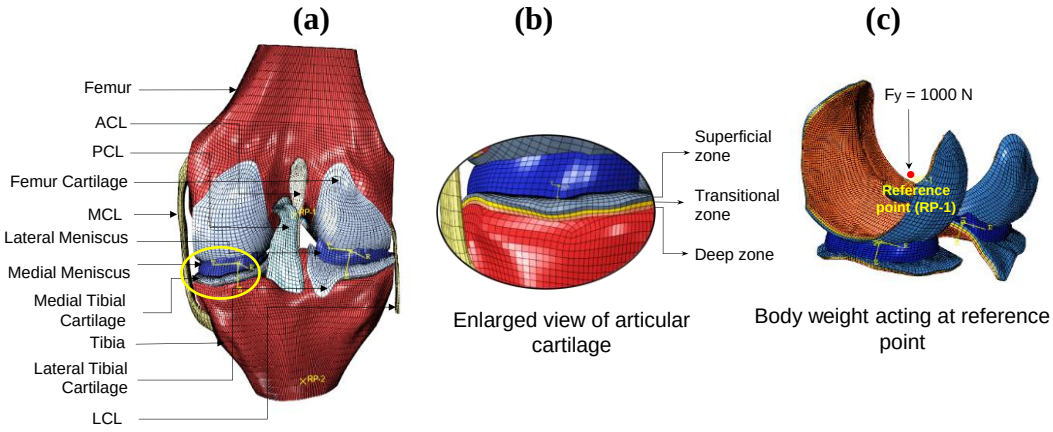

Figure 5.1 (a) The posterior view of 3D finite element knee joint model (b) enlarged view of tibial cartilage (c) bodyweight of 1000N acting.

In this study, the heterogeneity of the cartilage is defined in terms of material and geometrical heterogeneities. Material heterogeneity is the inhomogeneous distribution of material constituents (such as fiber density and orientation), and it is modelled using the corresponding constitutive models. The geometrical heterogeneity is the inhomogeneity in cartilage structure (such as superficial, transverse/middle, and deep zones), as shown in Figure 5.1 (b). It may be noted here that the native architecture of cartilage may have these individual layers with different thicknesses depending on the collagen fibre structural inhomogeneity. The current study, however, assumes each zone's mesh size is the same for numerical convergence purposes. These soft tissues are discretized into 56433 hexahedral elements with an element size of 0.5 mm each. The cartilage, meniscus, and ligaments have meshed with hexahedral brick elements (element type: C3D8), and the femur and tibia have meshed with shell elements (element type: S4) as per Abaqus/Standard user's manual (Smith 2009). Using an 8-node element in contact modelling can potentially improve contact response and numerical convergence than higher node elements.

5.3 Interface, constraints, loading and boundary conditions

The interaction between the cartilages at the articulating surface is assigned as frictionless contact. A rigid body tie constraint ties the ligaments and cartilage with bone nodes at the bone insertion points to retain their position. Another rigid body

constraint connects the tibia and femur to corresponding reference points (RP-1 and RP-2), such that the tibia and femur act as a rigid body. The RP-1 is at the centre position of lateral and medial femoral epicondyles for the femur. The femur can rotate about RP-1, and the meniscus is constrained to maintain its position between two cartilages.

All rotational and linear motions (6DOF) of the tibia are constrained, and the femur is set free to move in all five degrees of freedom but restricted in knee flexion. Since this study focuses on the maximum extension position of the gait cycle when the flexion angle is zero. Thus RP-1 is subjected to a load of 1000N (compressive), as shown in Figure 5.1 (c)

5.4 Material models

Using well-known material models, the influence of homogeneous and heterogeneous (both material and geometrical case) cartilage surface texture is compared for a mechanical response. These are IE, IPE, and TIE models. Note that the basic models, such as IE and IPE, assume collagen fibers are homogenized with the rest of the cartilage constituents. The TIE model is an extended version of these basic models where collagen contribution is considered reinforcement. The material constants of these models (the constitutive relation of all these models are given supplementary information S1) are provided in Table 5.1.

Table 5.1 The material parameters for modelling homogeneous and heterogeneous articular cartilage.

Material models	Homogeneous (non-gradient)	Heterogeneous (gradient)	Source
IE	$E = 15$ MPa $\nu = 0.475$	$E_s = 15$ MPa $E_t = 10$ MPa $E_d = 5$ MPa $\nu = 0.475$	(Li et al. 2019)*

IPE	$E = 15$ MPa $\nu = 0.475$ $S_l = 1$ $e = 4$ $k = 0.001\, mm^4/Ns$	$E_s = 15$ MPa $E_t = 10$ MPa $E_d = 5$ MPa $\nu = 0.475$ $S_l = 1, e = 4$ $k = 0.001\, mm^4/Ns$	(Li et al. 2019; Wilson et al. 2004)*
TIE	$E_p = 5.8\, MPa$ $E_t = 0.46\, MPa$ $\nu_p = 0.87\ (-)$** $\nu_t = 0.03(-)$ $G_t = 2.5\, MPa$	$E_{ps} = 5.8\, MPa$ $E_{ts} = 0.46\, MPa$ $\nu_{ps} = 0.87\ (-)$ $\nu_{ts} = 0.03(-)$ $G_{ts} = 2.5\, MPa$	(Klets et al. 2016; Vaziri et al. 2008; Wilson et al. 2003)*
		$E_{pt} = 4\, MPa$ $E_{tt} = 0.46\, MPa$ $\nu_{pt} = 0.87\ (-)$ $\nu_{tt} = 0.05(-)$ $G_{tt} = 2\, MPa$	
		$E_{pd} = 2\, MPa$ $E_{td} = 0.46\, MPa$ $\nu_{pd} = 0.87\ (-)$ $\nu_{td} = 0.2\ (-)$ $G_{td} = 1\, MPa$	

Notes: E = Elastic modulus, ν = Poisson's ratio, E_s, E_t, E_d = Elastic moduli of the superficial, transitional and deep layer, E_{ps}, E_{pt}, E_{pd} and E_{ts}, E_{tt}, E_{td} are in-plane and out of plane Young's moduli for the three layers, similarly $\nu_{ps}, \nu_{pt}, \nu_{pd}$ and $\nu_{ts}, \nu_{tt}, \nu_{td}$ are in-plane and out of plane Poisson's ratio for the three layers. G_{ts}, G_{tt}, G_{td} are out of plane shear modulus for all layers, respectively, S_l = specific weight of wetting liquid, k = permeability and e = void ratio. *Source for the homogeneous (non-gradient) model. **Poisson's ratio in the in-plane direction has been chosen from the article (Klets et al. 2016), but the value is altered to match the material's consistency in Abaqus.

The rest of the joint parts are modelled as per Table 5.2. Even though the bone (femur and tibia) consists of the cortical and cancellous parts, we approximated it as a uniform rigid body. Like articular cartilage, the meniscus also has complicated architecture, including a network of collagen fibers. To reduce the complexity of modelling, we modelled the meniscus (lateral and medial) with TIE material (Imeni et al. 2020). The ligaments are modelled with the Neo-Hookean isotropic hyperelastic material (nearly incompressible) model.

Mathematically for the isotropic poroelastic (IPE) cartilage model, the total stress generated is given by Equation 5.1.

$$\sigma_{tot} = \sigma_s + \sigma_{fl} \tag{5.1}$$

where σ_{tot} is the total stress tensor, σ_s is the stress component in solid matrix and σ_{fl} is the stress component in the fluid matrix of the cartilage. The total stress generated in the transversely isotropic elastic (TIE) cartilage model is given by,

$$\sigma = C\,\epsilon \tag{5.2}$$

where σ is the Cauchy stress tensor, C is the stiffness matrix, and ϵ is the strain. The stiffness matrix C can be expressed as,

$$C = \begin{pmatrix} \frac{1}{E_\mathrm{p}} & -\frac{\nu_\mathrm{p}}{E_\mathrm{p}} & -\frac{\nu_\mathrm{t}}{E_\mathrm{t}} & 0 & 0 & 0 \\ -\frac{\nu_\mathrm{p}}{E_\mathrm{p}} & \frac{1}{E_\mathrm{p}} & -\frac{\nu_\mathrm{t}}{E_\mathrm{t}} & 0 & 0 & 0 \\ -\frac{\nu_\mathrm{p}}{E_\mathrm{p}} & -\frac{\nu_\mathrm{t}}{E_\mathrm{p}} & \frac{1}{E_\mathrm{t}} & 0 & 0 & 0 \\ 0 & 0 & 0 & \frac{1}{G_\mathrm{t}} & 0 & 0 \\ 0 & 0 & 0 & 0 & \frac{1}{G_\mathrm{t}} & 0 \\ 0 & 0 & 0 & 0 & 0 & \frac{2(1+\nu_\mathrm{p})}{E_\mathrm{p}} \end{pmatrix} \tag{5.3}$$

Where $E_\mathrm{p}$and E_t are Young's moduli for in-plane and out of the plane, ν_p and ν_t are Poisson's ratio for in-plane and out of the plane, and G_t is the shear modulus for out of the plane, respectively. A nearly incompressible isotropic hyperelastic material model

(Neo-Hookean) is used to model all ligaments behaviour with strain energy density function given in chapter 3.

Table 5.2 The material parameters for the components of the knee joint other than cartilage

Parts	Components	C_1 (MPa)	D_1 $(MPa)^{-1}$	Source
Ligaments isotropic hyperelastic (Neo-Hookean)	ACL	1.95	0.00683	(Łuczkiewicz et al. 2015; Peña et al. 2006)
	PCL	3.25	0.0041	
	MCL	1.44	0.00126	
	LCL	1.44	0.00126	
Meniscus (TIE)	$E_p = 120\ MPa, E_t = 20\ MPa$ $\nu_p = 0.2\ (-), \nu_t = 0.3(-)$ $G_p = 8.33\ MPa, G_t = 57.7\ MPa$			(Łuczkiewicz et al. 2015)

Notes: C_1 and D_1 are Neo-Hookean material constants, E_p and E_t are in-plane and transverse-plane elastic modulus, ν_p and ν_t are in-plane and transverse plane Poisson's ratio, G_p and G_t are in-pane and transverse plane shear modulus.

5.5 Results and discussions

5.5.1 Comparison of different material models for homogeneous and heterogeneous cases

The contact pressure distribution in the tibial cartilage surface from the meniscus impact is compared for homogeneous and heterogeneous cartilage cases given in Figure 5.2. Though no significant difference is observable in Figure 5.2 (a), the homogeneous model provides higher contact pressure distribution compared to the heterogeneous case. TIE and IPE models show a clear impression of contact pressure on the cartilage surface among all the constitutive models compared. Also, the equivalent stress has an essential role in predicting knee pathologies. Figure 5.3 (a)

depicts the stress distribution on the tibial surface. Compared with the IE and TIE model, the IPE model showed maximum equivalent stress generated in the femur cartilage. This indicates the biphasic tissue model supports more load than the simple model during the load transfer mechanism.

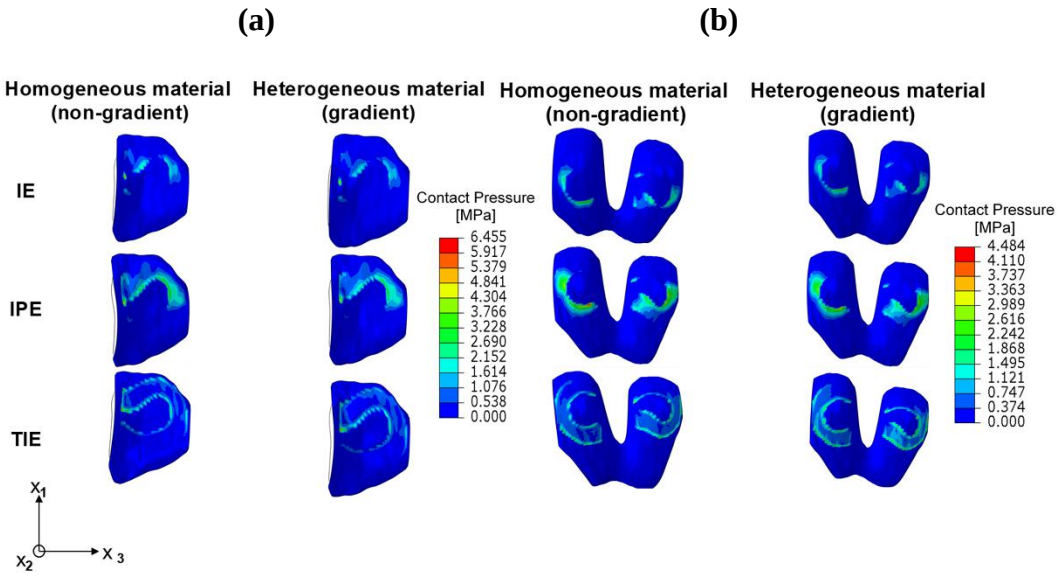

Figure 5.2 Distribution of contact pressure on (a) the tibial lateral surface; (b) the femoral surface

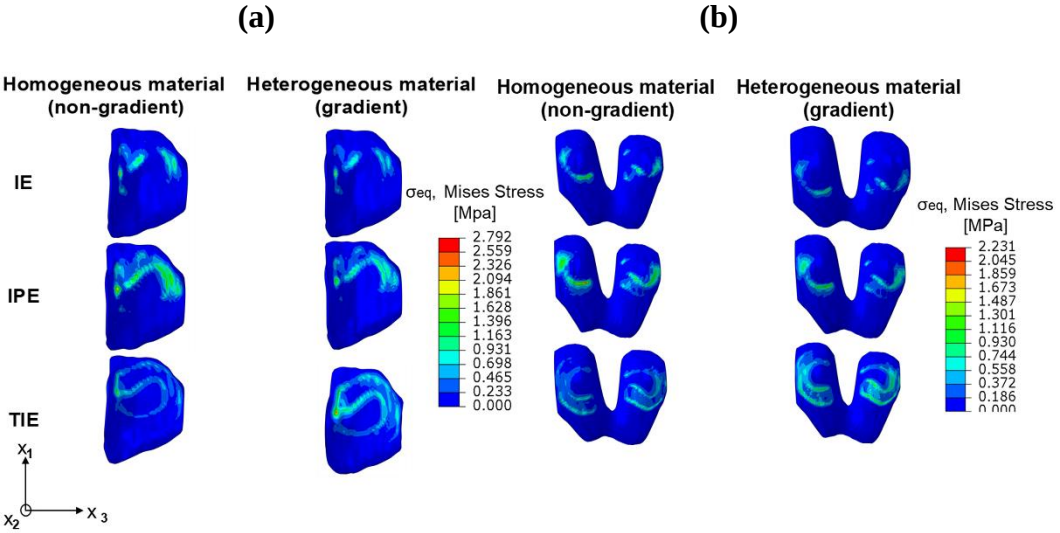

Figure 5.3 The contours for equivalent stress generation on (a) the tibial lateral surface (b) the femoral surface

Also, it is observed here that the IE and IPE geometrical heterogeneous models provide less uniformity in stress distribution with respect to the TIE model. Figure 5.3 (b)

shows the femoral stress distribution, which follows a similar pattern for all models, where the TIE model clearly understands the stress impression with no stress concentration. The maximum stress generated on the TIE model is 2.559 MPa and 2.792 MPa for the tibial cartilage, 2.045 MPa and 2.231 MPa for the femoral cartilage for the heterogeneous material homogeneous cases, respectively.

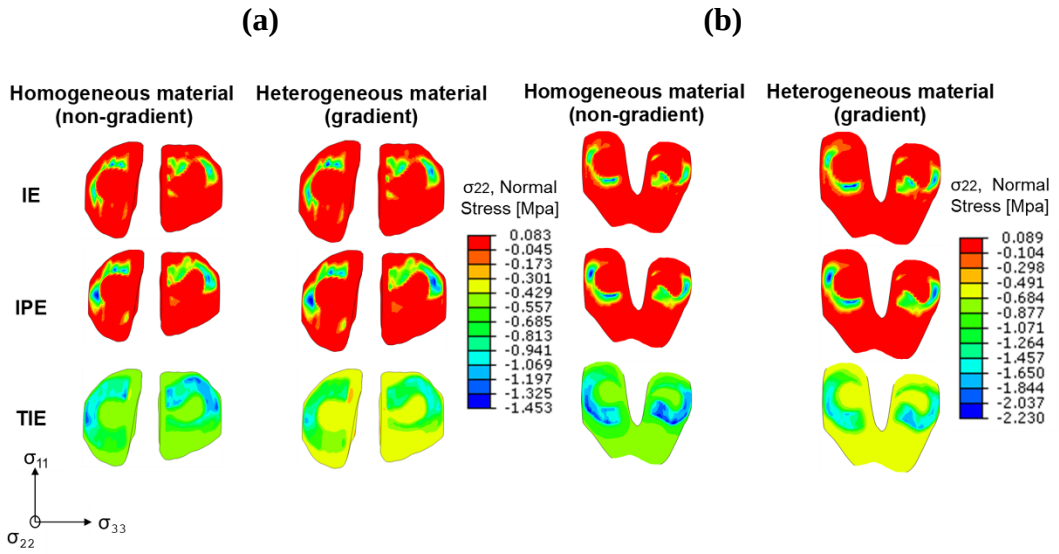

Figure 5.4 The normal stress distribution on (a) the tibial surface; (b) the femoral surface

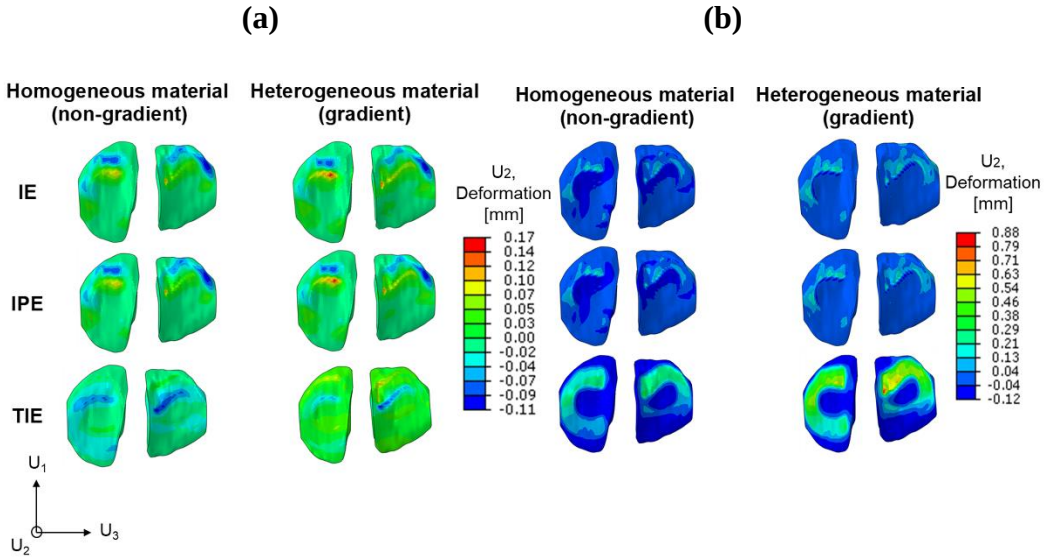

Figure 5.5 The cartilage deformation (a) U1 (anterior-posterior) (b) U2 (proximal-distal) at full extension position.

Directional stress may give better insights into knee mechanics. Figure 5.4 (a) and 5.4 (b) clearly distinguish the directional stress impression in the tibial and femoral surface. Figure 5.4 (a) shows a uniform stress distribution in heterogeneous (both material and geometrical) cases for all models compared to the homogeneous model. In the TIE model, the tibial cartilage has lower stress than the femur cartilage at -2.2 MPa and -1.4 MPa, respectively. Also, the TIE model's compression stress in the homogeneous situation is relatively high. This could be owing to the high rigidity provided by the cartilage's surface.

Table 5.3 The estimated over-prediction of mechanical measures in percentage for a homogeneous model relative to its heterogeneous alternative

Comparison of models	Zones	Mises stress (%)	Max. prin. Stress (%)	Max. prin. log. strain (%)	Min. prin. log. strain (%)	Max. def. (%)	Max. pres. generated (%)
Homo. IE	SZ	25	32	9	28	6	0.3
Vs	TZ	12	5	10	13	7	6
Hetro. IE	DZ	4	15	22	28	6	12
Homo. IPE	SZ	25	36	49	42	5	0.7
Vs	TZ	14	6	8	99	4	6
Hetro. IPE	DZ	22	15	23	4	5	12
Homo. TIE	SZ	60	42	4	95	3	47
Vs	TZ	4	88	71	98	3	37
Hetro. TIE	DZ	37	215	42	27	2	47

Note: Homogeneous isotropic elastic (Homo. IE), heterogeneous isotropic elastic (Hetro. IE), homogeneous isotropic poroelastic (Homo. IPE), heterogeneous isotropic poroelastic (Hetro. IPE), homogeneous transversely isotropic elastic (Homo. TIE),

heterogeneous transversely isotropic elastic (Hetro. IE), maximum principal (Max. prin.), maximum principal logarithmic strain (Max. prin. log. strain), maximum deformation (Max. def.), the maximum pressure (Max. pres.)

The tibial cartilage deformation U_2 (anterior-posterior) over the medial and lateral compartment of the tibial cartilage surface are shown for different material models and also for the deformation in U_1 (proximal-distal) given by Figure 5.5 (a) and 5.5 (b). The maximum tibial cartilage deformation for the IPE geometrical heterogeneous model is 0.17 mm in the posterior and 0.88 mm in the proximal direction, whereas the solid model has lesser deformation. It indicates that porosity impacts tibial deformation and pressure distribution in a knee joint during the standing position. It can be observed from Figure 5.5 that even with the homogeneous TIE model, the in-plane (anterior-posterior) and through-plane (proximal-distal) cartilage deformation is more pronounced and precise than the material heterogeneous IPE model. Therefore TIE models can safely be assumed to be reliable in predicting the onset and progression of OA.

In addition, Table 5.3 compares the maximum variation in Mises stress, principal stress, strain, deformation, and pressure generated on the cartilage with the homogeneous and heterogeneous entity. The maximum percentage change in stresses and strains is observed higher in the TIE model than in the IE and IPE models. The maximum primary stress varies by about 200 per cent in TIE models between homogeneous and heterogeneous entities.

5.5.2 Significance of cartilage heterogeneity in mechanical response

This study examines the influence of heterogeneous material characteristics on tissue depth from superficial to deep zone with multiple constitutive material models. Also, investigate the impact of stresses and strains during the full extension position (standing position) using the finite element knee model. Verifying simulation findings is a critical step, and we double-checked that our results for the intact knee model match those found in the literature (Allaire et al. 2008; Halonen et al. 2016b; Lee et al. 2006; Marzo and Gurske-DePerio 2009; Morimoto et al. 2009; Paletta et al. 1997). The

IE, IPE, and TIE cartilage material models are compared with homogeneous and heterogeneous entities. The contact pressure distribution is observed not so evident from IE models compared to IPE or TIE models, and the material heterogeneity produces a relatively lower magnitude of pressure distribution.

According to some studies, the material property of articular cartilage varies enormously with distance from the articular surface, especially in the superficial region; hence heterogeneous constitutive models suit well for such studies (Chen et al. 2001). Also, many constitutive models are proposed for implementing intact and OA heterogeneous characteristics. The heterogeneous behaviour of a finite element cartilage model with an incompressible, poroelastic solid matrix reinforced by an inhomogeneous, distributed fiber filled with an incompressible fluid in the collagen–solid proteoglycan matrix is well predicted (Pierce et al. 2013). The split-line patterns are utilized for FRPE inhomogeneous cartilage models to illustrate diverse cartilage influenced by collagen fibers. The average Mises stresses in the homogeneous IE model are 2.7 MPa in the tibial lateral compartment, and 2.2 MPa in the femoral lateral component, similar to the range reported in the previous work(Yang et al. 2010a; b). Also, with a load of 1000 N, the maximum contact pressure generated on the cartilage surface varies between 6 and 16 MPa (Mononen et al. 2012). Particularly in the geometrically heterogeneous model, the maximum principal stresses increased significantly in the cartilage's middle zone (Halonen et al. 2016a). The early OA model showed increased compressive strains in the articulating layer and decreased stresses and fibril strains, especially in the intermediate zone (Klets et al. 2018; Liukkonen et al. 2017a).

We assumed that IE models predict more accurate findings under short-term loading, similar to the assumptions made in other investigations (Mononen et al. 2015; Tanska et al. 2015). Moreover, in compression, the IE material model (elastic) showed the highest primary stresses, whereas the other models indicated tension. It's because the IE material model doesn't include fluid pressure. According to previous research, the load supported by fluid in cartilage can be as high as 5–15 MPa, which can support 80–90% of the BW when walking (Ateshian et al. 1998; Bursać et al. 1999; Halonen

et al. 2014) However, different parameters undoubtedly likewise influence the material heterogeneity characteristics in cartilage. This might alter minimally if more attributes were included (heterogeneity in fluid flow across cartilage thickness), but it should not change any conclusions about the correlation between the material models. The IE and IPE models are basic models which do not take into account of material heterogeneity of the cartilage. From the present study, material heterogeneous TIE models show a better impression of meniscus reaction on articular cartilage compared to its homogeneous alternative. At the same time, IE and IPE geometrically heterogeneous models predict poor impressions on the cartilage surface. Hence material heterogeneous TIE model can be used as a better alternative to fiber reinforced model in knee biomechanics studies. The Comparison of mechanical response on femoral/tibial cartilage for different material models are compared with the literatures is shown in Table 5.4.

Table 5.4 Comparison of mechanical response on femoral/tibial cartilage (maximum principal stress/contact pressure) for different material models from literature

Material Models		**Isotropic elastic**	**Isotropic porous elastic**	**Transversely isotropic porous elastic**	**Fiber-reinforced porous elastic**
Present study	Max. contact pressure [MPa]	6.45	5.91	2.79	-
	Max. effective stress [MPa]	2.70	2.23	2.55	-
(Klets et al. 2016)	Max. principal stress [MPa]	2.50	1.20	2.51	4.25
(Shriram et al. 2017)	Max. contact pressure [MPa]	5.7	-	-	-
	Max. principal stress [MPa]	3.5	-	-	-

In a wide range of biomedical engineering applications, developing better constitutive models for modelling soft tissue deformation is becoming increasingly important. Researchers can use these articular cartilage model comparisons to look into the tissue-

joint mechanism and implant material design and better understand tissues' microscale response.

5.6 Conclusions

In summary, the following conclusions were drawn. The maximum cartilage contact pressure induced by the knee joint with the geometrically heterogeneous material model is lower than the homogeneous model. The maximum Von-Mises stress may not present a quantitative assessment of cartilage damage. The poroelastic cartilage model can help estimate anterior/posterior deformation, whereas the material heterogeneous TIE model is suitable for understanding proximal/distal deformation limits. The maximum change in stresses and strains are observed in TIE models than in IE and IPE models.

The study has some limitations regarding model generation, input, and assumptions. The knee kinematics is very complex, and hard to simulate the exact motion; the tibia stresses are a combination of loading (compression), shear, and tensile. In this article, only the knee joint's standing (full extension) position is considered a simple loading case. Other soft tissues are left out (patella, patellar tendon, joint capsule, and skin) in the models because the focus of this investigation is to compare three distinct material models of cartilage having the geometry under the same applied load

5.7 Closure

This chapter explores the influence of different constitutive material models in the mechanical response of the cartilage model. The peak cartilage contact pressure induced by the knee joint with the heterogeneous material model is lower than in the homogeneous model. The poroelastic cartilage model can help estimate anterior/posterior deformation, whereas the TIE model is suitable for understanding proximal/distal deformation limits. The maximum change in stresses and strains are observed in TIE models than in IE and IPE models. The following chapter determined the effect of cartilage constituent structure and its influence on mechanical responses for the intact and arthritic knee during various activities.

CHAPTER 6

CARTILAGE CONSTITUENT'S INFLUENCE ON KNEE KINETICS/KINEMATICS

6.1 Introduction

This chapter determined the influence of cartilage constituent structure on the mechanical responses of the intact and arthritic knee during various activities. The inhomogeneous distribution of collagen fiber in cartilage can substantially influence knee kinematics. This becomes vital for understanding the mechanical response of soft tissues and cartilage deterioration, including osteoarthritis (OA). Though the conventional computational models consider geometrical heterogeneity along with fiber reinforcements in the cartilage model as material heterogeneity, the influence of fiber orientation on knee kinetics and kinematics is not fully explored. This work examines how the collagen fiber orientation in the cartilage affects the healthy (intact knee) and arthritic knee response over multiple gait activities like running and walking.

6.2 Methodology

A 3D finite element knee joint model is used to compute the articular cartilage response during the gait cycle—a fiber-reinforced porous hyperelastic material used to model the soft tissue. A split-line pattern is used to implement the fiber orientation in femoral and tibial cartilage. Four distinct intact models and three OA models with collagen fibers oriented parallel, perpendicular, and inclined with respect to the articular surface are analysed.

6.3 Finite element model

A case study is performed based on open-knee geometry (Erdemir, 2014), simulating the walking and running cycle to study the influence of collagen fiber orientation in multiple gait activities. The tibiofemoral joint is segmented from a female subject (70

years, 77 kg) into femur, tibia, collateral ligaments (MCL and LCL), cruciate ligaments (ACL and PCL), menisci (lateral and medial), and cartilage (femoral and tibial) as given in Figure 6.1 (d). The finite element model of the knee joint is imported in FEBio Studio 1.2.0 for the static analysis (Maas et al. 2012).

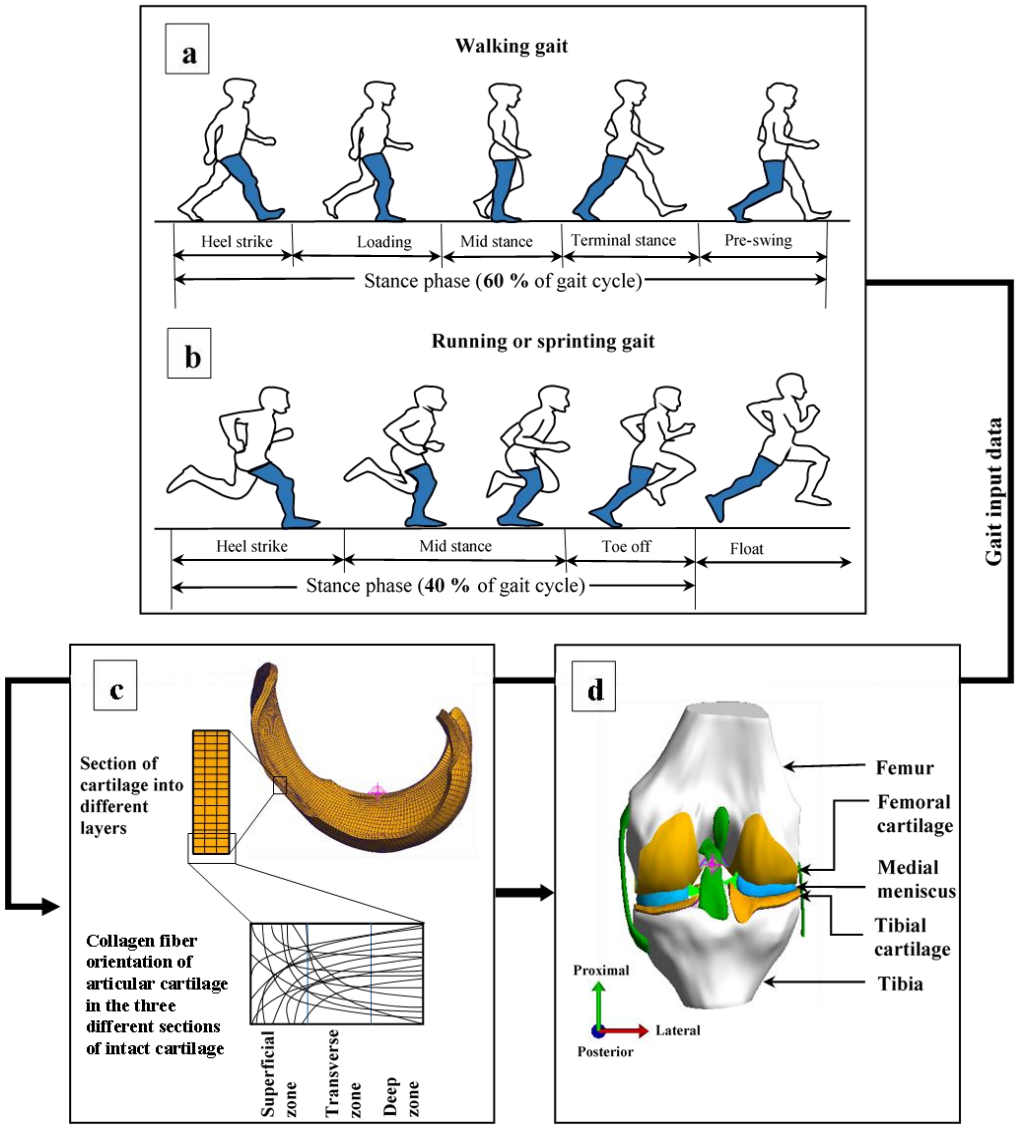

Figure 6.1 Schematic of workflow: (a) the stance phase of the walking gait (b) running gait (c) sagittal view of femoral cartilage with the orientation of collagen fibers (d) finite element model of the knee joint.

6.4 Gait input data

In this study, the gait input data is taken from the literature and imported into the model for simulation (Besier et al. 2009; Cappellini et al. 2006; Chan and Rudins 1994; Khassetarash et al. 2020; Orozco et al. 2018). During the walking and running gait cycle, six different but simultaneous movements occur between the femur and tibia. It is divided into three rotations (extension–flexion, internal-external, and varus-valgus) and three force components (anterior-posterior, medial-lateral, and proximal-distal) (Li et al. 2017).

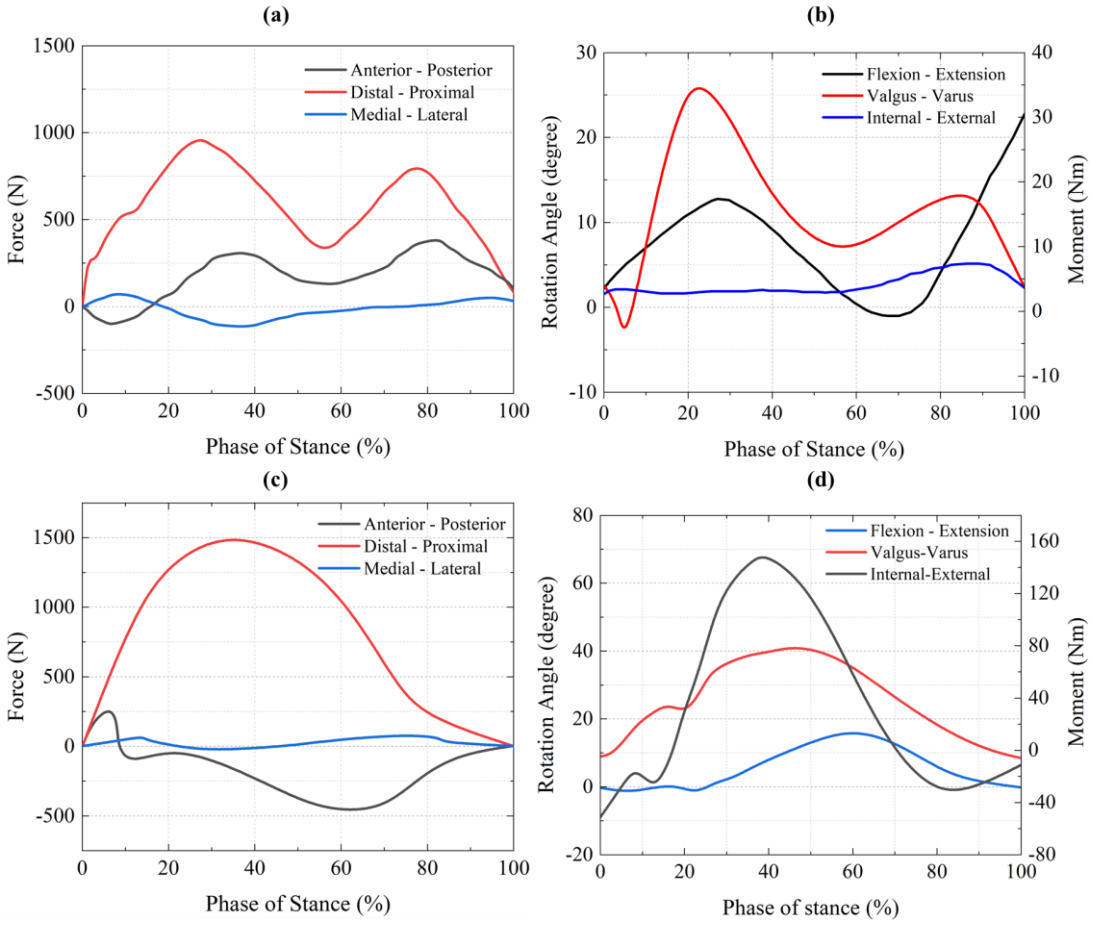

Figure 6.2 Input gait data for the analysis (a) the components of forces acting during stance phase of walking cycle (b) the rotation angle during walking cycle (c) the forces as acting during the running cycle (d) the rotation during running cycle

The walking kinetic and kinematic data are obtained from a subject (28 years old male, 82 kg) who walked on a 10 m track at an average speed of 1.7 m/s (Halonen et al.

2016a). The running data were obtained from a subject (22 years old male, 76 kg average) running at 4.07 m/s in a 30 m walkway (David et al. 2015b). The authors of both studies used 3D motion capture and anatomical marker systems to track walking and running data and converted them into knee kinetics and kinematics data with commercial software.

6.5 Contact and boundary conditions

In the model, the tibia is constrained in all degrees of freedom, whereas the femur is subjected to rotation for the gait input data. Also, translational forces are applied to the femur. The interaction between cartilage and meniscus is set to be frictionless.

The meniscus is connected to the tibial surface with elastic springs to mimic the anterior and posterior horn attachment. At the initial simulation stage, the cartilage and meniscus are made to make light contact to achieve the initial convergence. Following the initial conditions, forces and rotations applied during the stance phase of the gait cycle through a cylindrical joint in the analysis. The forces (proximal-distal, anterior-posterior, and medial-lateral) and rotations (flexion-extension, valgus-varus and internal-external) during the stance phase of the gait cycle for walking and running are applied to the model as illustrated in Figure 6.2.

6.6 Material models

The soft tissue is divided into fibrillar (collagen fibers) and non-fibrillar (proteoglycan matrix and interstitial fluid) components (Wilson et al. 2004). To simplify the model, the inhomogeneous compressive modulus of the matrix is neglected (Schinagl et al. 1997b; Todd et al. 2018). A fiber-reinforced porous hyperelastic (FRPHE) model is used for implementing the biphasic articular cartilage tissue (femoral and tibial cartilage). The collagen fibers are embedded in the ground matrix since fibers can only withstand tension and cannot sustain on their own. A fiber with exponential power-law provided by Equation 6.1 is utilized to model the collagen fibers. A neo-Hookean compressible hyperelastic material model given by Equation 6.3 is employed to model the proteoglycan ground matrix. The strain-dependent permeability nature of tissue is

implemented based on the Holmes-Mow model given by Equation 6.4 (Chen et al. 2016; Ebrahimi et al. 2019; Henak et al. 2014; Holmes and Mow 1990; Li 2021; Li et al. 1999; Mononen et al. 2013; Reuter and Hurschler 2018; Shegaf and Speirs 2020; Tomic et al. 2014).

The fiber strain energy density function is given by,

$$\psi = \frac{\xi}{\alpha\beta}\left(\exp\left[\alpha\left(I_n - 1\right)^{\beta}\right] - 1\right) \tag{6.1}$$

$$N = \sin\varphi\cos\theta e_1 + \sin\varphi\sin\theta e_2 + \cos\varphi e_3 \tag{6.2}$$

Where $I_n = \lambda_n^{\,2} = N.C.N$, λ_n = the fiber stretch, N = the fiber orientation represented by θ and φ [deg] given by Eq. (2), ξ = representing a measure of the fiber modulus [MPa], α = coefficient of exponential argument, β = power of exponential argument (fiber nonlinearity), θ, φ = spherical angle for fiber orientation [deg].

The proteoglycan matrix strain energy density function (Mooney-Rivlin) is given by:

$$\psi = C_1(I_1 - 3) + C_2(I_2 - 3) + \frac{1}{D}(\ln J)^2 \tag{6.3}$$

where C_1, C_2, D are hyperelastic material constants, when $C_2 = 0$ the model reduces to neo-Hookean constitutive model, I_1, I_2 are the first and second invariants corresponding to the left Cauchy-Green deformation tensor, J is Jacobian of the deformation given by $\det(F)$, and F is the deformation gradient. $D = 2/K$ and $C_1 = \mu/2$ where K is the bulk modulus, and μ is the shear modulus. The strain-dependent permeability of soft tissue is described using the Holmes-Mow constitutive equation given in Equation 6.4 and Equation 6.5 (Holmes and Mow 1990; Mononen et al. 2011, 2013).

$$K_s = k(J)I \tag{6.4}$$

$$k(J) = k_0 \left(\frac{J - \varphi_0}{1 - \varphi_0} \right)^{\alpha_1} e^{\frac{1}{2}M\left(J^2 - 1\right)} \tag{6.5}$$

Where $k(J)$ is a strain-dependent component, k_0 is isotropic hydraulic permeability, M is an exponential strain-dependent co-efficient and α_1 is a power-law exponent. The inhomogeneity in the solid phase of the tissue is modelled by varying the volume fraction along the thickness direction. The solid volume fraction φ_0 is given in Equation 6.6, where z varies from 0 to 1 from the cartilage surface to the subchondral bone (Tanska et al. 2015).

$$\varphi_0 = 1 - (.8 - .15z) \tag{6.6}$$

Seven different femoral and tibial cartilage models are created to investigate the influence of collagen fiber orientation in the superficial zone and depth direction for an intact and arthritic knee. The femoral cartilage models made are shown in Figure 6.3. The first four models represent the intact knee, and the rest three the arthritic knee cases. The collagen fiber orientation is defined using split-line patterns, and the direction of the fibers is controlled using the model. The split-line patterns are obtained from the literature (Below et al. 2002; Chahine et al. 2004; Huang et al. 2005; Li et al. 2016; Mononen et al. 2012; Rakhsha et al. 2019).

The following material models (intact and osteoarthritic) with different collagen fibre orientation directions are developed for the present investigation:

i) In intact model-1, the split lines are aligned in the medial-lateral direction in the femur and tibial cartilage. The split-line representation is shown in Figure 6.3 (a). Model-1 mimics the arcade-like collagen structure.

ii) In intact model-2, the split lines are aligned in the plane of the articulating surface, and the direction is pointed outward from the centre according to the geometry illustrated in Figure 6.3 (b). Also, the orientation along the depth-wise path mimics an arcade-like structure.

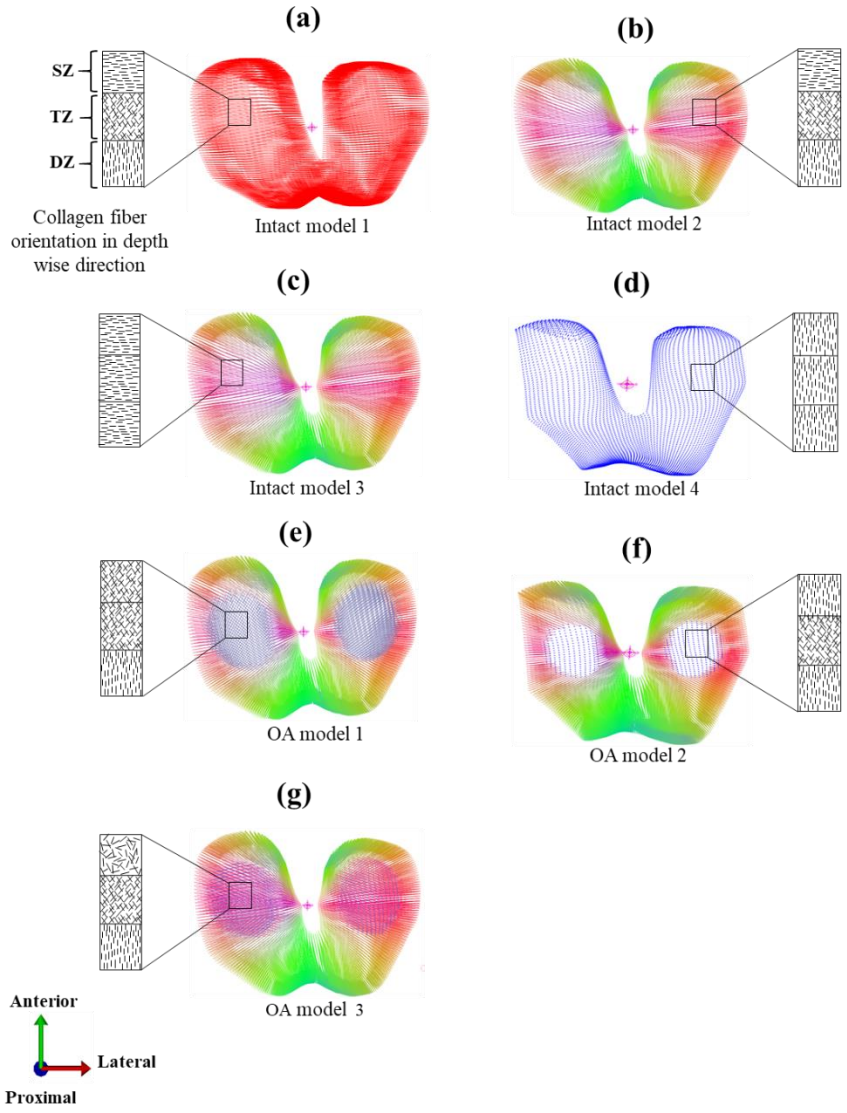

Figure 6.3 Femoral cartilage models based on distinct collagen fiber orientation (a-d) intact cartilage model (e-g) osteoarthritic models, the fiber orientation in the depth-wise direction is shown in the boxes.

iii) In intact model-3, the split line pattern is aligned similar to model-2; It is the same for all three zones, as shown in Figure 6.3 (c).

iv) In the intact model-4, the split-line pattern is aligned along the proximal-distal direction, as shown in Figure 6.3 (d), and it is the same for all zones.

The arthritic zone where fibrillation occurs for the osteoarthritic cartilage model is selected. The split-line pattern orientation is assigned to obtain the influence of

collagen orientation in the OA knee. Three different OA models are used to investigate the impact of collagen fiber orientation.

v) The split-line pattern is aligned such that it is equally inclined to the medial-lateral and proximal-distal axis in OA model-1. Also, the alignment is restricted inside the arthritic zone, as shown in Figure 6.3 (e).

vi) The split-line pattern is aligned in the proximal-distal direction, as shown in Figure 6.3 (f) in OA model-2.

vii) The OA model-3 represents the random split-line orientation of collagen fibers, as shown in Figure 6.3 (g).

The properties of the FRPHE cartilage material are implemented into the model according to Table 6.1. The menisci, collateral, and cruciate ligaments are modelled as transversely isotropic hyperelastic, and the constants are chosen from the literature (Deneweth et al. 2015; Donahue et al. 2002; Raju and Koorata 2022; Vaziri et al. 2008).

Table 6.1 Material constants for FRPHE intact and arthritic cartilage models (intact model-1 and OA model-1)

Material Constants		**Intact knee**				**Arthritic knee**				**Source**
		Deep zone	**Middle zone**		**Superficial zone**	**Deep zone**	**Middle zone**		**Superficial zone**	
Collagen fiber: (Fiber exponential power uncoupled)	ξ (MPa)	9.19	4.595	4.59	9.19	4.595	2.297	2.297	4.59	(Henak et al. 2014; Li et al. 2016)
	α	0	0		0	0	0		0	
	β	2	2		2	2	2		2	
	Θ (deg)	0	0	0	0	0	0	0	0	
	φ (deg)	0	45	-45	90	0	45	-45	90	

Proteoglycan matrix: (compressible hyperplastic neo-Hookean)	**μ** (MPa)	1.82	1.82	1.82	0.91	0.91	0.91	(Li 2021)
	K (MPa)	1860	1860	1860	930	930	930	
Interstitial fluid: Permeability (Perm-Holmes-Mow)	**K_o** (mm^4/Ns)	.00174	.00174	.00174	.00174	.00174	.00174	(Mononen et al. 2011, 2013)
	M	7.1	7.1	7.1	7.1	7.1	7.1	
	α	2	2	2	2	2	2	
Density	**ρ_s** (tonnes/mm^3)	1 x 10^{-9}	1 x 10^{-9}	1 x 10^{-9}	1 x 10^{-9}	1 x 10^{-9}	1 x 10^{-9}	(Todd et al. 2018)
	ρ_f (tonnes/mm^3)	1.5 x10^{-9}	1.5 x10^{-9}	1.5 x10^{-9}	1.5 x10^{-9}	1.5 x10^{-9}	1.5 x10^{-9}	
Volume fraction	φ_0	0.2	0.275	0.35	0.2	0.275	0.35	

6.7 Results and discussions

6.7.1 The tissue response during walking and running cycle

Figure 6.4 shows the contours of different mechanical responses of the femoral articular cartilage during the stance phase of the walking gait cycle. It displays the variation in various mechanical responses, such as contact pressure, principal elastic stress, Lagrange strain, fluid pressure, and fiber stretch of the biphasic cartilage. Throughout the cycle, it is seen that the contact pressure generated on the articulating surface varies, and maximum contact pressure of 2.5 MPa is observed at the end of the heel strike on the lateral side. According to published research, osteoarthritis is most

prone to develop on the articulating surface where the maximum contact pressure is generated (Wang et al. 2014).

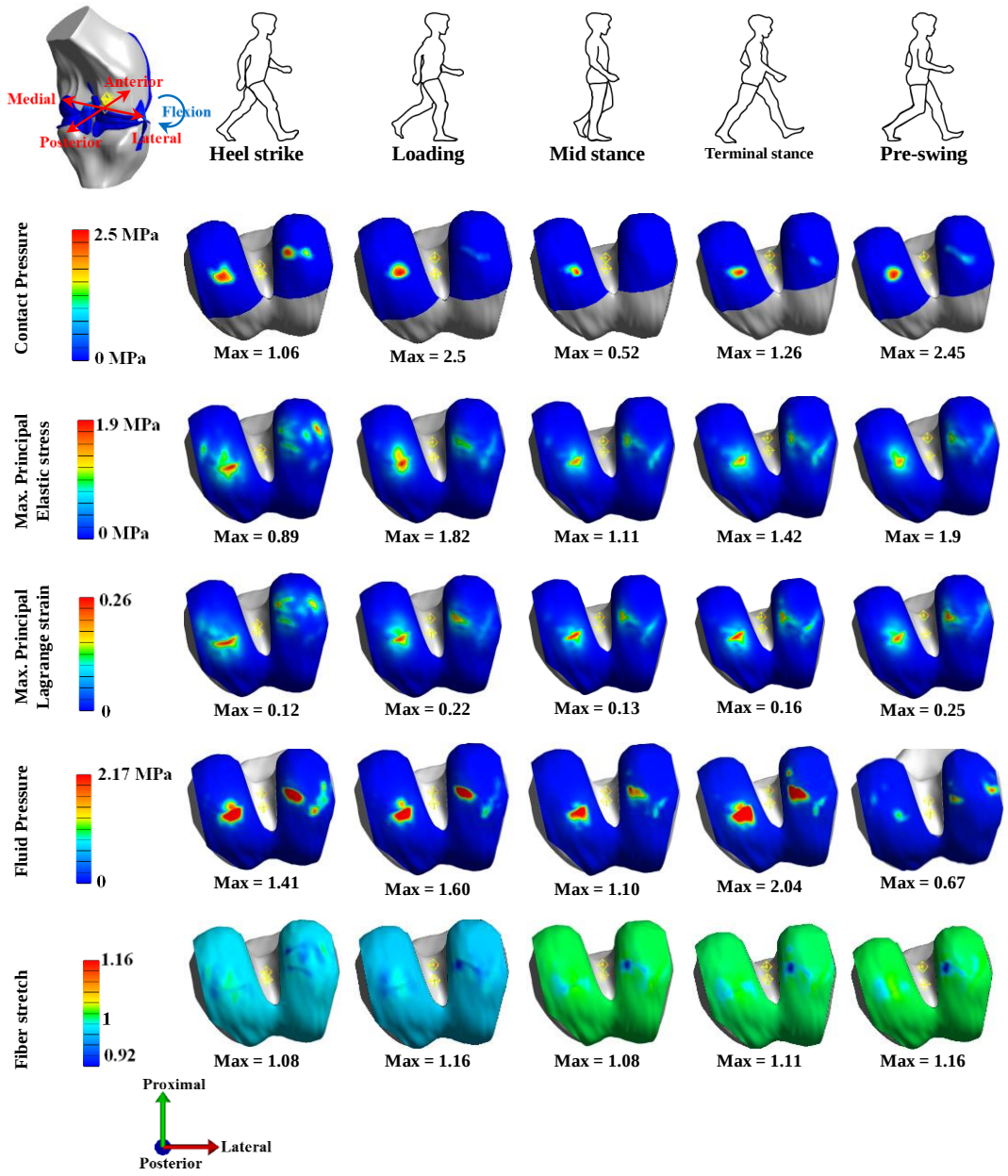

Figure 6.4 Contours of mechanical responses of femoral cartilage on the surface of intact model-1 during the stance phase of walking (60% gait cycle).

Figure 6.5 depicts the contours of various mechanical responses throughout the running gait cycle. However, this also shows a similar trend in the contact pressure, as the maximum value of 2.9 MPa is observed at the end of the heel strike. The location of maximum contact pressure is observed on the medial side of the cartilage as compared

to the lateral side. The maximum elastic stress and Lagrange strains are concentrated in the lateral-medial epicondyle area of the femoral cartilage during walking gait; however, during the running gait, these maximum values are observed in the posterior side of the knee cartilage.

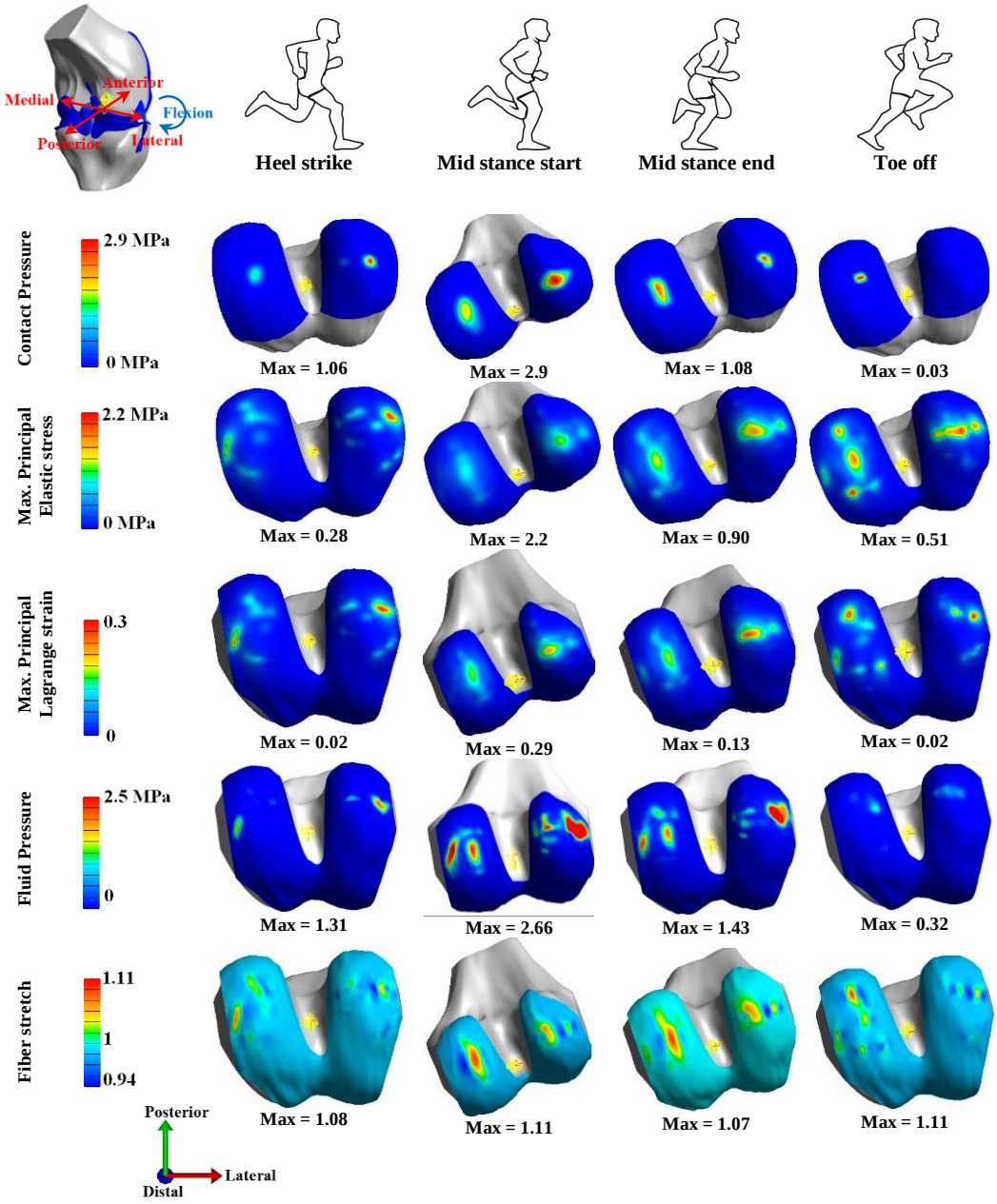

Figure 6.5 Contours of mechanical responses of femoral cartilage on the surface of intact model-1 during the stance phase of running (40% gait cycle).

6.7.2 Comparison of walking and running cycle

Maximum principal stress of 1.82 MPa is produced throughout the walking cycle, which is more than the fluid pressure of 1.60 MPa that is produced during the loading stance (first peak in the loading curve). However, the principal stress produced at the terminal stance, 1.42 MPa, is less than the fluid pressure, 2.04 MPa (second peak in the loading curve). A fluid pressure of 2.66 MPa is produced during the running cycle at the mid-stance start (the maximum peak in the loading curve), which is more than the maximum primary stress of 2.20 MPa produced. The medial side of the femoral cartilage experiences the maximum stresses and strains during the whole stance period of the walking gait. In contrast, the lateral compartment of the cartilage has the maximum responses during the running gait. The collagen fiber stretch also changes during the stance phase, with most variation seen in the running rather than walking cycle.

6.7.3 Importance of collagen fiber orientation in knee kinematics

Figure 6.6 shows the variation in mechanical responses for different collagen fiber-oriented models during the stance phase of the gait cycle. All intact and arthritic models show similar trends in contact pressure, maximum principal elastic stress, maximum principal Lagrange strain, and fluid pressure. The intact model aligned with the proximal-distal direction has a higher contact pressure than the other models shown in Figure 6.6 (a). Also, there is a 200% difference in the contact pressure for intact and OA models, and contact pressure reaches zero during the mid-stance (40-60% of the stance phase) for both models. In the walking gait, two contact pressure peaks are observed (during the 30% and 90% stance phases, respectively). During the first peak, contact pressure for intact models is two times higher than for OA models, and during the second peak, it is five times higher. Figure 6.6 (b) shows higher principal stress for the intact parallel split-line model and lower principal stress for the random split-line oriented OA model during walking gait. According to previous experimental research, Green-Lagrange strain is a crucial indication of cell damage compared to other results such as contact pressure, principal stress, and fluid pressure (Jeffrey et al. 1995; Wilson et al. 2006). As shown in Figure 6.6 (c), the maximum principal Lagrange strain has

higher values for intact models than OA models. One can observe that the strain difference between these two sets of models significantly increases from 20 to 90% of the stance phase. Figure 6.6 (d) shows maximal interstitial fluid pressure in soft tissue. As expected, intact models give rise to higher fluid pressure than OA models. Among intact models, models 1 and 2 (parallel-oriented collagen fiber models) show elevated responses.

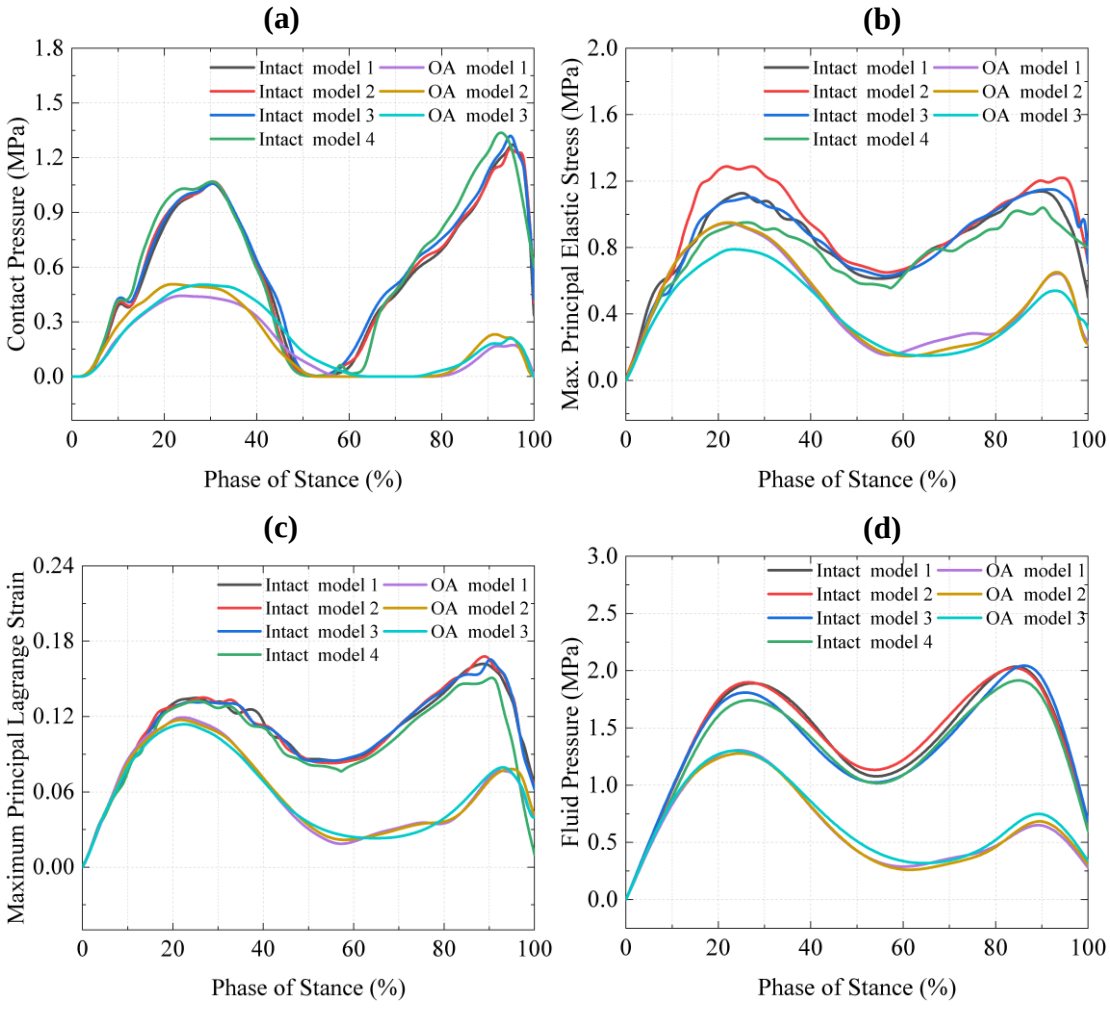

Figure 6.6 The comparison of mechanical responses of cartilage for different models (a) the contact pressure (b) maximum principal elastic stress (c) maximum principal Lagrange strain (d) maximum fluid pressure generated.

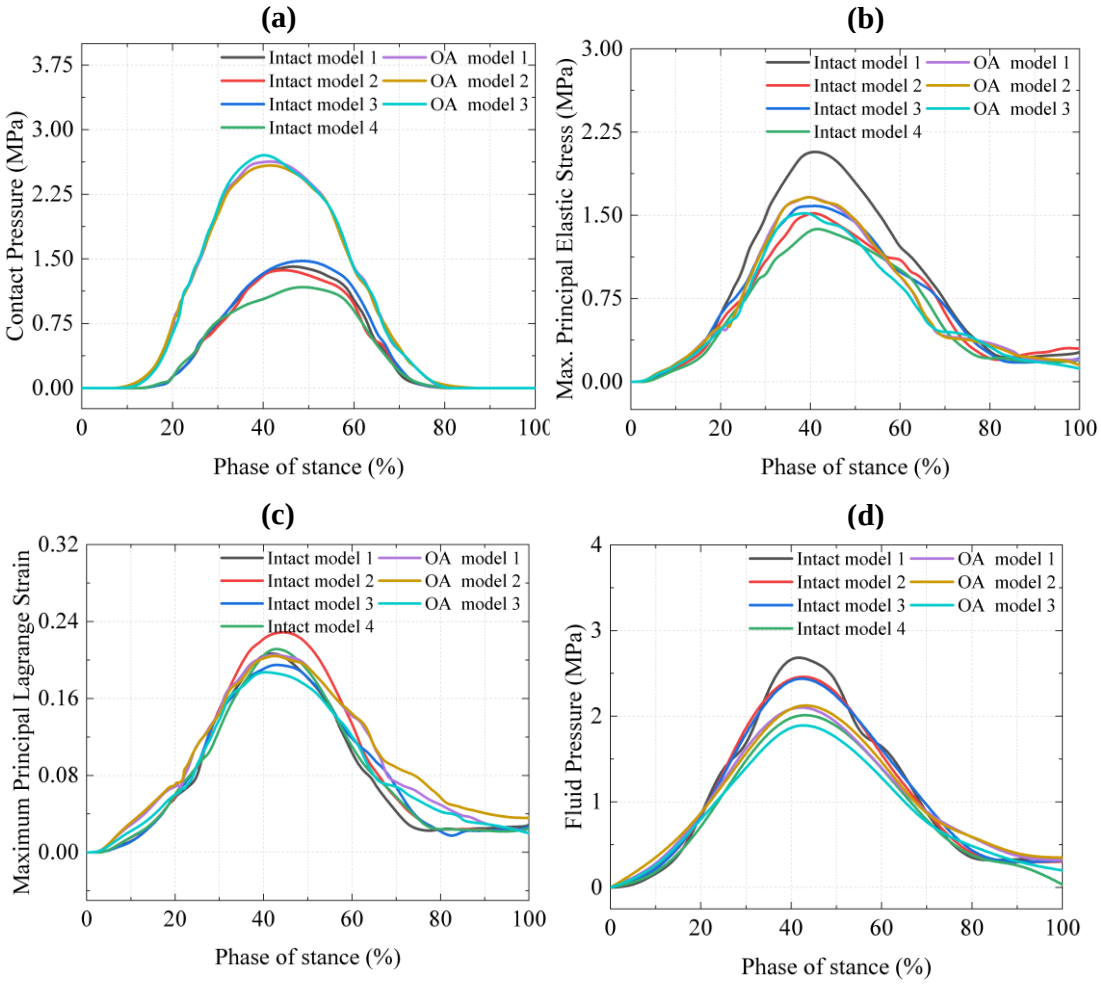

Figure 6.7 The comparison of mechanical characteristics of cartilage for different models (a) the contact pressure (b) maximum principal elastic stress (c) maximum principal Lagrange strain (d) maximum fluid pressure.

Figure 6.7 illustrates the mechanical responses of various models throughout the running gait. Even though the mechanical responses for both the walking and running cycles are comparable to the gait input data, it is interesting to note that the contact pressure created during the running cycle is more significant for the OA model than the intact model shown in Figure 6.7 (a). Also, the maximum contact pressure generated is higher for the randomly oriented OA model (OA model 3) and the minimum for the perpendicular oriented intact model (Intact model 4). Further, it can be observed that the contact pressure for walking gait (Figure 6.6(a)) is strikingly high for intact models than for OA models, which is not the case for running gait.

Figure 6.7 (b) shows elastic stress distribution, where the parallel split-line model (Intact model 1) exhibits the highest elastic stress, whereas the proximal-distal aligned model indicates lower elastic stress. The Lagrange strain is plotted in Figure 6.7 (c). One can observe that the strain distribution trend is almost similar for all the simulated cases. This response differs significantly from the walking gait scenario (Figure 6(c)). Like the Lagrange strain, the interstitial fluid pressure in Figure 6.7 (d) also shows a similar trend. However, a closer observation indicates an increase of ~ 40% in fluid pressure in the case of intact models with parallel-oriented intact models experiencing higher fluid pressure than perpendicular or inclined ones.

6.7.4 Significance of Lagrange strain in knee articulation between cartilages

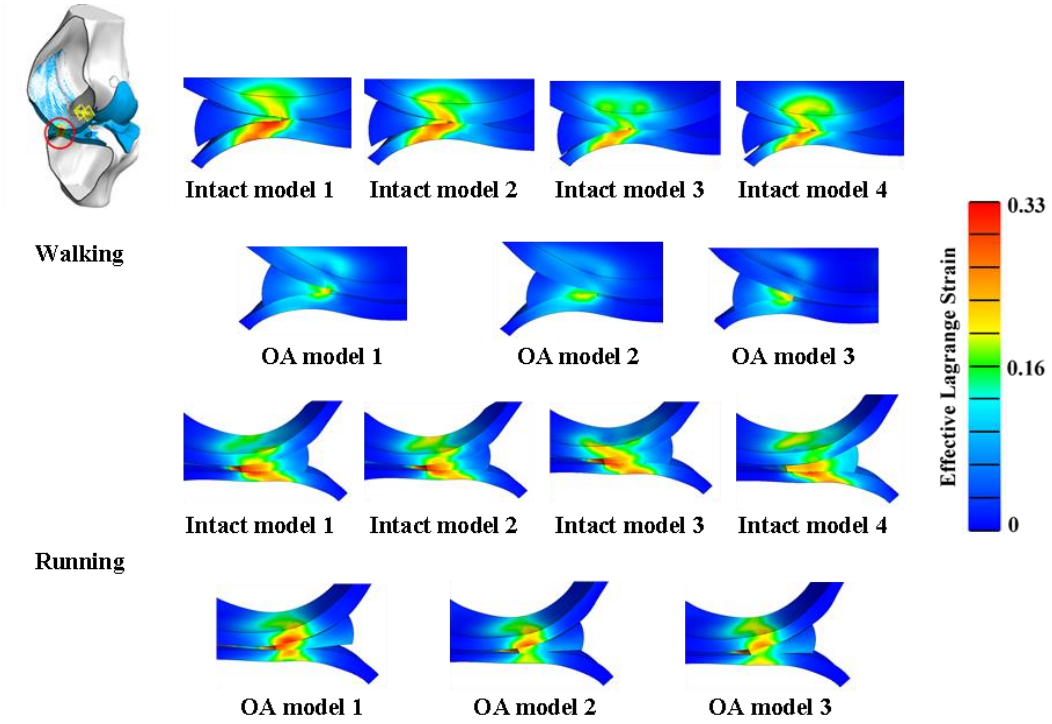

Figure 6.8 The effective Lagrange strain in the sagittal plane sectional view of the articulating region.

Figure 6.8 shows the effective Lagrange strain in the femoral-tibial cartilage and meniscus contact region for walking and running cases. During the walking cycle, the tibial cartilage exhibits a higher strain in the case of intact models, while only the meniscus has a higher strain in the case of OA models. Conversely, during the running

cycle, the meniscus shows a higher strain in the case of intact models, and the femoral cartilage exhibits a higher stain in the case of OA models. In addition, it can be observed that the inclined intact model-3 shows lower tibial cartilage strain than the parallel-oriented models during the walking case, and during the running cycle, the perpendicularly oriented intact model-4 exhibits lower tibial cartilage strain. Further, during the running cycle, the maximum strain is detected in the tibial cartilage-meniscus interface for intact models. In contrast, the maximum strain is observed in the femoral cartilage-meniscus interface for OA models.

6.7.5 Tissue responses on knee kinematics

A subject-specific knee geometry with six degrees of knee kinetics and kinematics data concerning walking and running gait is utilized for the present knee investigation. An FRPHE cartilage model with control on collagen fiber orientation and osteoarthritic characteristics are used for the analysis. Also, different fiber-oriented cartilage models are created for intact and osteoarthritic cases. The model determines contact pressure in the articulating area, principal stress, Lagrange strain, interstitial fluid pressure, and cartilage fiber stretch, all of which are essential factors in the evaluation of cartilage degradation (Haris and Beng Chye Tan 2020; Klets et al. 2018; Peters et al. 2018b; Raju et al. 2021; Shirazi and Shirazi-Adl 2009). The findings imply that the collagen fibril orientations, as revealed by split lines, play a significant role in regulating cartilage strains and stresses.

The experimental investigation by (Thambyah et al. 2005) predicted more significant contact pressures during the heel strike on the medial compartment than those on the lateral compartment, which is consistent with our model. Our model yielded contact pressures of 2 and 3 MPa at the lateral and medial compartments, respectively, at 50% of the stance phase (1500 N). These values are also in the same range as those found in past computational studies (1-5 MPa with loads between 1000 and 1800 N) (El-Rich 2022; Erbulut et al. 2021; Esrafilian et al. 2020, 2021; Halonen et al. 2014; Sylvia et al. 2015; Wang et al. 2014).

In the gait input data for knee kinetics and kinematics, forces and rotations corresponding to particular activities are applied to the FE knee model (Abid et al. 2019; Hall et al. 2012; Hyodo et al. 2020; Roberts et al. 2017; Schliemann et al. 2018). One limitation of the approach is that it uses a small force and rotation in the initial step to bring the model into contact with the cartilages and meniscus to achieve initial convergence. Moment-driven and rotation-driven are the two methods used to input flexion-extension, valgus-varus, and internal-external rotations to the knee model (Adouni et al. 2012b; Bennett et al. 2021). However, the present study uses a rotation-driven method to implement knee rotations, as shown in Figures 6.2 (b) and 6.2 (d). Also, it is unclear whether the FE model should be driven by a moment or a rotation because both methods predict identical measures in the literature (Wang et al. 2014).

Table 6.2 Comparison of mechanical response on femoral/tibial cartilage throughout the gait cycle (intact walking) of the present work with respect to the literature

Mechanical responses		**Loading stance**	**Mid stance**	**Toe-off**
Present study (Max 1000N input load)	Max. contact pressure [MPa]	1.11	0.15	1.20
	Max. Principal stress [MPa]	1.30	0.72	1.25
(Mononen et al. 2015) (Max 2000 N input load)	Max. stress [MPa]	7.50	1.50	10.5

The peak mechanical response magnitudes of the intact models are substantially more extensive than the OA model during walking gait, as shown in Figure 6.6; while running, peak magnitudes are observed for OA cases. However, during the running gait, the highest value for Lagrange strain is generated in the intact model-2 with split-line patterns parallel to the articulating surface, as shown in Figure 6.7 (c), and it indicated the higher risk of OA, as excessive strain contributes to OA (Below et al. 2002; Halonen et al. 2016a; Kazemi et al. 2013). The maximum fiber stretch is obtained in the deep zone during running gait, whereas a lesser fiber stretch is received in the superficial layer, as illustrated in Figure 6.5. It may be caused by impact loading in the

joint during running; however, the maximum fiber stretch in the superficial zone during walking can be seen in Figure 6.4. Hence, the fiber stretch values help to predict the gait data (Dhaher et al. 2010). The maximum elastic stresses during the walking and running cycle are obtained for models with split-line patterns parallel to the articulating surface for intact models, as shown in Figures 6.6 (b) and 6.7 (b). The study demonstrates that the direction of the cartilage's collagen fibres affects the maximum stress generated and, therefore, is associated with osteoarthritis. Comparison of mechanical response on femoral/tibial cartilage throughout the gait cycle (intact walking) of the present work with respect to the literature is given in Table 6.2.

6.8 Conclusions

The study presents a novel method to control collagen fiber orientation for FRPHE cartilage models for knee joint analysis. This study suggests during the walking cycle, the maximum contact pressure is observed to be greater in intact models than in OA models; however, during running, the ultimate value is observed to be greater in OA models than in intact models. Also, the maximum stresses and fluid pressure are obtained for parallel-oriented models than proximal-distal oriented models for both walking and running gait. However, the maximum principal Lagrange strain predicts a similar trend for both intact and OA models throughout the running stance phase; the parallel-oriented models exhibit a higher value than perpendicular and inclined ones. These results will aid researchers in developing improved assistive devices for arthritis patients who engage in subject-specific activities such as walking and running.

6.9 Closure

In this chapter an investigation of collagen fiber structure on the knee kinetics or kinematics. The study analysed the mechanical responses for intact and arthritic cartilage cases. In the following chapter, we design a knee implant based on a commercially available form and modify the design to improve contact pressure distribution and longevity.

CHAPTER 7

MODELING OF PROSTHETIC KNEE

7.1 Introduction

In this chapter, the prosthetic knee is designed and analysed for the mechanical responses on the polyethylene bearing. Prosthetic knee is implanted to individuals with end-stage osteoarthritis to restore knee function and alleviate joint discomfort. There have been recent developments in the design of customized implants based on patient-specific data obtained from MRI scans and subsequent image processing techniques. Here curvature of the femoral component plays an important role in effective implant design. Therefore the objective here is to investigate the influence of this curvature of the femoral component on the mechanical response of the bearing component.

7.2 Computational model of knee prosthesis

A 3D finite element knee implant model with a circular and elliptical femoral component is developed and investigated for gait kinetics and kinematics. The computational model used in this study is developed based on a commercially available implant Scorpio NRG CR (Stryker, USA), as shown in Figure 7.1 (a). In this work, we modified the present design's femoral component curvature to circular and elliptical, as shown in Figures 7.1 (b) and 7.1 (c). Also, the fixed-bearing, cruciate-retaining type finite element model is selected for the present analysis. The Co-Cr metal components are modelled as a rigid body. The parts are meshed with 10-node quadratic tetra elements with a femoral component average element edge length of 3.2 mm and a tibial insert average element edge length of 2.2 mm. The tibial tray contains 8-node, 5-mm linear brick elements.

A mesh convergence test is conducted in the study to ensure that the solution should not change when the mesh is refined. The optimum element length concerning the contact pressure generated on the surface is 2.2 mm, based on the tibial insert edge

length of 4 models ranging from 1 to 4 mm in 1 mm increments. There is a total of 20155 elements in the tibial insert. The pre-processing and post-processing analysis is performed on FEBio Studio (University of Utah and Columbia University), an open-source finite element analysis software (Maas et al. 2012).

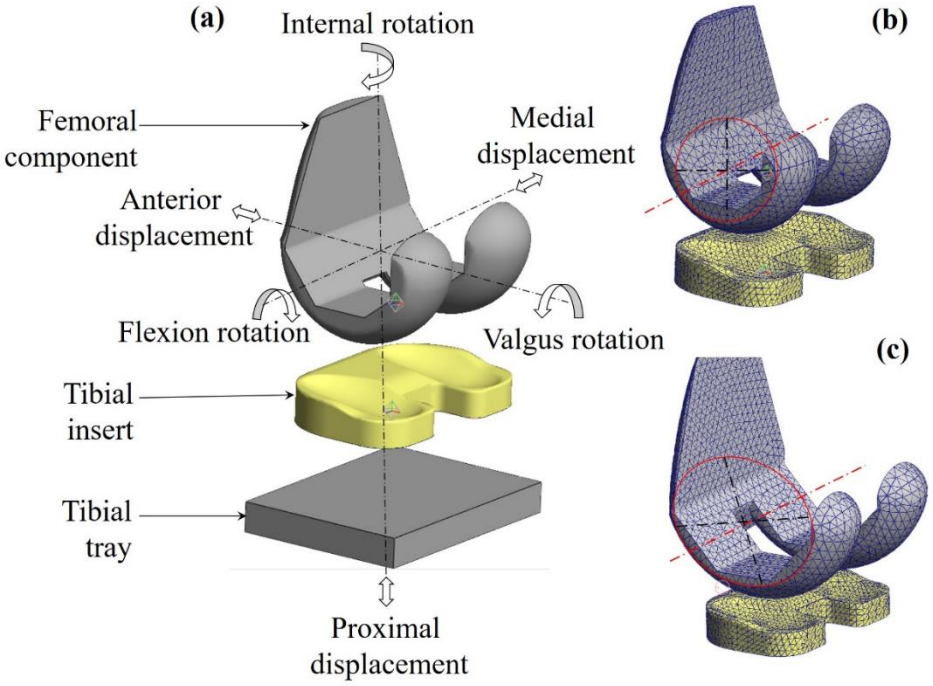

Figure 7.1 (a) The 3D finite element model of the TKA (b) circular design femoral component (c) elliptical design femoral component

7.3 Loading and boundary conditions

An explicit TKA finite element analysis is performed to predict the knee joint movements and contact pressure on the tibial insert under gait loading conditions. The tibial tray and tibial insert are constrained in all directions, whereas the femur rotates in relation to the gait input data. In addition, all translational forces are applied to the femur component. The femoral component and tibial insert are designed to engage without friction. The master surface is the articular surface of the femoral component, whereas the slave surface is the tibial insert surface beneath it. During the gait cycle, the forces and rotations are applied to the centre of mass of the femoral component. The forces and rotations during the phase stance of the gait cycle are applied to the model, as illustrated in Figure 7.2.

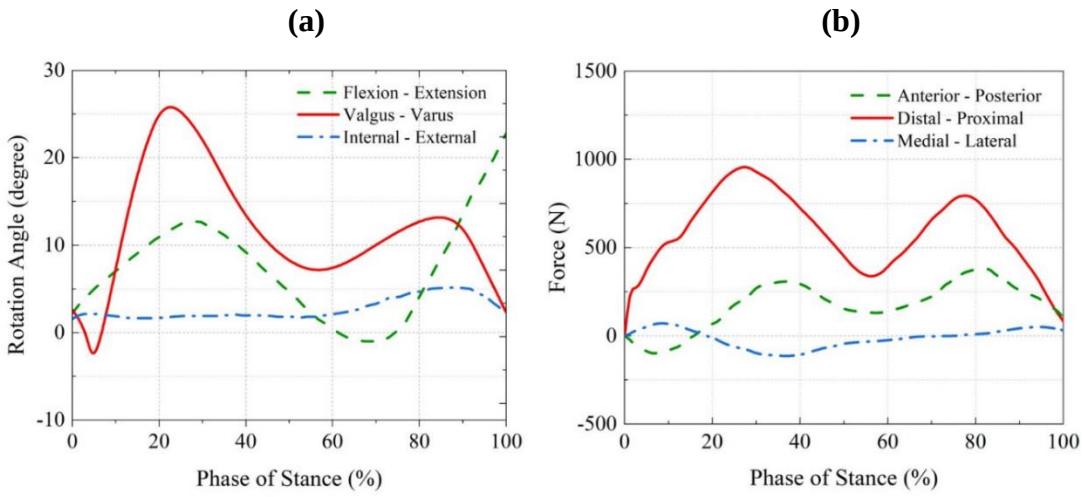

Figure 7.2 The input gait data for the analysis (a) the rotation angle in all 3 dof (b) the components of forces.

The gait input data are taken from the literature and imported into the model for simulation (Besier et al. 2009; Cappellini et al. 2006; Chan and Rudins 1994; Khassetarash et al. 2020; Orozco et al. 2018). The walking kinematics data are obtained from the subject (28-year male, 82 kg) who walked on a 10 m track at an average speed (of 1.7 m/s) (Halonen et al. 2016a). Their study used 3D motion capture and anatomical marker systems to track walking and running data and converted them into knee kinematics data with commercial software.

7.4 Material models

Table 7.1 The material constants for the components of the TKA implant

Implant Components	Mechanical properties		Source
Femoral component	Cobalt-Chromium (rigid)	Rigid body	(Koh et al. 2019)
Tibial tray			
Tibial insert	UHMWPE (Isotropic elastic)	ρ=9.38x10-10 tonnes/mm^3	(Malito et al. 2018)
		E=800 MPa	

	ν=0.459

The UHMWPE tibial insert is modelled as a linear isotropic elastic material, and the material constants are given in Table 7.1. The Co-Cr metal components are chosen as rigid bodies because their material constants are substantially higher than the tibial insert

7.5 Contact pressure distribution and Lagrange strain measurement

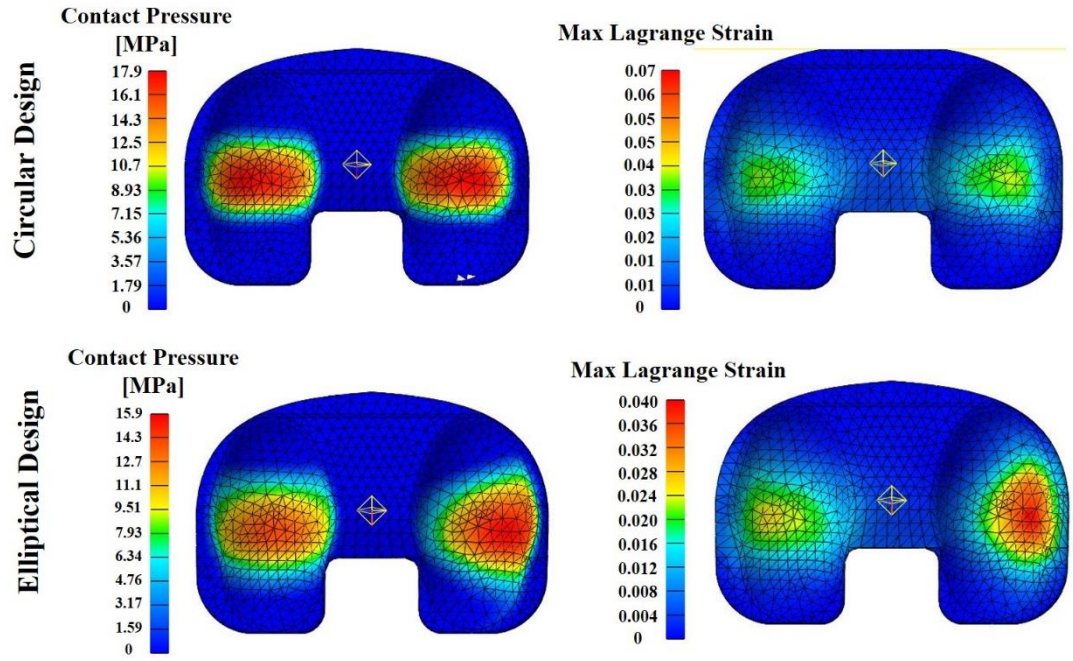

Figure 7.3 Contours of maximum contact pressure and Max Lagrange strain generated on UHMWPE tibial insert.

The contour of the maximum Lagrange strain and contact pressure created on the surface of the UHMWPE tibial insert during a gait is shown in Figure 7.3. It is observed that the circular design has higher contact pressure and Lagrange strain compared to the elliptical alternative design. However, as shown in Figure 7.4, the maximum values of mechanical responses are achieved during the first 20–30% of the stance phase. The contact pressure generated in the circular design is higher than in the elliptical design given in Figure 7.4 (a). Also, the principal and effective stresses have similar trends

with respect to the contact pressure shown in Figure 7.4 (b-d). In addition, the elliptical design achieves a larger contact area on the articulating site than the circular design. The patient's comfort decreases as the curvature flattens; however, the contact pressure reduces, which is observed in Figures 7.4 (a) and 7.4 (f).

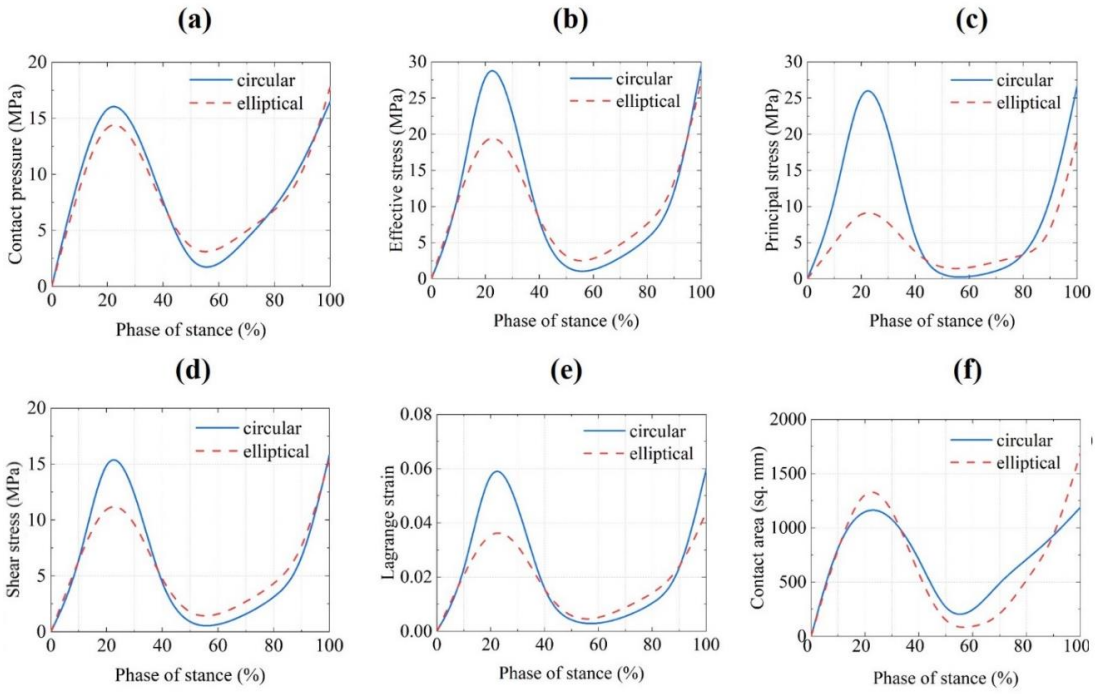

Figure 7.4 The mechanical responses of UHMWPE tibial inserts (a) the contact pressure (b-d) Effective stress, principal stress and shear stress (e) Lagrange strain (f) the articulating area of contact.

The wear depth is calculated according to equation (1) concerning the maximum contact pressure generated for circular and elliptical designs, as in Table 7.2. The comparison of maximum femoral translation over tibial insert is plotted in Figure 7.5 for circular and elliptical designs. It is observed that the elliptical design has higher translation in all directions compared to the circular design. There is a 40 per cent difference in anterior-posterior translation between the two designs

7.6 Wear Calculation

Archard devised an equation for determining the linear wear depth from articulating surfaces between two moving metal surfaces (Archard 1953; Haider and Baykal 2016;

Ramírez et al. 2020). The current investigation's wear calculation on the tibial insert uses Equation 7.1.

$$H = K_w PS \tag{7.1}$$

where H is the linear wear depth, P is the contact pressure, K_w is the wear factor which can be calculated experimentally, and S is the total sliding distance for 1 lakh cycles. A pin-on-disk tribometer calculates the co-Cr wear factor on UHMWPE experimentally (TRB 3, Anton-Paar, Austria). The wear track profile on the UHMWPE surface for a 1 million cycle is plotted with a profilometer. The wear factor or wear rate is calculated using Equation 7.2.

$$K_w = \frac{V}{F_n S} \tag{7.2}$$

where V is the measured wear volume $388.9 * 10^6\ \mu m^3$, F_n is the applied load 40N, and S is the sliding distance of 1200m. The calculated wear factor is $9.05 * 10^{-6}\ mm^3/Nm$.

Table 7.2 The wear depth produced on the tibial insert during the gait cycle

	Circular Design	**Elliptical Design**
Max. contact pressure (MPa)	17.9	15.9
Measured wear depth (mm)	0.194	0.172
(Kang et al. 2017) **(mm)**	0.25	-

7.7 Discussions

The current work uses a knee implant geometry and data from all six degrees of knee kinematics. The effectiveness of the prosthetics and surgical success depends on the kinematic behaviour after TKA. According to a computational assessment of TKA design and subsequent wear analysis, the clinically observed anterior femoral translation is caused by a rapid decrease in the radii-of-curvature of the femur. As seen

in Figure 7.5, a shift from a smaller to a greater curvature radius caused the femur to translate posteriorly.

Table 7.3 Comparison of wear rate/factor of the UHMWPE tibial insert obtained from the present study with respect to the literatures

	Wear rate/factor [10^{-6} mm^3/Nm]
Present study	9.05
(Hussain et al. 2020a)	1.25 - 3.1
(Baykal et al. 2014)	3.5 - 9.5

In reality, in vivo wear measurement in TKA is quite tricky. The in vitro wear simulation results have been quite predictive of the wear behaviour seen in clinical settings. It's time-efficient and economical to finish the equivalent of the last five years' worth of clinical wear data (McKellop and D'Lima 2008; Netter et al. 2015). As a result, computer modelling and simulation in this sector have grown more prevalent (Fregly et al. 2005; Knight et al. 2007; Netter et al. 2015; Zhao et al. 2008). Comparison of wear rate/factor of the UHMWPE tibial insert obtained from the present study with respect to the literatures is given in Table 7.3.

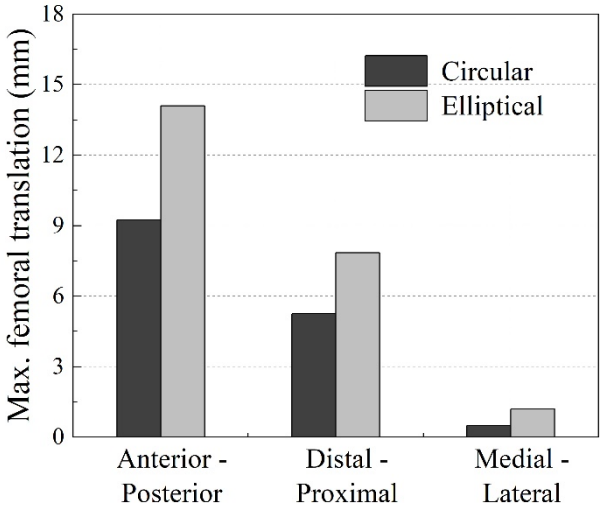

Figure 7.5 The maximum femoral component translation for circular and elliptical design

Despite being ineffective in terms of cost and time, experimental investigations are often carried out and can only study a restricted number of configurations and load circumstances (Scholes and Unsworth 2009). However, experimental research is eventually required to have a complete understanding of the way materials behave. According to pin-on-disc testing, the amount of wear caused by UHMWPE decreases as contact pressure increases. Consequently, an implant with lower conformity with a constrained articulating area and high contact stress would experience less wear than an implant with more excellent conformance (Barbour et al. 1997; Galvin et al. 2009).

It's uncertain if kinematic differences caused by patient characteristics and surgical technique exceed the impact of implant design (Fitzpatrick et al. 2012). Changes in reported kinematics were exclusively attributable to differences in articulating geometry since all geometric alterations to the implant geometry were analysed in the computational model under comparable boundary circumstances. In the future, researchers will investigate how these implants work under more physiological loading settings and the in vitro variation that might be predicted.

7.8 Conclusions

The computational method used here successfully establishes the connection between the design of TKR implants and the mechanical responses of bearing materials. The model's sensitivity is shown by its ability to identify differences in kinematic patterns resulting from implant design changes to curvature. Now, it will be used to examine a variety of additional design aspects, including the reduction of UHMWPE tibial insert stress and the optimization of insert wear behaviour.

7.9 Closure

This chapter discusses the computational investigation of prosthetic knee-bearing material mechanical reactions during the gait cycle. The current study also predicts the material's wear rate and contact pressure distribution. The following chapter examines the bearing material's mechanical and chemical properties under identical knee joint loading conditions.

CHAPTER 8

EXPERIMENTAL STUDY OF PROSTHETIC KNEE-BEARING MATERIAL (UHMWPE)

8.1 Introduction

This chapter discusses a novel technique used to incorporate material heterogeneity in prosthetic knee-bearing material. In actuality, cartilage structure is heterogeneous, and the third and fourth chapter shows the importance of heterogeneity in the knee joint's mechanical response. Conventionally, the bearing material for knee implants (UHMWPE) is homogeneous. Incorporating heterogeneous characteristics into the bearing material may improve the mechanical properties of the implant. Using gamma irradiation, the suggested model develops property-modulated features in the bearing material, which are then included in the knee implant. UHMWPE's tribological and chemical properties are experimentally analysed, and the wear rate and volume are estimated.

8.2 Radiation crosslinking (γ ray)

Radiation cross-linking is a vital technique to enhance the UHMWPE's wear resistance (Baena et al. 2015; Dhar Badgayan et al. 2020). Studies suggested in vitro (McKellop et al. 1999; Muratoglu et al. 2003), and in vivo cross-linking of UHMWPE has been effectively utilised to reduce wear (Digas et al. 2007). The cross-linking of UHMWPE is accomplished through ionising radiation (gamma or electron beam) (Charlesby and A 1952). Irradiation of UHMWPE generates free radicals by radiolytically cleaving C-H and C-C bonds in polyethylene, the majority of which recombine to form cross-links in the amorphous region of the polymer shown in Figure 8.1. The red dots are the new crosslinks formed after irradiation. The uncombined free radicals (green dots in Figure 8.1) generated get trapped in the amorphous area, and the oxidation of those residual free radicals cause degradation of mechanical properties (Oral et al. 2008). Radiation

cross-linking followed by heat treatments and antioxidant additives are used to overcome the oxidation stability and bearing performance (Muratoglu et al. 1999, 2003; Oral et al. 2010).

Conventional polyethylene is replaced by first-generation HXLPE with annealing or remelting thermal treatment to improve wear resistance and minimise oxidation. Second-generation annealed HXLPE has been created to enhance first-generation annealed HXLPE in terms of oxidative resistance, low wear, and mechanical strength (D'Antonio et al. 2012; Dumbleton et al. 2002). A second generation HXLPE (X3, Stryker, USA) were cross-linked in three cycles by a sequential irradiating and annealing procedure (total radiation dose was 90 kGy). This method increases the number of cross-links. Compared to the first-generation annealed material, a 60% reduction in wear is observed (Dumbleton et al. 2002).

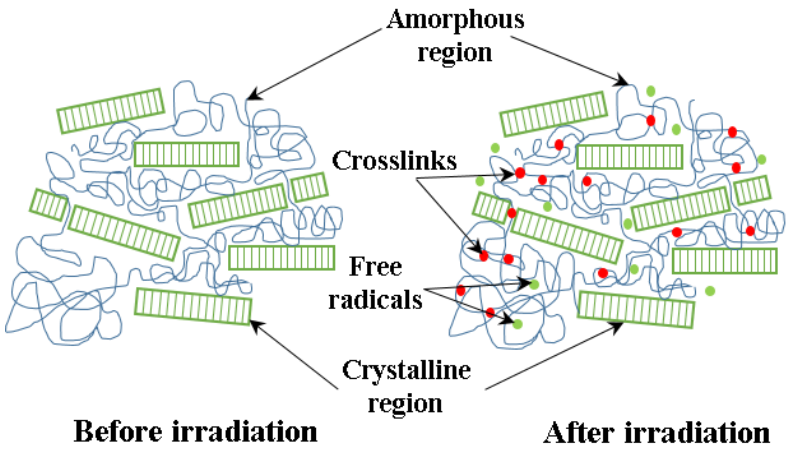

Figure 8.1 Crosslinking of UHMWPE samples using gamma irradiation

Currently, thermal annealing below the material's melting point is employed to stabilise cross-linked UHMWPE and eliminate free radicals. Melting after radiation cross-linking reduces leftover free radical concentration to undetectable levels and prevents long-term oxidation. However, melting diminishes the irradiated polymer's crystallinity and mechanical characteristics (Oral et al. 2006). Stabilizing radiation-induced free radicals with vitamin E can help build an oxidation-resistant UHMWPE and improve the fatigue properties of cross-linked UHMWPE without post-irradiation melting (Bracco and Oral 2011). Enhancing the longevity of implants is the primary emphasis of the research on highly cross-linked UHMWPE right now.

8.3 Methodology

8.3.1 Materials and sample preparation

Ram extruded virgin UHMWPE rod (GUR 1020 medical grade) of 70 mm diameter, and 500 mm length is procured from Orthoplastics Ltd. (Lancashire, UK). Multiple samples of 35 mm diameter and 12 mm thickness are cut from the rod for radiation crosslinking of UHMWPE using a CNC lathe, shown in Figure 8.2.

Figure 8.2 Samples prepared from ram extruded UHMWPE by CNC machining

8.3.2 Preparation of cross-linked UHMWPE

It is hypothesised that the physical property modulation of UHMWPE is achieved through gamma irradiation of UHMWPE samples through the led block cage (40 x 40 x 36 mm) with holes. A schematic of irradiation used for the present investigation is shown in Figure 8.3. A lead block cage is built with the top surface having a pattern of holes and a cavity beneath for keeping samples. The cage's thickness is designed so that the amount of gamma irradiation that falls on the sample from all directions is equal except the top surface. Five different samples such as (exposure through a 2 mm hole pattern, exposure through a 1.5 mm hole pattern, exposure through a 1 mm hole pattern, top surface exposure and full exposure) are prepared by gamma irradiating UHMWPE samples with different configurations such as lead block surface with 1 mm, 1.5 mm and 2 mm holes, with no lead shield above the top surface of the sample, and without lead block cage. Then the samples are irradiated at lower, moderate and high doses (30 kGy, 100 kGy and 150 kGy, respectively) using gamma rays from a Co-60 source at Microtrol Sterilisation Services Pvt. Ltd. Bangalore, India.

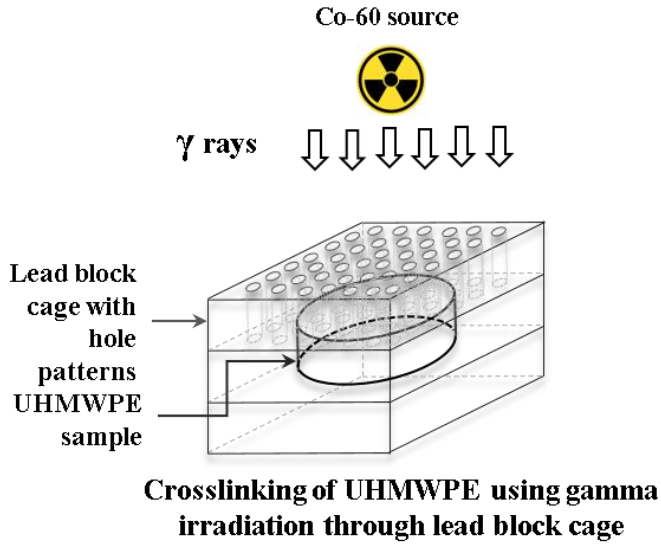

Figure 8.3 Irradiation of UHMWPE samples through lead block with hole patterns

8.3.3 Calculation of thickness for lead block

The thickness of the lead block cage is critical, and its value was chosen as the same as the half-value layer (HVL) for lead from the Cobalt-60 source. The linear attenuation varied with the density of the absorber, and the amount of gamma rays that come out from the absorber can be controlled with the density and thickness of the material. The thickness of the absorber can be calculated based on the attenuation law given by Equation 8.1.

$$\frac{I_x}{I_0} = e^{-\left(\frac{\mu}{\rho}\right)x} \tag{8.1}$$

where I_o = initial intensity, I_x = intensity after path length, ρ = mass density of element, μ = mass attenuation coefficient, and x is the shield thickness. The attenuation coefficient describes the attenuation of radiation as it passes through the matter (g/cm^2), ρ is the density of the lead (11.35 g/cm^3). Two wavelength gamma rays are emitted from the Cobalt-60 source, and the energy of the rays is 1.17 MeV and 1.33 MeV. For the present calculation, an approximation of 1.25 MeV is used for the average energy. The mass attenuation coefficient for the lead block can be obtained from the mass attenuation vs photon energy (MeV) chart from the NIST standard chart through the interpolation technique (Gual et al. 2017; J. H. Hubbell and S. M. Seltzer

1995). To obtain half the irradiation intensity, the initial intensity is set to 1, and the intensity after the path length is set to 0.5. The mass attenuation coefficient for the lead at 1 MeV is $7.102 * 10^{-2} \frac{cm^2}{g}$ and for 2 MeV is $4.606 * 10^{-2} \frac{cm^2}{g}$. Using Equation 8.1 and interpolation technique the thickness of the thickness of the lead is calculated 11.5 mm. The thickness of the lead cage the present investigation was selected as 11.5 mm based on the attenuation law.

8.4 Mechanical characterisation

A number of tribological parameters, including friction coefficient (COF), wear volume, and wear rate, are investigated for the cross-linked UHMWPE material. Additionally, the surface hardness of the irradiation samples is evaluated by comparing the values obtained from exposed and unexposed regions. Also, the storage and loss modulus of the material is measured to understand the stiffness

8.4.1 Wear and friction measurement

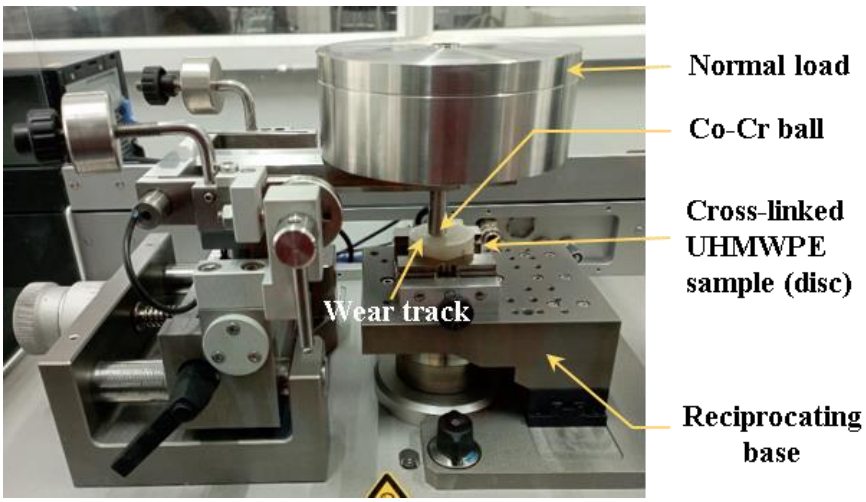

Figure 8.4 The gamma-irradiated UHMWPE sample mounted on a reciprocating tribometer

The tribological characteristics, such as wear volume and wear rate of the samples, are measured using a linear reciprocating tribometer (TRB-3, Anton Paar GmbH, Austria), as shown in Figure 8.4. Fifteen samples are created using irradiation doses of 30, 100,

and 150 kGy. The samples are subjected to a ball-on-disc test with a normal force of 40 N, resulting in normal contact pressure of nearly 6 MPa, within the computationally estimated range of the maximum pressure generated in the knee joint. The amplitude used for the present investigation is 600 mm with a maximum linear speed of 13.19 cm/s. A frequency of 7.00 Hz is selected, with a data acquisition rate of 80.00 Hz used in the study. For the wear analysis, the metal-on-polymer test is employed, with the ball made of Co-Cr and the disc made of UHMWPE to simulate actual conditions. The wear track area is measured using the instrument's attached profilometer as the ball reciprocates over polymer for up to 1 lakh cycles (1,200 meters). The track area and width are used to compute the wear rate and volume. Similarly, the friction coefficient is measured from the tribometer for the same number of cycles and from the same wear track.

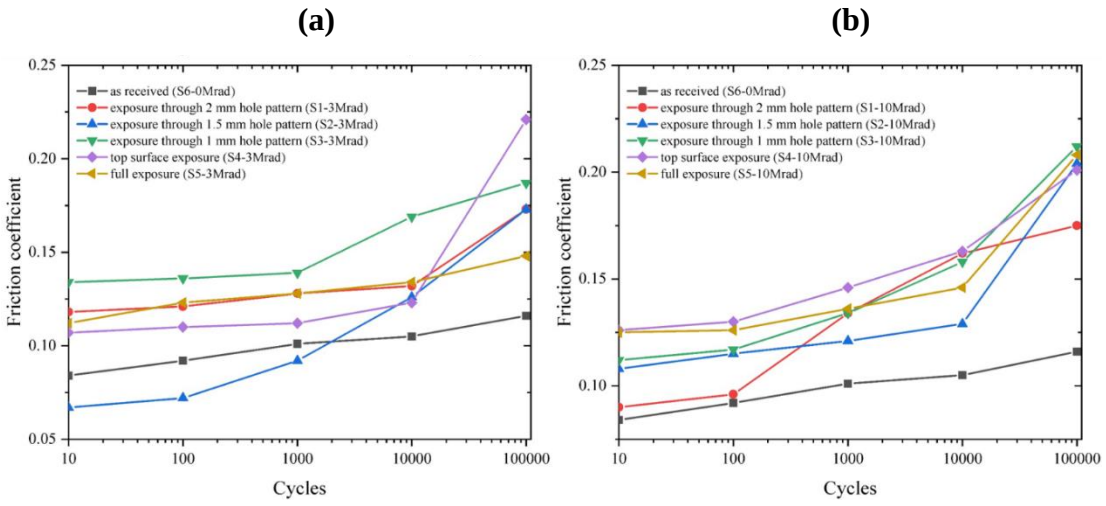

Figure 8.5 The comparison of coefficient of friction for lower and higher irradiation dose (a) lower irradiation dose 30 kGy (b) higher lower irradiation dose 150 kGy

Several tribological measurements, including friction coefficient (COF), wear volume and wear rate, are used to test the wear resistance of cross-linked UHMWPE. The friction coefficient is plotted against the number of cycles and compared with low and high irradiation doses. It is observed the coefficient of friction increases as the radiation dose increases; however, samples exposed through a 1 mm hole pattern exhibit a lower

friction coefficient than other models shown in Figure 8.5. The cross-linked samples have higher COFs and lower wear rates compared with as received virgin UHMWPE.

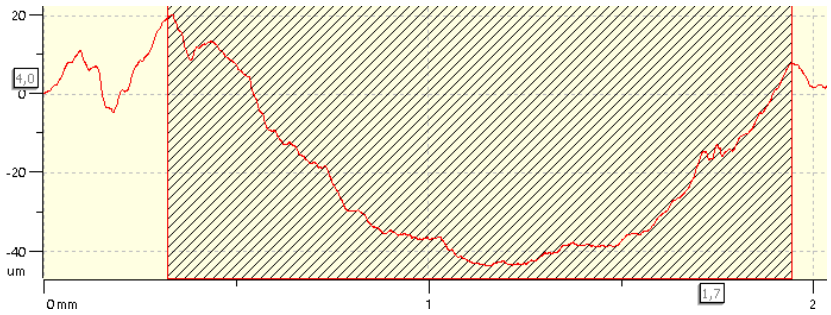

Figure 8.6 Profile of the wear track on the sample for 1 x 10^5 cycles obtained from profilometer

The wear track profile is captured using a profilometer, and the cross-section area of the profile is measured from the profilometer spectrum, as shown in Figure 8.6 for 1x10^5 cycles. The width and depth of penetration are measured from the profile, and the wear volume is measured. The wear rate/wear factor for all samples is calculated using Equation 8.2.

$$K = \frac{V}{F_n * L} \tag{8.2}$$

where V is the wear volume measured from the profilometer, F_n is the normal force applied (40N), and L is the sliding distance. For 1x10^5 cycles, 1200 m is the sliding distance considered for the calculation. The wear volume and wear rate for all the samples are calculated and plotted.

The calculated wear volume with respect to the number of cycles is plotted and shown in Figure 8.7. The wear volume is observed lower for irradiated samples with regard to as received samples. Also, exposure through 1 mm hole pattern samples shows a reduction in wear volume compared to fully exposed samples. The improved wear resistance mainly results from the property modulation technique achieved, as hypothesised in the study.

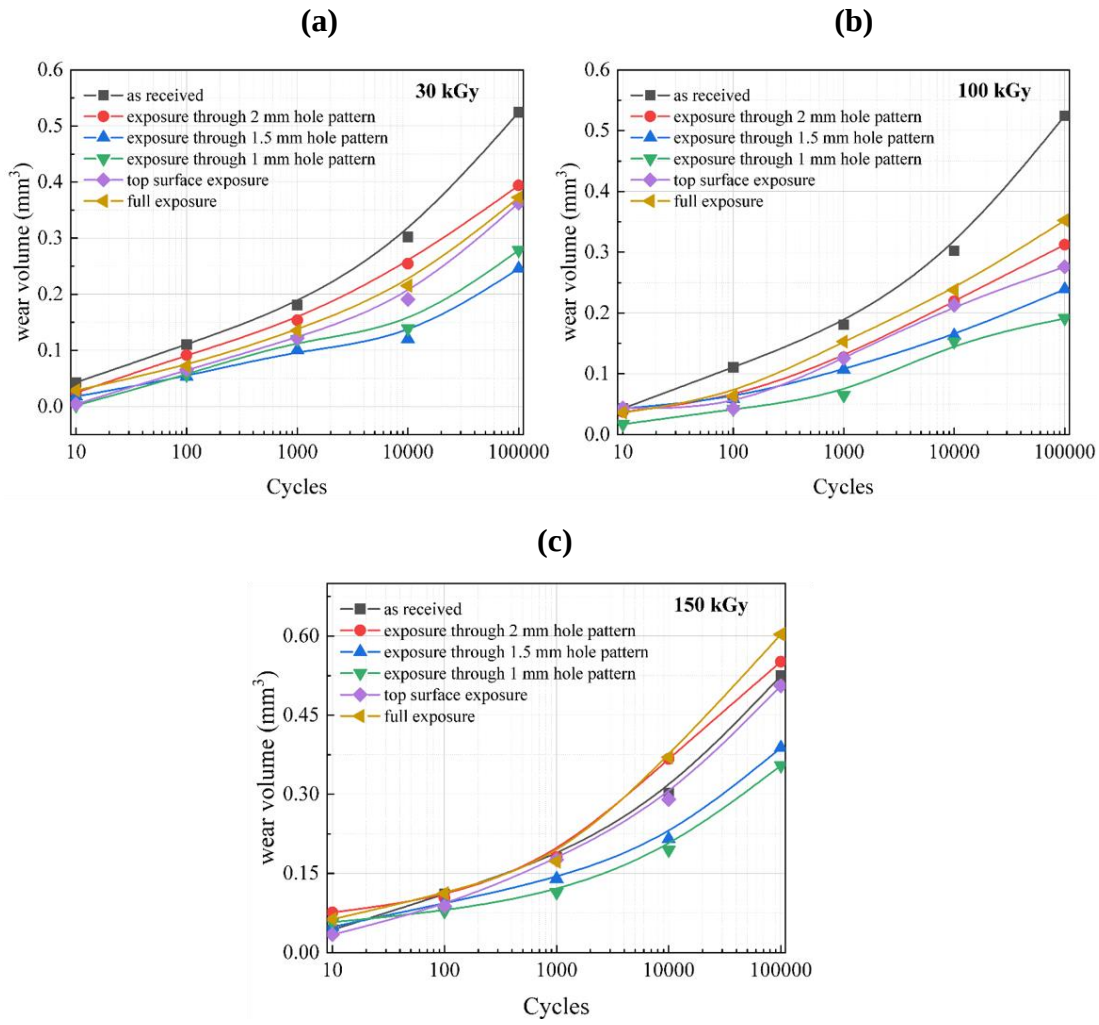

Figure 8.7 The wear volume plotted against the number of cycles obtained from the samples irradiated (a) low dose, (b) moderate dose and (c) high dose.

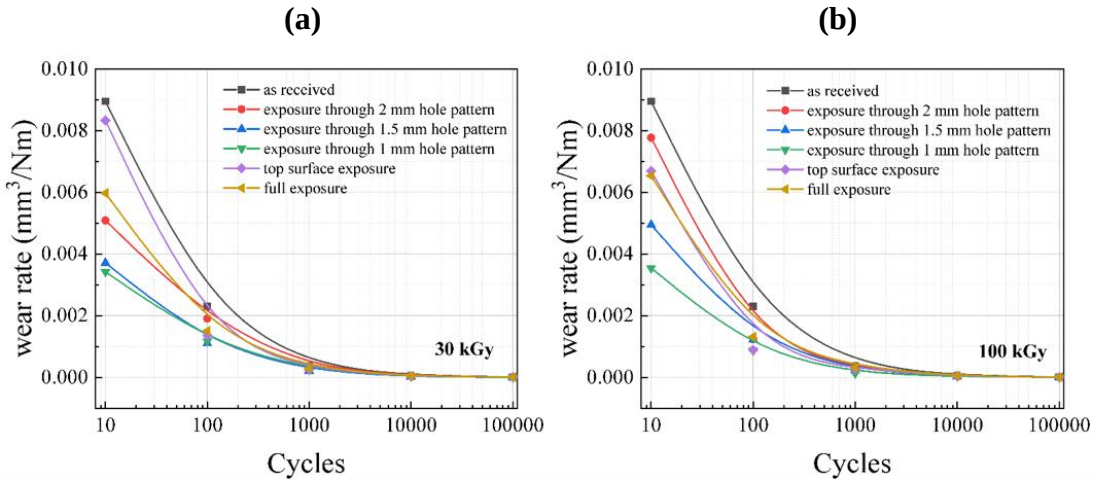

(c)

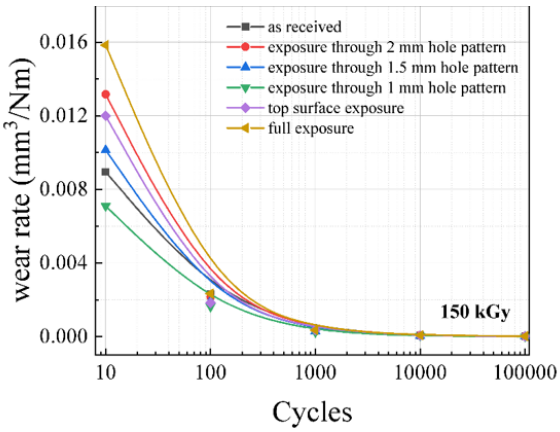

Figure 8.8 The wear rate/wear factor of UHMWPE obtained for different radiation dose levels (a) low dose, (b) moderate dose and (c) high dose.

Similarly, the wear rate is calculated and plotted against the number of cycles shown in Figure 8.8. It is observed there is a reduction in wear for irradiated samples compared with as received ones. Also, the samples exposed through a 1 mm hole pattern show less wear than other samples. Also, for a higher dose (150 kGy) wear rate is higher than as received samples which are not advised.

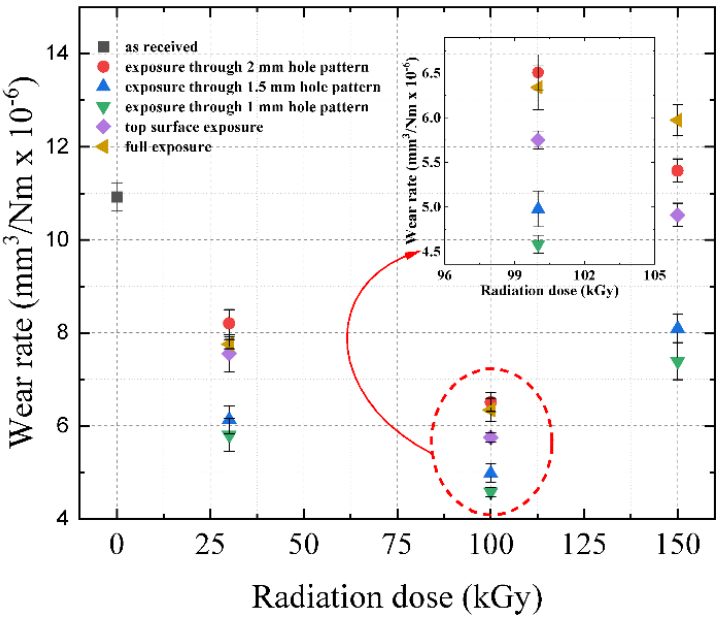

Figure 8.9 The wear rate/wear factor of UHMWPE obtained for different radiation dose levels at $1x10^5$ cycles

The wear rate/wear factor versus the radiation dose is plotted in Figure 8.9. The wear rate decreases as the dose increase to 100 kGy and then increases at higher doses. The wear rate of virgin UHMWPE as received is 11.05 x 10^{-6} mm^3/Nm, and it has been reduced up to 4.6 x 10^{-6} mm^3/Nm with an irradiation dose of 100 kGy. In addition, samples with a 1mm hole pattern exhibit a more significant reduction in wear rate than other samples. It is seen that the sample at a higher dose (150 kGy) demonstrates a higher rate of wear than the sample received, which is not advised.

8.4.2 Hardness measurement

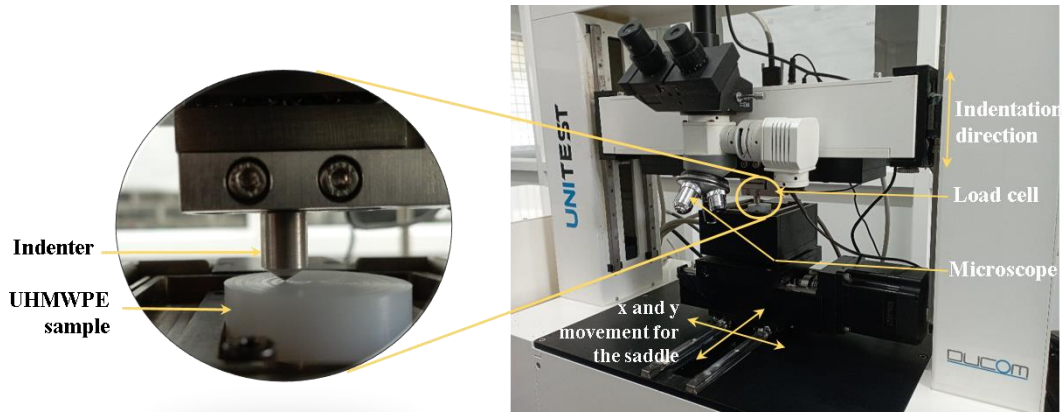

Figure 8.10 The hardness of UHMWPE is measured using the indentation test

The surface hardness is measured using the Rockwell hardness method on the UNITEST scratch testing configuration (Ducom, India), shown in Figure 8.10. A Rockwell cone-type diamond stylus of 120 degrees and 200-micron radius is used for the hardness measurement. The indentation test is performed on the exposed and unexposed regions on the sample surface. All samples are tested for a 5 N load at a loading rate of 1 N/s. The indentation diameter is measured using a digital microscope attachment, and the Rockwell hardness number is calculated from the indentation depth using the following Equation 8.3.

$$HR = N - \frac{d}{s} \tag{8.3}$$

HR is the Rockwell hardness number, and N and s are scale factors depending on the test being used. The value of N is either 100 or 130, depending on the Rockwell

hardness scale used. Similarly, the value of s is either 0.001 mm or 0.002 mm, and d is the penetration depth measured from zero points (in mm).

The microhardness test is performed for 5, 10 and 50 N indentation loads. The indentation dimension is measured from a digital microscope setup attached to the apparatus. The indentation under 5N load is captured and measured as shown in Figure 8.11. These values help in approximating the hardness values. For more precise readings, calculate Rockwell hardness values using Equation 8.3. Similarly, hardness tests are conducted on each sample, and indentation impressions are recorded.

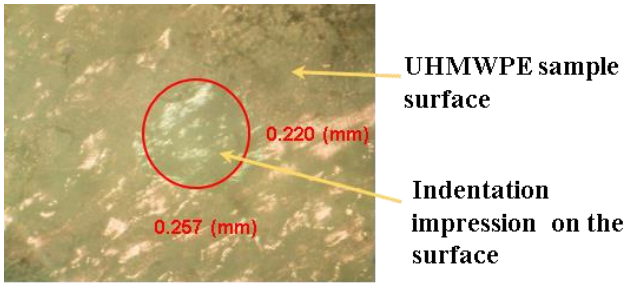

Figure 8.11 The digital microscopic view (10x) of the indentation under 5N load on the UHMWPE surface

The indentation test is performed on the exposed and unexposed regions for all the samples. The Rockwell hardness values are calculated from surface locations with and without radiation exposure and plotted with surface points, as shown in Figure 8.12. As received samples show a lower hardness than irradiated ones, top-exposed and full-exposed samples show the maximum hardness. The samples with exposure through a lead hole block show a non-uniform hardness on the surface, indicating that the physical property modulation of UHMWPE is achieved using the proposed novel technique.

The penetration depth of the indenter is compared for all the samples at 5N, 20N and 50N indentation loads, respectively, as shown in Figure 8.13. As the irradiation dose increases, the penetration depth decreases, indicating that the hardness increases as the exposure increases. At 5N indentation load, a maximum depth of 56 μm is found for the unirradiated sample. As radiation exposure increases to 150 kGy, the indentation

depth for a fully exposed sample becomes 39 μm. Consequently, a 30% reduction in indentation depth relative to as received samples. In addition, a comparison of each sample reveals that exposure through a hole pattern has a higher hardness than full exposure. And a 1.5 mm hole pattern indicates a difference of 28% between the low and high dose levels. Figures 8.13 (b) and (c) depict similar trends for 20N and 50N indentation loads, respectively. It implies that the material's hardness represents its resistance to wear, and as the irradiation dose increases, the material's hardness increases while its toughness decreases.

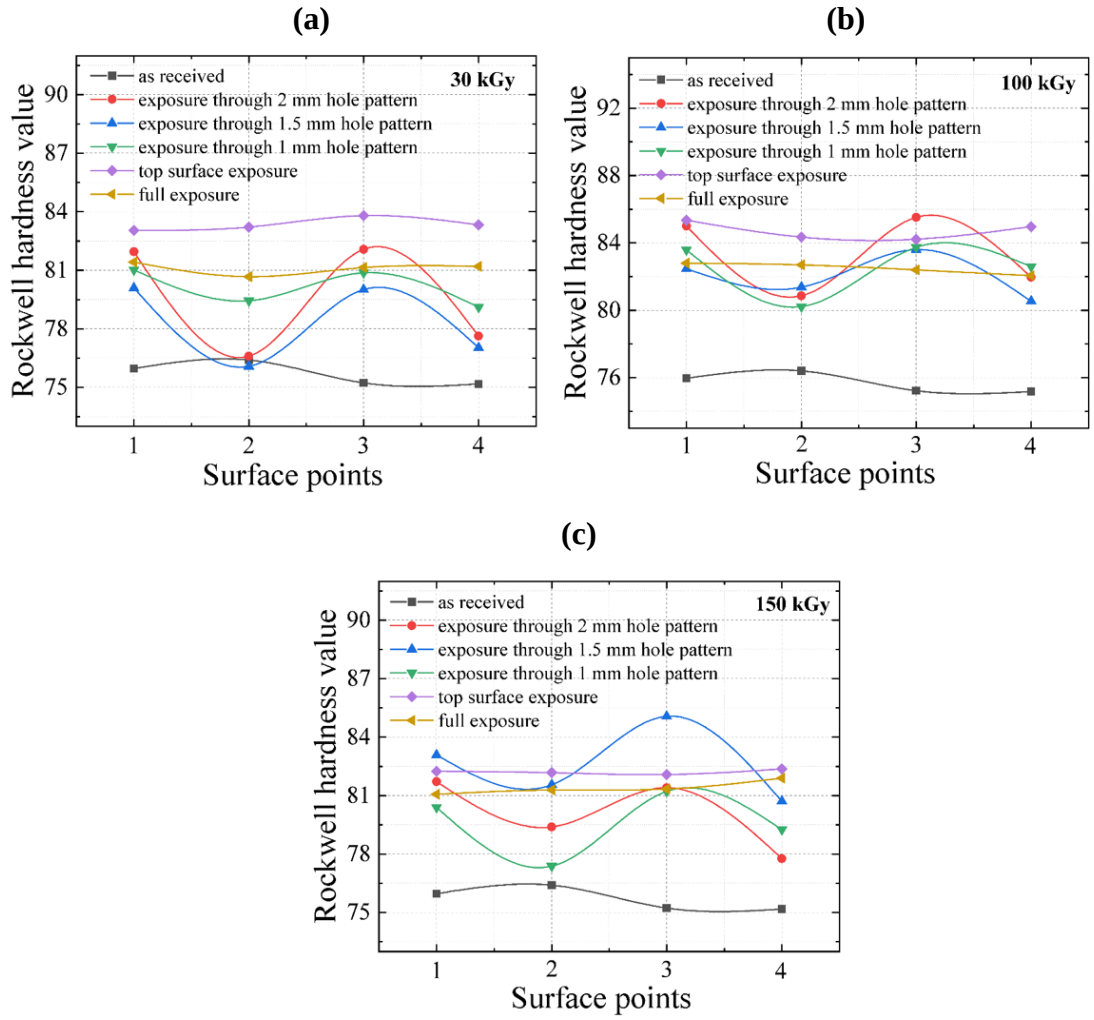

Figure 8.12 The Rockwell hardness values on the surface of different samples at different irradiation dose levels (a) low dose, (b) moderate dose and (c) high dose.

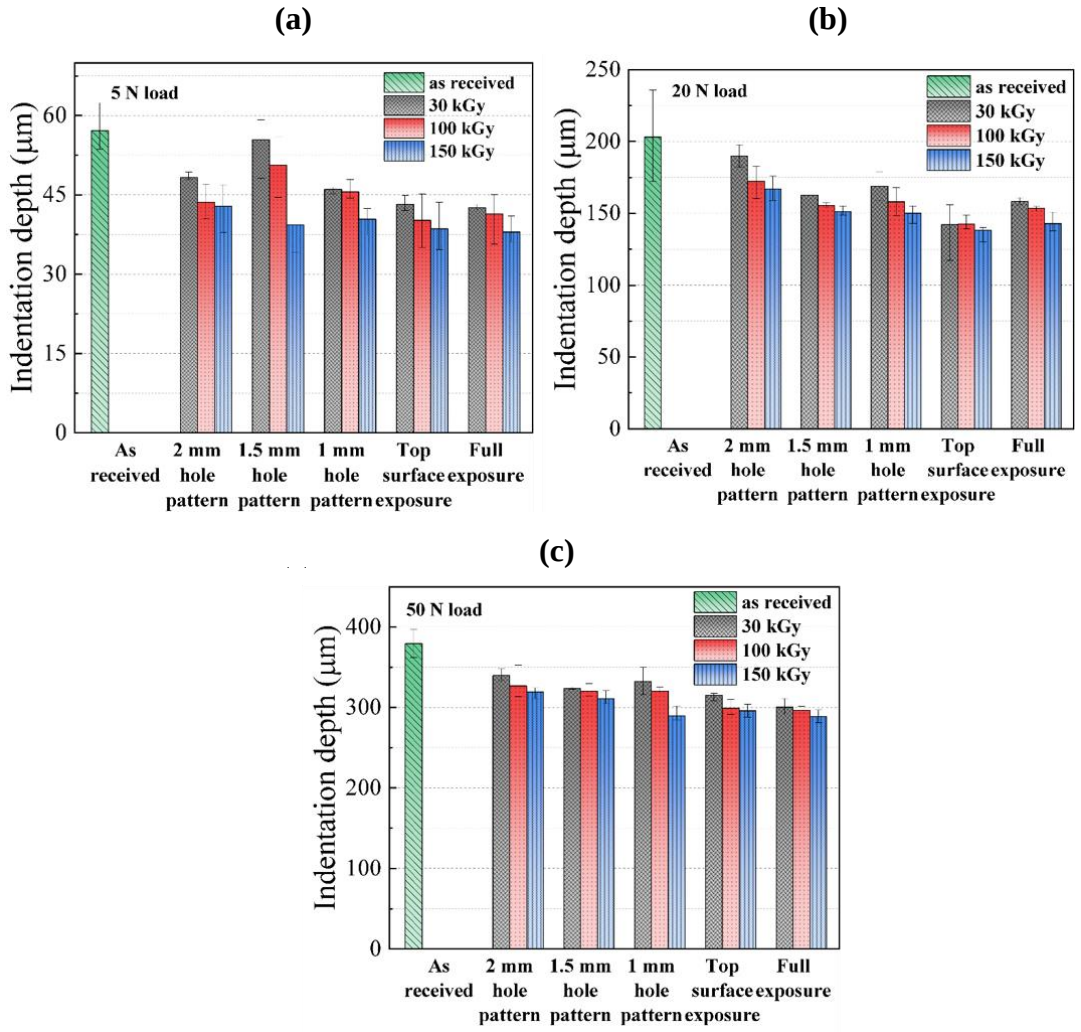

Figure 8.13 The comparison of indentation depth with respect to the irradiation dose (a) 5N indentation load, (b) 20N indentation load, and (c) 50N indentation load.

8.4.3 Storage and loss modulus

Dynamic mechanical characteristics of the UHMWPE, such as storage and loss modulus, are calculated using the dynamic mechanical analysis (DMA) technique. Three thin films are sliced from each sample using a fully automated rotary microtome (Leica RM2255, Wetzlar, Germany) of 50 μm thickness. From each film, a strip is cut 20 mm in length and 4.1 mm in width using a cutting die with two adjustable parallel blades. The DMA analysis of the specimen is performed on a discovery hybrid rheometer (DHR-20, TA Instruments, New Castle, DE, USA), as shown in Figure 8.14. Samples are mounted in the testing chamber with an initial gauge length of 16 mm.

The temperature is swept from 25^0 C to 175^0 C at a constant rate of 3^0C/min. The strain is modulated up to 0.2% at a rate of 1 Hz.

Figure 8.14 The DMA analysis of UHMWPE thin film using a dynamic hybrid rheometer

The storage modulus indicates the material's capacity to store the energy of external forces without permanent deformation. Consequently, a more significant storage modulus is related to a material's more excellent elasticity and stiffness. Also, according to ISO 6721, the loss modulus represents the viscous response of a material by measuring the energy dissipated during a loading cycle (Dayyoub et al. 2019). This has to do with the stress and elongation of the materials. The storage and loss modulus are measured and plotted in Figure 8.15. The storage modulus value is increased by analysing the graphs for low, moderate, and high irradiation doses. Also, as the temperature rises from 25^0C to 175^0C, the storage modulus decreases to a particular temperature (approximately above 70^0C) and then continues at an approximately constant value.

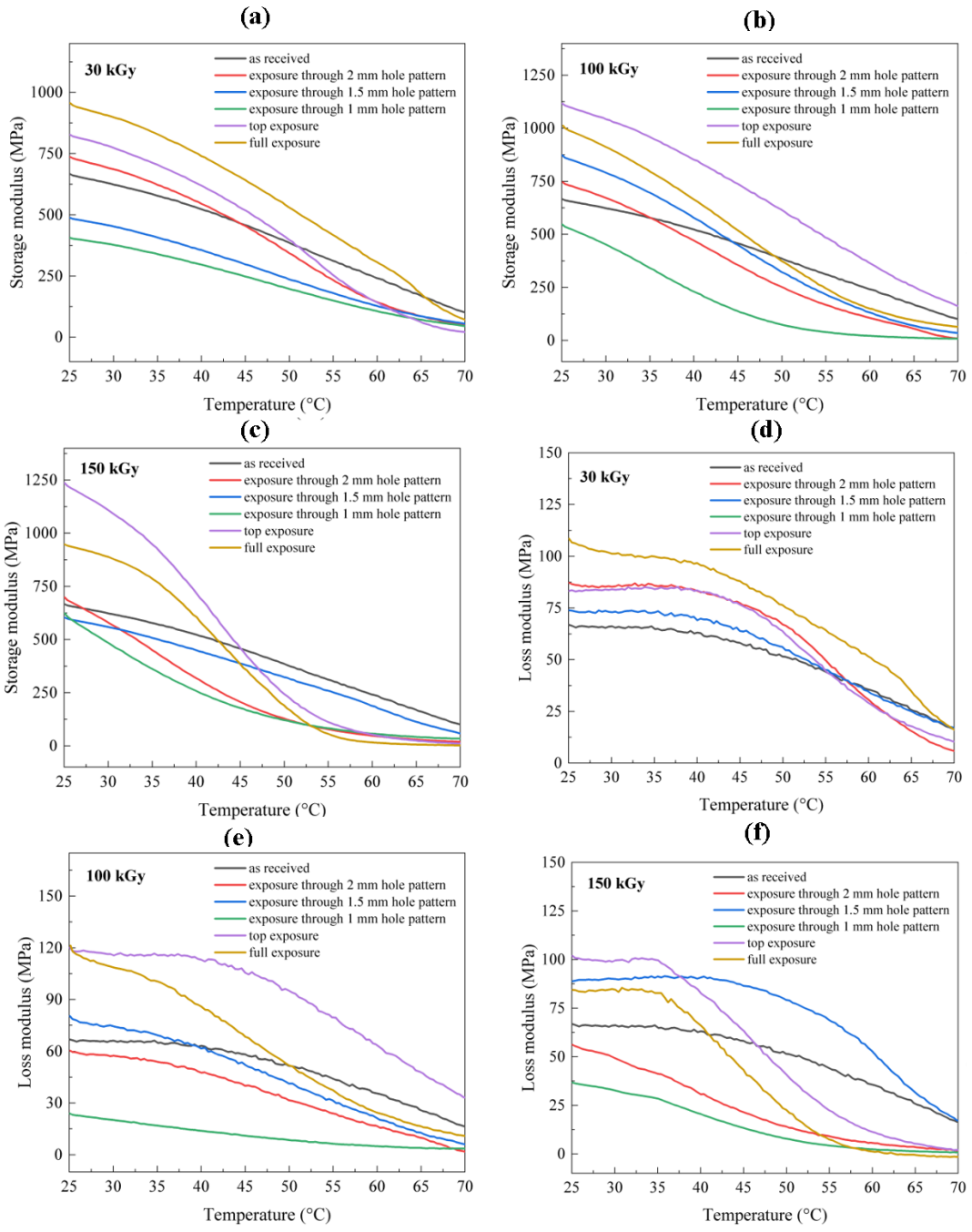

Figure 8.15 (a-c) The storage modulus of samples at 30, 100 and 150 kGy (d-f) the loss modulus of samples at 30, 100 and 150 kGy

As shown in Figure 8.15 (a-c), the initial storage modulus for the top exposed sample is 810 MPa at 30 kGy irradiation and reached up to 1250 MPa for 150 kGy. In addition, samples exposed through a 1mm hole pattern had a lower storage modulus than other samples at all irradiation dose levels. Therefore modifying the material with irradiation

could increase the mechanical resistance of the material, leading to a decrease in its toughness. Similar trends are observed for loss modulus shown in Figure 8.15 (d-f). Compared to all other samples, the exposure through hole pattern samples has a lower value, implying that viscous response is more inadequate, and less energy is lost through the sample.

8.5 Chemical characterisation

The chemical properties of each sample, including crosslink density, molecular weight, and oxidation index, are analysed and compared. The two most prevalent techniques for chemical characterization are dynamic mechanical analysis (DMA) and Fourier transform infrared spectroscopy (FTIR).

8.5.1 FTIR analysis

Fourier Transform Infrared Spectroscopy (FTIR) is utilized in the present work (Spectrum 2 FTIR Spectrometer, Perkin-Elmer, USA) to measure the chemical structure of UHMWPE. The same microtomed UHMWPE thin films of 50 μm and 1mm x 1 mm is used. The sample is positioned on a micro-FTIR device's FTIR bench or microscope stage as per ASTM F2102 and F2381 standards. The ATR mode is selected since the sample is solid and a minimum of twelve scans is performed, and their average should be compared to a white background.

Table 8.1 Prominent FTIR bands of UHMWPE and its oxidised species.

Band region (cm^{-1})	**Functional groups**	**Source**
800 – 1000	Unsaturated C = C	(Azam et al. 2016; Kwak et al. 2009; Rocha et al. 2009; Spiegelberg et al. 2016)
1100 - 1400	Ethers and C – O – C group	
1600	COO	
1650,1850	C = C	
1727	Carbonyl species (ethers, esters and ketones) C – O	
3300, 3695	OH	

The spectrum is collected in transmission mode, ranging from 4,000 to 400 cm^{-1}. Figure 8.16 shows the FTIR spectrum of all the samples at 30, 100 and 150 kGy irradiation doses. The spectrum confirms the evidence of functional groups such as hydroperoxides, carbonyl species, ethers and other unsaturated bonds in Table 8.1.

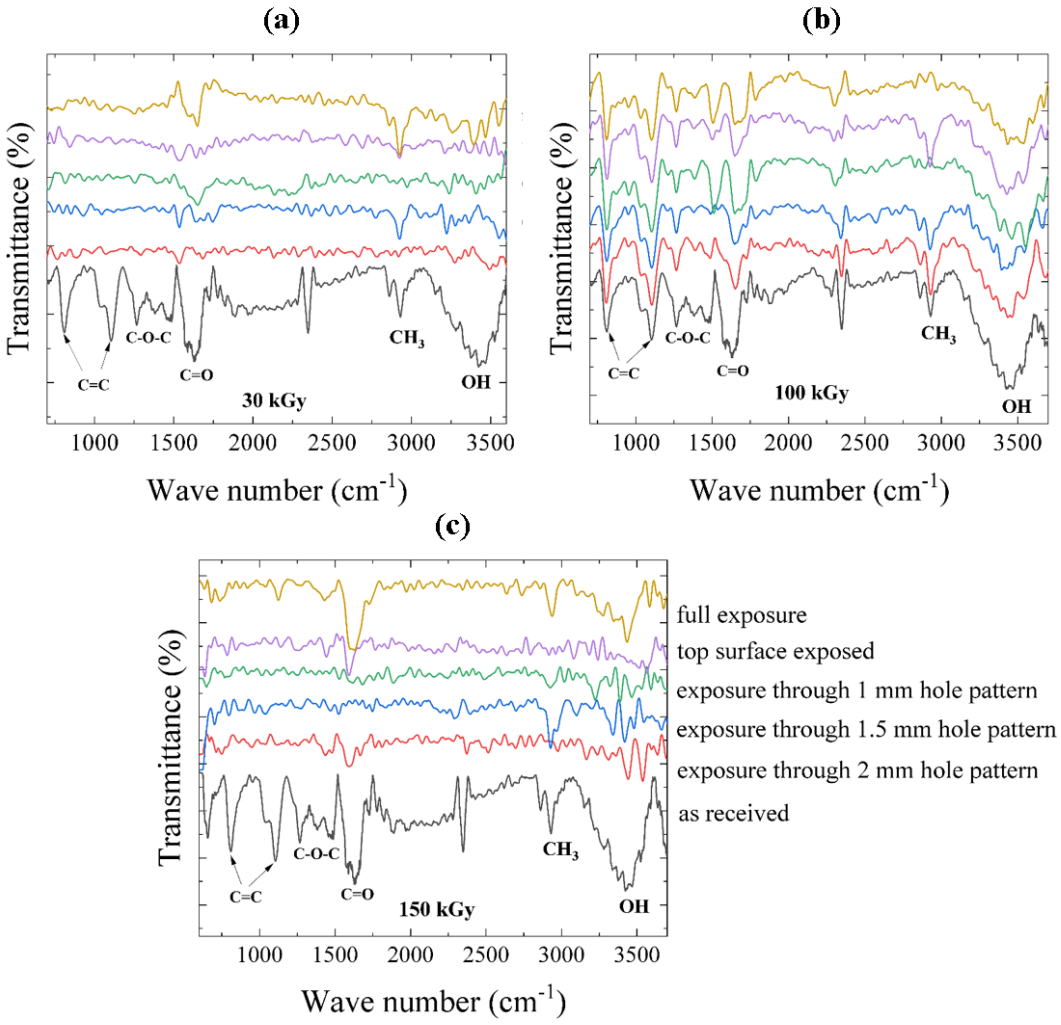

Figure 8.16 The FTIR spectrum for all the UHMWPE samples at different irradiation (a) 30 kGy dose (b) 100 kGy dose (c) 150 kGy dose

From Figure 8.16, the transmission at 910 cm^{-1} owing to the terminal vinyl group indicates evidence of deterioration. Typically, a terminal vinyl group suggests that the polymer chain has been broken. The amount of radiolytic transvinylene groups in UHMWPE is proportional to the number of cross-links generated when the material is exposed to ionising radiation. The spectral differences between as-received and

irradiated samples were significant in the 3300-3695 cm^{-1} and 1670-1775 cm^{-1} areas. The low and narrow transmittance peaks of about 3695 cm^{-1} were attributed to alcohols and hydroperoxides without hydrogen bonds. Hydrogen-bonded hydroxyl groups, including alcohols, hydroperoxides, and carboxylic acids, are attributed to the broad transmittance band around 3300 cm^{-1}.

8.5.2 Cross-link density and molecular weight

DMA is an alternative technique to determine the cross-link density and molecular weight between cross-links rather than the gravimetric gel swell chemical analysis technique (Reinitz et al. 2015). Storage modulus (E') in the rubbery plateau is defined as the storage modulus at 160^0C. Molecular weight (M_c) and the cross-link density (ν_d) are calculated using Equations 8.4 and 8.5.

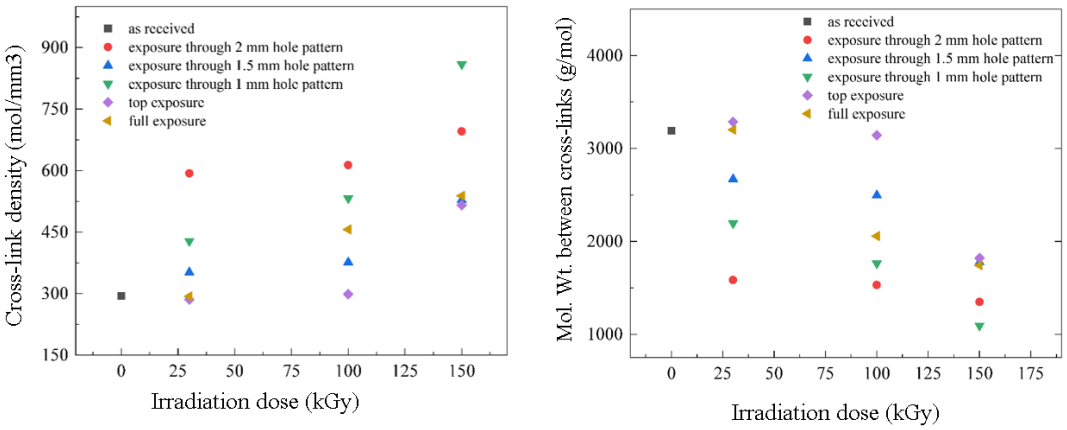

Figure 8.17 The crosslink density and molecular weight between crosslinks against the irradiation dose

$$M_c = \frac{2(1+\nu)\rho RT}{E'} \tag{8.4}$$

$$\nu_d = \frac{1}{M_c \nu'} \tag{8.5}$$

where ρ is the density of the amorphous polymer (for UHMWPE, ρ = 0.94 g/cm^3), R is the gas constant (8.314 J/molK), T is the absolute temperature (160^0C), E' is the

storage modulus, ν is the Poisson's ratio (ν = 0.4), and ν' is the specific volume of the polymer (Chen et al. 2018).

Molecular weight (Mc) values ranged from 3300 g/mol for 30 kGy to 1100 g/mol for 150 kGy irradiation dosage as determined by DMA, as shown in Figure 8.17. Our findings can be validated by comparing them to earlier experimental studies (Reinitz et al. 2015). In their research, the maximum molecular weight ranges from 1850 to 1380 g/mol, while the radiation dose ranges from 35 to 200 kGy. The study confirms the molecular weight decreases ad the irradiation dose increases. In addition, when comparing various samples, physical property-modified samples had a lower molecular weight than conventionally treated samples. The density of crosslinks is inversely proportional to the molecular weight, with property-modulated samples possessing more crosslinks than fully exposed materials.

8.5.3 Oxidation index

Oxidation levels were quantified as a function of depth from a free surface. Oxidation levels were expressed as an oxidation index, and the total oxidation level is determined by FTIR according to ISO 5834 and ASTM Standard F648, as shown in Equation 8.6. A_O is the integrated area from 1650 cm^{-1} to 1850 $cm^{-1,}$ referred to as the ketone (C=O) group transmittance band, and A_R is the integrated area referred to as the methyl group from 1330 cm^{-1} to 1396 cm^{-1}. The areas are calculated using the software Origin Pro Program, version 9.8.

$$I_{ox} = \frac{A_O}{A_R} \tag{8.6}$$

The oxidation index for all the samples at different radiation doses is plotted and shown in Figure 8.18. Conventional UHMWPE showed a lower oxidation index of 2.7, whereas irradiated UHMWPE showed a higher oxidation index of 7.0 on the surface. Interestingly, materials irradiated using the suggested technique have a lower oxidation index at greater doses than those irradiated using the conventional approach.

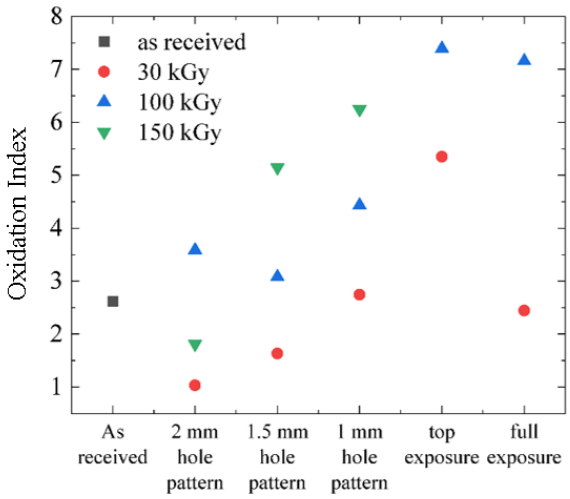

Figure 8. 18 The oxidation index calculated from the FTIR spectrum for all the UHMWPE samples at a different irradiation dose

8.6 Conclusions

The proposed novel approach achieves the physical property modulation of UHMWPE. The surface hardness from exposed and unexposed regions indicates non-uniformity in hardness on the surface. The wear rate and wear volumes show good improvement compared with the conventional technique. The study suggests the wear rate decreases as the radiation dose increases to 100 kGy and then rises to 150 kGy. The results indicate the molecular weight increases as the irradiation dose increases. Also, the cross-link density of UHMWPE between molecules of the proposed model suggests that property-modulated material possesses more crosslinks than fully exposed material. Interestingly, materials irradiated using the proposed approach show a lower oxidation index at higher dosage levels than materials irradiated with the conventional technique.

8.7 Closure

This chapter discusses the experimental investigation of UHMWPE knee implant-bearing material to enhance wear resistance. The novel physical property modulation techniques improve the wear resistance and other mechanical characteristics. The next chapter discusses the summary of the work's conclusions and future scopes.

CHAPTER 9

CONCLUSIONS

This work focuses on the computational research of soft tissues and the effect of heterogeneity on the knee joint's mechanical response. Also implemented material heterogeneity in TKR bearing material of total knee replacement knee implants and examined the responses experimentally after implementation. **Chapter 1** described the introduction of knee problems, soft tissue microstructure, knee implants' components, and the importance of knee implants for osteoarthritis patients. **Chapter 2** provided a concise literature review on the computational techniques of articular cartilage mechanics in knee joint analysis and the various methods used to enhance the design and durability of knee implants from the past to the present. Literature-identified research gaps contributed to the development of the objectives for this study.

The computational study of the knee joint and the influence of soft tissues in knee kinematics is investigated using the finite element simulation. A graded material is modelled and analysed for the mechanical response described in **Chapter 3.** The results suggest the proposed graded implant material can be used as an implant material for osteoarthritis patients. Also, these discoveries and proposals are applicable in biomechanical models to investigate treatments (surgical or traditionalist) related to knee osteoarthritis. **Chapter 4** further discussed the investigation of mechanical responses of knee joint soft tissues during the gait cycle. The contact pressure, effective Lagrange strain, maximum shear stress, effective stress, and total displacement are compared on all soft tissues. The discoveries might contribute to developing comprehensive computational tools that help us better understand the causes of knee injury and illness.

Chapter 5 briefly describes the influence of different constitutive material models in the mechanical response of the cartilage model; the peak cartilage contact pressure induced by the knee joint with the heterogeneous material model is lower than in the

homogeneous model. The poroelastic cartilage model can help estimate anterior/posterior deformation, whereas the TIE model is suitable for understanding proximal/distal deformation limits. The maximum change in stresses and strains are observed in TIE models than in IE and IPE models.

Chapter 6 explains the computational study on the influence of soft tissues in knee kinetics/kinematics for intact and arthritic cases is investigated. The study presents a novel method to control collagen fiber orientation for FRPHE cartilage models for knee joint analysis. This study suggests that maximum stresses are obtained for models with parallel split-line walking and proximal-distal split-line while running gait. However, the effective Lagrange strain and maximum principal strain behave similarly for both intact and OA models throughout the stance phase; the OA cartilage has higher contact pressure and stress than the intact model. These results will aid researchers in developing improved assistive devices and implant material for arthritis patients who engage in subject-specific activities such as walking and running.

The modelling of knee prostheses and the enhancement of mechanical properties through design modifications relative to conventional knee prostheses is described in **Chapter 7.** The investigation successfully determines the link between TKR implant designs and bearing material mechanical responses. The model's sensitivity is demonstrated by the ability to detect changes in kinematic patterns due to curvature modifications in implant design. It will now be used to study a variety of additional design concerns, such as decreasing UHMWPE tibial insert stress and optimising insert wear behaviour.

In reality, cartilage structure is heterogeneous, and the computer work demonstrates the significance of heterogeneity in the knee joint's mechanical response. Conventionally, the bearing material for knee implants (UHMWPE) is homogenous. Incorporating heterogeneous qualities into the bearing material may improve the mechanical properties of the implant. A novel physical property modulation technique for UHMWPE through gamma irradiation technique is discussed in **Chapter 8.** Utilizing the novel method suggested, the physical property modification of UHMWPE is accomplished. The surface hardness of exposed and unexposed regions

indicates that the surface hardness is not homogeneous. The wear rate and wear volumes demonstrate significant improvement over conventional techniques. The study shows that the wear rate reduces as the radiation dosage increases from 100 kGy to 150 kGy. The results also suggested that molecular weight increases with increasing irradiation dosage. In addition, the cross-link density of UHMWPE between molecules in the proposed model indicates that property-modulated material has more cross-links than completely exposed material. Interestingly, materials irradiated using the suggested method have a lower oxidation index at greater doses than materials irradiated with the conventional technique.

9.1 Future scope

The computational part presented in this thesis shows the investigation of soft tissue mechanical responses for intact and arthritic knee joint cases. However, some of the future scopes for the computational works are:

1. A more realistic cartilage model can be created by incorporating the inhomogeneous compressive modulus of the matrix and inhomogeneity in fluid content. The study may predict more accurate results compared with the current work.
2. A new knee model could be created from the present geometry by including the patella, patellar tendon, joint capsule, and tendons, which aids in predicting knee reactions by taking their effects into account.
3. A specimen-specific cartilage response of soft tissues can be predicted by recording the knee kinematics using the gait lab and inputting the corresponding gait data into the finite element model. Obtain the responses and compare them to the intact cartilage responses to predict the severity and progression of cartilage disease. Similarly, different specimen-specific model responses can be expected using the current model.

However, successful experimental work on the knee implant material has been completed, and the wear characteristics have been assessed using a tribometer; the scope of future experimental work is outlined below.

4. The proposed property modulation technique can be implemented on actual UHMWPE tibial inserts of commercially available knee implants, and the wear characteristics can be calculated using knee simulators.
5. It is hypothesised that a smaller hole pattern on the irradiation shielding material to provide the physical property modulation characteristic will produce better wear resistance than the current findings.
6. The wear data received from the ball-on-disc experimental data may be used for computational wear simulation.

REFERENCES

Abid, M., Mezghani, N., and Mitiche, A. (2019). “Knee joint biomechanical gait data classification for knee pathology assessment: A literature review.” *Appl. Bionics Biomech.*, 2019.

Adouni, M., and Shirazi-Adl, A. (2014). “Evaluation of knee joint muscle forces and tissue stresses-strains during gait in severe OA versus normal subjects.” *J. Orthop. Res.*, 32(1), 69–78.

Adouni, M., Shirazi-Adl, A., and Shirazi, R. (2012a). “Computational biodynamics of human knee joint in gait: From muscle forces to cartilage stresses.” *J. Biomech.*, 45(12), 2149–2156.

Adouni, M., Shirazi-Adl, A., and Shirazi, R. (2012b). “Computational biodynamics of human knee joint in gait: From muscle forces to cartilage stresses.” *J. Biomech.*, 45(12), 2149–2156.

Akagi, M., Asano, T., Clarke, I. C., Niiyama, N., Kyomoto, M., Nakamura, T., and Hamanishi, C. (2006). “Wear and toughness of crosslinked polyethylene for total knee replacements: a study using a simulator and small-punch testing.” *J. Orthop. Res.*, 24(10), 2021–7.

Allaire, R., Muriuki, M., Gilbertson, L., and Harner, C. D. (2008). “Biomechanical consequences of a tear of the posterior root of the medial meniscus: Similar to total meniscectomy.” *J. Bone Jt. Surg. - Ser. A*, 90(9), 1922–1931.

Anderson, A. E., Ellis, B. J., Maas, S. A., Peters, C. L., and Weiss, J. A. (2008). “Validation of finite element predictions of cartilage contact pressure in the human hip joint.” *J. Biomech. Eng.*, 130(5), 1–10.

Archard, J. F. (1953). “Contact and rubbing of flat surfaces.” *J. Appl. Phys.*, 24(8), 981–988.

Asano, T., Akagi, M., Clarke, I. C., Masuda, S., Ishii, T., and Nakamura, T. (2007).

"Dose effects of cross-linking polyethylene for total knee arthroplasty on wear performance and mechanical properties." *J. Biomed. Mater. Res. B. Appl. Biomater.*, 83(2), 615–22.

Ateshian, G. A., Wang, H., and Lai, W. M. (1998). "The role of interstitial fluid pressurization and surface porosities on the boundary friction of articular cartilage." *J. Tribol.*, 120(2), 241–248.

Azam, A. M., Ali, A., Khan, H., Yasin, T., and Mehmood, M. S. (2016). "Analysis of degradation in UHMWPE a comparative study among the various commercial and laboratory grades UHMWPE." *IOP Conf. Ser. Mater. Sci. Eng.*, 146(1), 012025.

Baena, J. C., Wu, J., and Peng, Z. (2015). "Wear performance of UHMWPE and reinforced UHMWPE composites in arthroplasty applications: A review." *Lubricants*, 3(2), 413–436.

Baker, D. A., Bellare, A., and Pruitt, L. (2003). "The effects of degree of crosslinking on the fatigue crack initiation and propagation resistance of orthopedic-grade polyethylene." *J. Biomed. Mater. Res. - Part A*.

Bao, H. R. C., Zhu, D., Gong, H., and Gu, G. S. (2013). "The effect of complete radial lateral meniscus posterior root tear on the knee contact mechanics: A finite element analysis." *J. Orthop. Sci.*, 18(2), 256–263.

Barbour, P. S. M., Barton, D. C., and Fisher, J. (1997). "The influence of stress conditions on the wear of UHMWPE for total joint replacements." *J. Mater. Sci. Mater. Med.*, 8(10), 603–611.

Baykal, D., Siskey, R. S., Haider, H., Saikko, V., Ahlroos, T., and Kurtz, S. M. (2014). "Advances in tribological testing of artificial joint biomaterials using multidirectional pin-on-disk testers." *J. Mech. Behav. Biomed. Mater.*, 31, 117–134.

Beck, R. T., Illingworth, K. D., and Saleh, K. J. (2012). "Review of periprosthetic osteolysis in total joint arthroplasty: An emphasis on host factors and future directions." *J. Orthop. Res.*, 30(4), 541–546.

Bei, Y., Fregly, B. J., Sawyer, W. G., Banks, S. A., and Kim, N. H. (2004). "The relationship between contact pressure, insert thickness, and mild wear in total knee replacements." *C. - Comput. Model. Eng. Sci.*, 6(2), 145–152.

Below, S., Arnoczky, S. P., Dodds, J., Kooima, C., and Walter, N. (2002). "The split-line pattern of the distal femur: A consideration in the orientation of autologous cartilage grafts." *Arthroscopy*, 18(6), 613–617.

Bennett, H. J., Valenzuela, K. A., Lynn, S. K., and Weinhandl, J. T. (2021). "Foot Rotation Gait Modifications Affect Hip and Ankle, but Not Knee, Stance Phase Joint Reaction Forces during Running." *J. Biomech. Eng.*, 143(2).

Besier, T. F., Fredericson, M., Gold, G. E., Beaupré, G. S., and Delp, S. L. (2009). "Knee muscle forces during walking and running in patellofemoral pain patients and pain-free controls." *J. Biomech.*, 42(7), 898–905.

Besier, T. F., Gold, G. E., Beaupré, G. S., and Delp, S. L. (2005). "A modeling framework to estimate patellofemoral joint cartilage stress in vivo." *Med. Sci. Sports Exerc.*, 37(11), 1924–1930.

Blankevoort, L., and Huiskes, R. (1991). "Ligament-bone interaction in a three-dimensional model of the knee." *J. Biomech. Eng.*, 113(3), 263–269.

Bolcos, P. O., Mononen, M. E., Mohammadi, A., Ebrahimi, M., Tanaka, M. S., Samaan, M. A., Souza, R. B., Li, X., Suomalainen, J. S., Jurvelin, J. S., Töyräs, J., and Korhonen, R. K. (2018). "Comparison between kinetic and kinetic-kinematic driven knee joint finite element models." *Sci. Rep.*, 8(1), 1–11.

Bracco, P., and Oral, E. (2011). "Vitamin E-stabilized UHMWPE for total joint implants: A review." *Clin. Orthop. Relat. Res.*, 469(8), 2286–2293.

Brown, T. S., Citters, D. W. Van, Berry, D. J., and Abdel, M. P. (2017). "The use of highly crosslinked polyethylene in total knee arthroplasty." *Bone Jt. J.*, 99B(8), 996–1002.

Bursać, P. M., Obitz, T. W., Eisenberg, S. R., and Stamenović, D. (1999). "Confined

and unconfined stress relaxation of cartilage: appropriateness of a transversely isotropic analysis." *J. Biomech.*, 32(10), 1125–1130.

Cappellini, G., Ivanenko, Y. P., Poppele, R. E., and Lacquaniti, F. (2006). "Motor patterns in human walking and running." *J. Neurophysiol.*, 95(6), 3426–3437.

Chahine, N. O., Wang, C. C. B., Hung, C. T., and Ateshian, G. A. (2004). "Anisotropic strain-dependent material properties of bovine articular cartilage in the transitional range from tension to compression." *J. Biomech.*, 37(8), 1251–1261.

Chan, C. W., and Rudins, A. (1994). "Foot Biomechanics During Walking and Running." *Mayo Clin. Proc.*, 69(5), 448–461.

Charlesby, A., and A, P. R. S. L. (1952). "Cross-linking of polythene by pile radiation." *Proc. R. Soc. London. Ser. A. Math. Phys. Sci.*, 215(1121), 187–214.

Chawla, M. (2019). "Advances in Total Knee Replacement surgery." *BioSpectrum Bus. Bio Heal. Sci.*, (January).

Chen, A. C., Bae, W. C., Schinagl, R. M., and Sah, R. L. (2001). "Depth- and strain-dependent mechanical and electromechanical properties of full-thickness bovine articular cartilage in confined compression." *J. Biomech.*, 34(1), 1–12.

Chen, T., Li, Q., Fu, Z., Sun, L., Guo, W., and Wu, C. (2018). "The shape memory effect of crosslinked ultra-high-molecular-weight polyethylene prepared by silane-induced crosslinking method." *Polym. Bull.*, 75(5), 2181–2196.

Chen, X., Zhou, Y., Wang, L., Santare, M. H., Wan, L. Q., and Lu, X. L. (2016). "Determining Tension–Compression Nonlinear Mechanical Properties of Articular Cartilage from Indentation Testing." *Ann. Biomed. Eng.*, 44(4), 1148–1158.

Clark, J. M. (1990). "The organisation of collagen fibrils in the superficial zones of articular cartilage." *J. Anat.*, 171, 117–30.

Clark, J. M. (1991). "Variation of collagen fiber alignment in a joint surface: A scanning electron microscope study of the tibial plateau in dog, rabbit, and man." *J.*

Orthop. Res., 9(2), 246–257.

Clary, C. W., Fitzpatrick, C. K., Maletsky, L. P., and Rullkoetter, P. J. (2013). "The influence of total knee arthroplasty geometry on mid-flexion stability: An experimental and finite element study." *J. Biomech.*, 46(7), 1351–1357.

Cohen, N. P., Foster, R. J., and Mow, V. C. (1998). "Composition and dynamics of articular cartilage: Structure, function, and maintaining healthy state." *J. Orthop. Sports Phys. Ther.*, JOSPT, Inc. JOSPT, 1033 North Fairfax Street, Suite 304, Alexandria, VA 22134-1540.

D'Antonio, J. A., Capello, W. N., and Ramakrishnan, R. (2012). "Second-generation annealed highly cross-linked polyethylene exhibits low wear." *Clin. Orthop. Relat. Res.*, 470(6), 1696–1704.

David, A. C., Carpes, F. P., and Stefanyshyn, D. (2015a). "Effects of changing speed on knee and ankle joint load during walking and running." *J. Sports Sci.*, 33(4), 391–397.

David, A. C., Carpes, F. P., and Stefanyshyn, D. (2015b). "Effects of changing speed on knee and ankle joint load during walking and running." *J. Sports Sci.*, 33(4), 391–397.

Dayyoub, T., Maksimkin, A. V., Kaloshkin, S., Kolesnikov, E., Chukov, D., Dyachkova, T. P., and Gutnik, I. (2019). "The structure and mechanical properties of the UHMWPE films modified by the mixture of graphene nanoplates with polyaniline." *Polymers (Basel).*, 11(1).

Deneweth, J. M., Arruda, E. M., and McLean, S. G. (2015). "Hyperelastic modeling of location-dependent human distal femoral cartilage mechanics." *Int. J. Non. Linear. Mech.*, 68, 146–156.

Deneweth, J. M., McLean, S. G., and Arruda, E. M. (2013). "Evaluation of hyperelastic models for the non-linear and non-uniform high strain-rate mechanics of tibial cartilage." *J. Biomech.*, 46(10), 1604–1610.

Dhaher, Y. Y., Kwon, T. H., and Barry, M. (2010). “The effect of connective tissue material uncertainties on knee joint mechanics under isolated loading conditions.” *J. Biomech.*, 43(16), 3118–3125.

Dhar Badgayan, N., Kumar Sahu, S., Samanta, S., and Rama Sreekanth, P. S. (2020). “An insight into mechanical properties of polymer nanocomposites reinforced with multidimensional filler system: A state of art review.” *Mater. Today Proc.*, 24, 422–431.

Digas, G., Kärrholm, J., Thanner, J., and Herberts, P. (2007). “5-Year experience of highly cross-linked polyethylene in cemented and uncemented sockets: Two randomized studies using radiostereometric analysis.” *Acta Orthop.*, 78(6), 746–754.

Donahue, T. L. H., Hull, M. L., Rashid, M. M., and Jacobs, C. R. (2002). “A finite element model of the human knee joint for the study of tibio-femoral contact.” *J. Biomech. Eng.*, 124(3), 273–280.

Donzelli, P. S., Spilker, R. L., Ateshian, G. A., and Mow, V. C. (1999). “Contact analysis of biphasic transversely isotropic cartilage layers and correlations with tissue failure.” *J. Biomech.*, 32(10), 1037–1047.

Drake, R. L., Vogel, A. W., and Mitchell, A. W. M. (2019). *Gray’s Anatomy for Students*. Philadelphia: Elsevier.

Dumbleton, J. H., Manley, M. T., and Edidin, A. A. (2002). “A literature review of the association between wear rate and osteolysis in total hip arthroplasty.” *J. Arthroplasty*, 17(5), 649–661.

Ebrahimi, M., Ojanen, S., Mohammadi, A., Finnilä, M. A., Joukainen, A., Kröger, H., Saarakkala, S., Korhonen, R. K., and Tanska, P. (2019). “Elastic, Viscoelastic and Fibril-Reinforced Poroelastic Material Properties of Healthy and Osteoarthritic Human Tibial Cartilage.” *Ann. Biomed. Eng.*, 47(4), 953–966.

Edidin, A. A., and Kurtz, S. M. (2000). “Influence of mechanical behavior on the wear of 4 clinically relevant polymeric biomaterials in a hip simulator.” *J. Arthroplasty*,

15(3), 321–331.

El-Rich, M. (2022). “Orthopedic biomechanics: stress analysis.” *Hum. Orthop. Biomech. Fundam. Devices Appl.*, 25–37.

Enab, T. A. (2014). “Performance improvement of total knee replacement joint through bidirectional functionally graded material.” *Int. J. Mech. Mechatronics Eng.*, 14(2), 104–113.

Erbulut, D. U., Sadeqi, S., Summers, R., and Goel, V. K. (2021). “Tibiofemoral Cartilage Contact Pressures in Athletes During Landing: A Dynamic Finite Element Study.” *J. Biomech. Eng.*, 143(10).

Erdemir, A. (2014). “Open Knee: Open Source Modeling and Simulation in Knee Biomechanics.” *J. Knee Surg.*, 29(2), 107–116.

Erdemir, A., and Sibole, S. (2010). “Open Knee: A Three-Dimensional Finite Element Representation of the Knee Joint.” *User’s Guid. Version 1.0.0*.

Esrafilian, A., Stenroth, L., Mononen, M. E., Tanska, P., Avela, J., and Korhonen, R. K. (2020). “EMG-Assisted Muscle Force Driven Finite Element Model of the Knee Joint with Fibril-Reinforced Poroelastic Cartilages and Menisci.” *Sci. Rep.*, 10(1), 1–16.

Esrafilian, A., Stenroth, L., Mononen, M. E., Tanska, P., Rossom, S. Van, Lloyd, D. G., Jonkers, I., and Korhonen, R. K. (2021). “12 Degrees of Freedom Muscle Force Driven Fibril-Reinforced Poroviscoelastic Finite Element Model of the Knee Joint.” *IEEE Trans. Neural Syst. Rehabil. Eng.*, 29, 123–133.

Essinger, J. R., Leyvraz, P. F., Heegard, J. H., and Robertson, D. D. (1989). “A mathematical model for the evaluation of the behaviour during flexion of condylar-type knee prostheses.” *J. Biomech.*, 22(11–12), 1229–1241.

Faisal, T. R., Adouni, M., and Dhaher, Y. Y. (2019). “The effect of fibrillar degradation on the mechanics of articular cartilage: a computational model.” *Biomech. Model. Mechanobiol.*, 18(3), 733–751.

Fisher, J., McEwen, H. M. J., Tipper, J. L., Galvin, A. L., Ingram, J., Kamali, A., Stone, M. H., and Ingham, E. (2004). "Wear, debris, and biologic activity of cross-linked polyethylene in the knee: Benefits and potential concerns." *Clin. Orthop. Relat. Res.*, 428, 114–119.

Fitzpatrick, C. K., Clary, C. W., Laz, P. J., and Rullkoetter, P. J. (2012). "Relative contributions of design, alignment, and loading variability in knee replacement mechanics." *J. Orthop. Res.*, 30(12), 2015–2024.

Fregly, B. J., Sawyer, W. G., Harman, M. K., and Banks, S. A. (2005). "Computational wear prediction of a total knee replacement from in vivo kinematics." *J. Biomech.*, 38(2), 305–314.

Galvin, A. L., Kang, L., Udofia, I., Jennings, L. M., McEwen, H. M. J., Jin, Z., and Fisher, J. (2009). "Effect of conformity and contact stress on wear in fixed-bearing total knee prostheses." *J. Biomech.*, 42(12), 1898–1902.

Gannon, A. R., Nagel, T., Bell, A. P., Avery, N. C., and Kelly, D. J. (2015). "The changing role of the superficial region in determining the dynamic compressive properties of articular cartilage during postnatal development." *Osteoarthr. Cartil.*, 23(6), 975–984.

Gual, M. R., Mesquita, A. Z., Ribeiro, E., and Grossi, P. A. (2017). "Shielding Verifications for a Gamma Irradiation Facility Considering the Installation of a New Automatic Product Loading System." *Sci. Technol. Nucl. Install.*, 2017.

Guilak, F., Ratcliffe, A., Lane, N., Rosenwasser, M. P., and Mow, V. C. (1994). "Mechanical and biochemical changes in the superficial zone of articular cartilage in canine experimental osteoarthritis." *J. Orthop. Res.*, 12(4), 474–484.

Haider, H., and Baykal, D. (2016). *Wear Assessment of UHMWPE with Pin-on-Disc Testing. UHMWPE Biomater. Handb. Ultra High Mol. Weight Polyethyl. Total Jt. Replace. Med. Devices Third Ed.*, Elsevier Inc.

Hall, M., Stevermer, C. A., and Gillette, J. C. (2012). "Gait analysis post anterior

cruciate ligament reconstruction: Knee osteoarthritis perspective." *Gait Posture*, 36(1), 56–60.

Halloran, J. P., Sibole, S., Donkelaar, C. C. van, Turnhout, M. C. van, Oomens, C. W. J., Weiss, J. A., Guilak, F., and Erdemir, A. (2012). "Multiscale Mechanics of Articular Cartilage: Potentials and Challenges of Coupling Musculoskeletal, Joint, and Microscale Computational Models." *Ann. Biomed. Eng.*, 40(11), 2456–2474.

Halonen, K. S., Dzialo, C. M., Mannisi, M., Venäläinen, M. S., Zee, M. De, and Andersen, M. S. (2017). "Workflow assessing the effect of gait alterations on stresses in the medial tibial cartilage - Combined musculoskeletal modelling and finite element analysis." *Sci. Rep.*, 7(1), 1–14.

Halonen, K. S., Mononen, M. E., Jurvelin, J. S., Töyräs, J., Kłodowski, A., Kulmala, J. P., and Korhonen, R. K. (2016a). "Importance of patella, quadriceps forces, and depthwise cartilage structure on knee joint motion and cartilage response during gait." *J. Biomech. Eng.*, 138(7), 1–11.

Halonen, K. S., Mononen, M. E., Jurvelin, J. S., Töyräs, J., and Korhonen, R. K. (2013). "Importance of depth-wise distribution of collagen and proteoglycans in articular cartilage-A 3D finite element study of stresses and strains in human knee joint." *J. Biomech.*, 46(6), 1184–1192.

Halonen, K. S., Mononen, M. E., Jurvelin, J. S., Töyräs, J., Salo, J., and Korhonen, R. K. (2014). "Deformation of articular cartilage during static loading of a knee joint - Experimental and finite element analysis." *J. Biomech.*, 47(10), 2467–2474.

Halonen, K. S., Mononen, M. E., Töyräs, J., Kröger, H., Joukainen, A., and Korhonen, R. K. (2016b). "Optimal graft stiffness and pre-strain restore normal joint motion and cartilage responses in ACL reconstructed knee." *J. Biomech.*, 49(13), 2566–2576.

Haris, A., and Beng Chye Tan, V. (2020). "Stress response envelopes of intact tibiofemoral joint and knee osteoarthritis." *Proc. Inst. Mech. Eng. Part H J. Eng. Med.*, 234(10), 1151–1161.

Heisel, C., Silva, M., Rosa, M. A. Dela, and Schmalzried, T. P. (2004). “Short-Term in Vivo Wear of Cross-Linked Polyethylene.” *J. Bone Jt. Surg. - Ser. A*, 86(4), 748–751.

Henak, C. R., Ateshian, G. A., and Weiss, J. A. (2014). “Finite element prediction of transchondral stress and strain in the human hip.” *J. Biomech. Eng.*, 136(2).

Holmes, M. H., and Mow, V. C. (1990). “The nonlinear characteristics of soft gels and hydrated connective tissues in ultrafiltration.” *J. Biomech.*, 23(11), 1145–1156.

Huang, C. Y., Stankiewicz, A., Ateshian, G. A., and Mow, V. C. (2005). “Anisotropy, inhomogeneity, and tension-compression nonlinearity of human glenohumeral cartilage in finite deformation.” *J. Biomech.*, 38(4), 799–809.

Hussain, M., Naqvi, R. A., Abbas, N., Khan, S. M., Nawaz, S., Hussain, A., Zahra, N., and Khalid, M. W. (2020a). “Ultra-high-molecular-weight-polyethylene (UHMWPE) as a promising polymer material for biomedical applications: A concise review.” *Polymers (Basel).*, 12(2), 1–27.

Hussain, Naqvi, Abbas, Khan, Nawaz, Hussain, Zahra, and Khalid. (2020b). “Ultra-High-Molecular-Weight-Polyethylene (UHMWPE) as a Promising Polymer Material for Biomedical Applications: A Concise Review.” *Polymers (Basel).*, 12(2), 323.

Hyodo, K., Kanamori, A., Kadone, H., Takahashi, T., Kajiwara, M., and Yamazaki, M. (2020). “Gait Analysis Comparing Kinematic, Kinetic, and Muscle Activation Data of Modern and Conventional Total Knee Arthroplasty.” *Arthroplast. Today*, 6(3), 338–342.

Imeni, M., Seyfi, B., Fatouraee, N., and Samani, A. (2020). “Constitutive modeling of menisci tissue: a critical review of analytical and numerical approaches.” *Biomech. Model. Mechanobiol.*, (0123456789).

Is, O., Guide, S., Messier, S. P., Gutekunst, D. J., Davis, C., DeVita, P., Sharma, L., Lou, C., Cahue, S., and Dunlop, D. D. (2005). “Osteoarthritis as a Chronic Disease.” *Arthritis Rheum.*, 21(7), 2026–2032.

J. H. Hubbell and S. M. Seltzer. (1995). “Tables of X-Ray Mass Attenuation.”

Jeffery, A. K., Blunn, G. W., Archer, C. W., and Bentley, G. (1991). “Three-dimensional collagen architecture in bovine articular cartilage.” *J. Bone Jt. Surg. - Ser. B*, 73(5), 795–801.

Jeffrey, J. E., Gregory, D. W., and Aspden, R. M. (1995). “Matrix Damage and Chondrocyte Viability Following a Single Impact Load on Articular-Cartilage.” *Arch. Biochem. Biophys.*, 322(1), 87–96.

Julkunen, P., Wilson, W., Jurvelin, J. S., Rieppo, J., Qu, C. J., Lammi, M. J., and Korhonen, R. K. (2008). “Stress-relaxation of human patellar articular cartilage in unconfined compression: Prediction of mechanical response by tissue composition and structure.” *J. Biomech.*, 41(9), 1978–1986.

Kandahari, A. M., Yang, X., Laroche, K. A., Dighe, A. S., Pan, D., and Cui, Q. (2016). “A review of UHMWPE wear-induced osteolysis: The role for early detection of the immune response.” *Bone Res.*, 4(November 2015).

Kang, K. T., Son, J., Kim, H. J., Baek, C., Kwon, O. R., and Koh, Y. G. (2017). “Wear predictions for UHMWPE material with various surface properties used on the femoral component in total knee arthroplasty: a computational simulation study.” *J. Mater. Sci. Mater. Med.*, 28(7).

Kazemi, M., Dabiri, Y., and Li, L. P. (2013). “Recent advances in computational mechanics of the human knee joint.” *Comput. Math. Methods Med.*, 2013.

Kazemi, M., Li, L. P., Buschmann, M. D., and Savard, P. (2012). “Partial Meniscectomy Changes Fluid Pressurization in Articular Cartilage in Human Knees.” *J. Biomech. Eng.*, 134(2).

Khassetarash, A., Vernillo, G., Martinez, A., Baggaley, M., Giandolini, M., Horvais, N., Millet, G. Y., and Edwards, W. B. (2020). “Biomechanics of graded running: Part II—Joint kinematics and kinetics.” *Scand. J. Med. Sci. Sport.*, 30(9), 1642–1654.

Klets, O., Mononen, M. E., Liukkonen, M. K., Nevalainen, M. T., Nieminen, M. T.,

Saarakkala, S., and Korhonen, R. K. (2018). “Estimation of the Effect of Body Weight on the Development of Osteoarthritis Based on Cumulative Stresses in Cartilage: Data from the Osteoarthritis Initiative.” *Ann. Biomed. Eng.*, 46(2), 334–344.

Klets, O., Mononen, M. E., Tanska, P., Nieminen, M. T., Korhonen, R. K., and Saarakkala, S. (2016). “Comparison of different material models of articular cartilage in 3D computational modeling of the knee: Data from the Osteoarthritis Initiative (OAI).” *J. Biomech.*, 49(16), 3891–3900.

Klika, V., Gaffney, E. A., Chen, Y. C., and Brown, C. P. (2016). “An overview of multiphase cartilage mechanical modelling and its role in understanding function and pathology.” *J. Mech. Behav. Biomed. Mater.*, 62, 139–157.

Knight, L. A., Pal, S., Coleman, J. C., Bronson, F., Haider, H., Levine, D. L., Taylor, M., and Rullkoetter, P. J. (2007). “Comparison of long-term numerical and experimental total knee replacement wear during simulated gait loading.” *J. Biomech.*, 40(7), 1550–1558.

Koh, Y. G., Lee, J. A., and Kang, K. T. (2019). “Prediction of wear on tibial inserts made of UHMWPE, PEEK, and CFR-PEEK in total knee arthroplasty using finite-element analysis.” *Lubricants*, 7(4).

Korhonen, R. K., and Herzog, W. (2008). “Depth-dependent analysis of the role of collagen fibrils, fixed charges and fluid in the pericellular matrix of articular cartilage on chondrocyte mechanics.” *J. Biomech.*, 41(2), 480–485.

Korhonen, R. K., Laasanen, M. S., Töyräs, J., Lappalainen, R., Helminen, H. J., and Jurvelin, J. S. (2003). “Fibril reinforced poroelastic model predicts specifically mechanical behavior of normal, proteoglycan depleted and collagen degraded articular cartilage.” *J. Biomech.*, 36(9), 1373–1379.

Kurtz, S. M. (2009). *The Clinical Performance of UHMWPE in Knee Replacements*. *UHMWPE Biomater. Handb.*, Elsevier Inc.

Kurtz, S. M. (2016). *UHMWPE Biomaterials Handbook*. MA: Elsevier.

Kurtz, S. M., Gawel, H. A., and Patel, J. D. (2011). “History and systematic review of wear and osteolysis outcomes for first-generation highly crosslinked polyethylene.” *Clin. Orthop. Relat. Res.*, 469(8), 2262–2277.

Kurtz, S. M., Muratoglu, O. K., Evans, M., and Edidin, A. A. (1999). “Advances in the processing, sterilization, and crosslinking of ultra-high molecular weight polyethylene for total joint arthroplasty.” *Biomaterials*, 20(18), 1659–1688.

Kurtz, S., Ong, K., Lau, E., Mowat, F., and Halpern, M. (2007). “Projections of primary and revision hip and knee arthroplasty in the United States from 2005 to 2030.” *J. Bone Jt. Surg. - Ser. A*, 89(4), 780–785.

Kwak, S., Noh, D. Il, Chun, H. J., Lim, Y. M., Nho, Y. C., Jang, J. W., and Shim, Y. B. (2009). “Effect of γ-ray irradiation on surface oxidation of ultra high molecular weight polyethylene/zirconia composite prepared by in situ Ziegler-Natta polymerization.” *Macromol. Res.*, 17(8), 603–608.

Lachiewicz, P. F., and Geyer, M. R. (2011). “The use of highly cross-linked polyethylene in total knee arthroplasty.” *J. Am. Acad. Orthop. Surg.*, 19(3), 143–51.

Lee, S. J., Aadalen, K. J., Malaviya, P., Lorenz, E. P., Hayden, J. K., Farr, J., Kang, R. W., and Cole, B. J. (2006). “Tibiofemoral contact mechanics after serial medial meniscectomies in the human cadaveric knee.” *Am. J. Sports Med.*, 34(8), 1334–1344.

Li, J. (2021). “Development and validation of a finite-element musculoskeletal model incorporating a deformable contact model of the hip joint during gait.” *J. Mech. Behav. Biomed. Mater.*, 113(October 2020), 104136.

Li, J., Hua, X., Jones, A. C., Williams, S., Jin, Z., Fisher, J., and Wilcox, R. K. (2016). “The influence of the representation of collagen fibre organisation on the cartilage contact mechanics of the hip joint.” *J. Biomech.*, 49(9), 1679–1685.

Li, J. S., Tsai, T. Y., Felson, D. T., Li, G., and Lewis, C. L. (2017). “Six degree-of-freedom knee joint kinematics in obese individuals with knee pain during gait.” *PLoS One*, 12(3), 1–11.

Li, L. P., Soulhat, J., Buschmann, M. D., and Shirazi-Adl, A. (1999). “Nonlinear analysis of cartilage in unconfined ramp compression using a fibril reinforced poroelastic model.” *Clin. Biomech.*, 14(9), 673–682.

Li, L., Yang, X., Yang, L., Zhang, K., Shi, J., Zhu, L., Liang, H., Wang, X., and Jiang, Q. (2019). “Biomechanical analysis of the effect of medial meniscus degenerative and traumatic lesions on the knee joint.” *Am. J. Transl. Res.*, 11(2), 542–556.

Lin, J., Shi, Y., Men, Y., Wang, X., Ye, J., and Zhang, C. (2020). “Mechanical roles in formation of oriented collagen fibers.” *Tissue Eng. - Part B Rev.*, 26(2), 116–128.

Liukkonen, M. K., Mononen, M. E., Klets, O., Arokoski, J. P., Saarakkala, S., and Korhonen, R. K. (2017a). “Simulation of subject-specific progression of knee osteoarthritis and comparison to experimental follow-up data: Data from the osteoarthritis initiative.” *Sci. Rep.*, 7(1), 1–14.

Liukkonen, M. K., Mononen, M. E., Tanska, P., Saarakkala, S., Nieminen, M. T., and Korhonen, R. K. (2017b). “Application of a semi-automatic cartilage segmentation method for biomechanical modeling of the knee joint.” *Comput. Methods Biomech. Biomed. Engin.*, 20(13), 1453–1463.

Losina, E., Ts, T., Bn, R., Wright, J., and Jn, K. (2012). “The Dramatic Increase in Total Knee Replacement Size and the Obesity Epidemic.” 201–207.

Łuczkiewicz, P., Daszkiewicz, K., Witkowski, W., Chróścielewski, J., and Zarzycki, W. (2015). “Influence of meniscus shape in the cross sectional plane on the knee contact mechanics.” *J. Biomech.*, 48(8), 1356–1363.

Maas, S. A., Ellis, B. J., Ateshian, G. A., and Weiss, J. A. (2012). “FEBio: Finite elements for biomechanics.” *J. Biomech. Eng.*, 134(1).

Malito, L. G., Arevalo, S., Kozak, A., Spiegelberg, S., Bellare, A., and Pruitt, L. (2018). “Material properties of ultra-high molecular weight polyethylene: Comparison of tension, compression, nanomechanics and microstructure across clinical formulations.” *J. Mech. Behav. Biomed. Mater.*, 83(January), 9–19.

Marzo, J. M., and Gurske-DePerio, J. (2009). “Effects of medial meniscus posterior horn avulsion and repair on tibiofemoral contact area and peak contact pressure with clinical implications.” *Am. J. Sports Med.*, 37(1), 124–129.

McKellop, H. A., and D’Lima, D. (2008). “How have wear testing and joint simulator studies helped to discriminate among materials and designs?” *J. Am. Acad. Orthop. Surg.*, 16 Suppl 1.

McKellop, H., Shen, F. W., Lu, B., Campbell, P., and Salovey, R. (1999). “Development of an extremely wear-resistant ultra high molecular weight polyethylene for total hip replacements.” *J. Orthop. Res.*, 17(2), 157–167.

Meng, Q., An, S., Damion, R. A., Jin, Z., Wilcox, R., Fisher, J., and Jones, A. (2017). “The effect of collagen fibril orientation on the biphasic mechanics of articular cartilage.” *J. Mech. Behav. Biomed. Mater.*, 65, 439–453.

Meng, Q., Jin, Z., Wilcox, R., and Fisher, J. (2014). “Computational investigation of the time-dependent contact behaviour of the human tibiofemoral joint under body weight.” *Proc. Inst. Mech. Eng. Part H J. Eng. Med.*, 228(11), 1193–1207.

Messier, S. P. (1994). “Osteoarthritis of the knee and associated factors of age and obesity: Effects on gait.” *Med. Sci. Sports Exerc.*

Mizrahi, J., Maroudas, A., Lanir, Y., Ziv, I., and Webber, T. J. (1986). “The ‘instantaneous’ deformation of cartilage: Effects of collagen fiber orientation and osmotic stress.” *Biorheology*, 23(4), 311–330.

Moger, C. J., Arkill, K. P., Barrett, R., Bleuet, P., Ellis, R. E., Green, E. M., and Winlove, C. P. (2009). “Cartilage collagen matrix reorientation and displacement in response to surface loading.” *J. Biomech. Eng.*, 131(3), 1–9.

Mommersteeg, T. J. A., Huiskes, R., Blankevoort, L., Kooloos, J. G. M., Kauer, J. M. G., and Maathuis, P. G. M. (1996). “A global verification study of a quasi-static knee model with multi-bundle ligaments.” *J. Biomech.*, 29(12), 1659–1664.

Mononen, M. E., Julkunen, P., Töyräs, J., Jurvelin, J. S., Kiviranta, I., and Korhonen,

R. K. (2011). “Alterations in structure and properties of collagen network of osteoarthritic and repaired cartilage modify knee joint stresses.” *Biomech. Model. Mechanobiol.*, 10(3), 357–369.

Mononen, M. E., Jurvelin, J. S., and Korhonen, R. K. (2013). “Effects of radial tears and partial meniscectomy of lateral meniscus on the knee joint mechanics during the stance phase of the gait cycle - A 3D finite element study.” *J. Orthop. Res.*, 31(8), 1208–1217.

Mononen, M. E., Jurvelin, J. S., and Korhonen, R. K. (2015). “Implementation of a gait cycle loading into healthy and meniscectomised knee joint models with fibril-reinforced articular cartilage.” *Comput. Methods Biomech. Biomed. Engin.*, 18(2), 141–152.

Mononen, M. E., Mikkola, M. T., Julkunen, P., Ojala, R., Nieminen, M. T., Jurvelin, J. S., and Korhonen, R. K. (2012). “Effect of superficial collagen patterns and fibrillation of femoral articular cartilage on knee joint mechanics-A 3D finite element analysis.” *J. Biomech.*, 45(3), 579–587.

Moratoglu, O. K. (2009). *15 - Highly Crosslinked and Melted UHMWPE, in UHMWPE Biomaterials Handbook. UHMWPE Biomater. Handb.*, Elsevier Inc.

Morimoto, Y., Ferretti, M., Ekdahl, M., Smolinski, P., and Fu, F. H. (2009). “Tibiofemoral Joint Contact Area and Pressure After Single- and Double-Bundle Anterior Cruciate Ligament Reconstruction.” *Arthrosc. - J. Arthrosc. Relat. Surg.*, 25(1), 62–69.

Muratoglu, O., Bragdon, C., O’Connor, D., Jasty, M., and Harris, W. (2001). “A novel method of crosslinking UHMWPE to improve wear, reduce oxidation, and retain mechanical properties.” *J Arthroplast.*, 16(2), 149–160.

Muratoglu, O. K., Bragdon, C. R., O’Connor, D. O., Jasty, M., Harris, W. H., Rizwan, G., and McGarry, F. (1999). “Unified wear model for highly crosslinked ultra-high molecular weight polyethylenes (UHMWPE).” *Biomaterials*, 20(16), 1463–1470.

Muratoglu, O. K., Merrill, E. W., Bragdon, C. R., O'Connor, D., Hoeffel, D., Burroughs, B., Jasty, M., and Harris, W. H. (2003). "Effect of radiation, heat, and aging on in vitro wear resistance of polyethylene." *Clin. Orthop. Relat. Res.*, (417), 253–262.

Naghibi Beidokhti, H., Janssen, D., Khoshgoftar, M., Sprengers, A., Perdahcioglu, E. S., Boogaard, T. Van den, and Verdonschot, N. (2016). "A comparison between dynamic implicit and explicit finite element simulations of the native knee joint." *Med. Eng. Phys.*, 38(10), 1123–1130.

Netter, J., Hermida, J., Flores-Hernandez, C., Steklov, N., Kester, M., and D'Lima, D. D. (2015). "Prediction of Wear in Crosslinked Polyethylene Unicompartmental Knee Arthroplasty." *Lubr. 2015, Vol. 3, Pages 381-393*, 3(2), 381–393.

Nuckols, R. W., Takahashi, K. Z., Farris, D. J., Mizrachi, S., Riemer, R., and Sawicki, G. S. (2020). "Mechanics of walking and running up and downhill: A joint-level perspective to guide design of lower-limb exoskeletons." *PLoS One*, 15(8 August), 1–20.

Oral, E., Ghali, B. W., Rowell, S. L., Micheli, B. R., Lozynsky, A. J., and Muratoglu, O. K. (2010). "A surface crosslinked UHMWPE stabilized by vitamin E with low wear and high fatigue strength." *Biomaterials*, 31(27), 7051–7060.

Oral, E., Malhi, A. S., and Muratoglu, O. K. (2006). "Mechanisms of decrease in fatigue crack propagation resistance in irradiated and melted UHMWPE." *Biomaterials*, 27(6), 917–925.

Oral, E., Malhi, A. S., Wannomae, K. K., and Muratoglu, O. K. (2008). "Highly Cross-Linked Ultrahigh Molecular Weight Polyethylene With Improved Fatigue Resistance for Total Joint Arthroplasty. Recipient of the 2006 Hap Paul Award." *J. Arthroplasty*, 23(7), 1037–1044.

Orozco, G. A., Tanska, P., Mononen, M. E., Halonen, K. S., and Korhonen, R. K. (2018). "The effect of constitutive representations and structural constituents of ligaments on knee joint mechanics." *Sci. Rep.*, 8(1), 1–15.

Pachore, J. A., Vaidya, S. V., Thakkar, C. J., Bhalodia, H. K. P., and Wakankar, H. M. (2013). “ISHKS joint registry: A preliminary report.” *Indian J. Orthop.*, 47(5), 505–509.

Paletta, G. A., Manning, T., Snell, E., Parker, R., and Bergfeld, J. (1997). “The effect of aiiograft meniscal replacement on intraarticular contact area and pressures in the human knee: A biomechanical study.” *Am. J. Sports Med.*, 25(5), 692–698.

Panula, H. E., Hyttinen, M. M., Arokoski, J. P. A., Långsjö, T. K., Pelttari, A., Kiviranta, I., and Helminen, H. J. (1998). “Articular cartilage superficial zone collagen birefringence reduced and cartilage thickness increased before surface fibrillation in experimental osteoarthritis.” *Ann. Rheum. Dis.*, 57(4), 237–245.

Park, S., Krishnan, R., Nicoll, S. B., and Ateshian, G. A. (2003). “Cartilage interstitial fluid load support in unconfined compression.” *J. Biomech.*, 36(12), 1785–1796.

Peña, E., Calvo, B., Martínez, M. A., and Doblaré, M. (2006). “A three-dimensional finite element analysis of the combined behavior of ligaments and menisci in the healthy human knee joint.” *J. Biomech.*, 39(9), 1686–1701.

Peña, E., Pérez Del Palomar, A., Calvo, B., Martínez, M. A., and Doblaré, M. (2007). “Computational modelling of diarthrodial joints. Physiological, pathological and post-surgery simulations.” *Arch. Comput. Methods Eng.*, 14(1), 47–91.

Peters, A. E., Akhtar, R., Comerford, E. J., and Bates, K. T. (2018a). “Tissue material properties and computational modelling of the human tibiofemoral joint: A critical review.” *PeerJ*, 2018(1), 1–48.

Peters, A. E., Akhtar, R., Comerford, E. J., and Bates, K. T. (2018b). “The effect of ageing and osteoarthritis on the mechanical properties of cartilage and bone in the human knee joint.” *Sci. Rep.*, 8(1), 1–13.

Pierce, D. M., Ricken, T., and Holzapfel, G. A. (2013). “A hyperelastic biphasic fibre-reinforced model of articular cartilage considering distributed collagen fibre orientations: Continuum basis, computational aspects and applications.” *Comput.*

Methods Biomech. Biomed. Engin., Taylor & Francis.

Raju, V., and Koorata, P. K. (2022). “Influence of material heterogeneity on the mechanical response of articulated cartilages in a knee joint.” *Proc. Inst. Mech. Eng. Part H J. Eng. Med.*, 236(9), 1340–1348.

Raju, V., Koorata, P. K., and Kamat, Y. (2021). “Case study for contact pressure improvisation with graded implant material in articular cartilages of knee joint.” *J. Mech. Sci. Technol.*, 35(3), 1049–1054.

Rakhsha, M., Smith, C. R., Recuero, A. M., Brandon, S. C. E., Vignos, M. F., Thelen, D. G., and Negrut, D. (2019). “Simulation of surface strain in tibiofemoral cartilage during walking for the prediction of collagen fibre orientation.” *Comput. Methods Biomech. Biomed. Eng. Imaging Vis.*, 7(4), 396–405.

Ramírez, T. D. la M., Cruz, I. H., Ruiz, M. A. D., Perrusquia, N. L., Bustos, D. G., and Martínez, M. F. (2020). “Numerical Model of Ultra-High Molecular Weight Polyethylene Abrasive Wear Tests.” *Model. Numer. Simul. Mater. Sci.*, 10(01), 1–14.

Reinitz, S. D., Carlson, E. M., Levine, R. A. C., Franklin, K. J., and Citters, D. W. Van. (2015). “Dynamical mechanical analysis as an assay of cross-link density of orthopaedic ultra high molecular weight polyethylene.” *Polym. Test.*, 45, 174–178.

Reuter, T., and Hurschler, C. (2018). “Comparison of biphasic material properties of equine articular cartilage from stress relaxation indentation tests with and without tension-compression nonlinearity.” *Curr. Dir. Biomed. Eng.*, 4(1), 485–488.

Roberts, M., Mongeon, D., and Prince, F. (2017). “Biomechanical parameters for gait analysis: a systematic review of healthy human gait.” *Phys. Ther. Rehabil.*, 4(1), 6.

Rocha, M., Mansur, A., and Mansur, H. (2009). “Characterization and Accelerated Ageing of UHMWPE Used in Orthopedic Prosthesis by Peroxide.” *Materials (Basel).*, 2(2), 562–576.

Ruggiero, L., Zimmerman, B. K., Park, M., Han, L., Wang, L., Burris, D. L., and Lu, X. L. (2015). “Roles of the Fibrous Superficial Zone in the Mechanical Behavior of

TMJ Condylar Cartilage." *Ann. Biomed. Eng.*, 43(11), 2652–2662.

Saxby, D. J., and Lloyd, D. G. (2017). "Osteoarthritis year in review 2016: mechanics." *Osteoarthr. Cartil.*, 25(2), 190–198.

Schinagl, R. M., Gurskis, D., Chen, A. C., and Sah, R. L. (1997a). "Depth-dependent confined compression modulus of full-thickness bovine articular cartilage." *J. Orthop. Res.*, 15(4), 499–506.

Schinagl, R. M., Gurskis, D., Chen, A. C., and Sah, R. L. (1997b). "Depth-dependent confined compression modulus of full-thickness bovine articular cartilage." *J. Orthop. Res.*, 15(4), 499–506.

Schliemann, B., Glasbrenner, J., Rosenbaum, D., Lammers, K., Herbort, M., Domnick, C., Raschke, M. J., and Kösters, C. (2018). "Changes in gait pattern and early functional results after ACL repair are comparable to those of ACL reconstruction." *Knee Surgery, Sport. Traumatol. Arthrosc.*, 26(2), 374–380.

Scholes, S. C., and Unsworth, A. (2009). "Wear studies on the likely performance of CFR-PEEK/CoCrMo for use as artificial joint bearing materials." *J. Mater. Sci. Mater. Med.*, 20(1), 163–170.

Schroer, W. C., Berend, K. R., Lombardi, A. V., Barnes, C. L., Bolognesi, M. P., Berend, M. E., Ritter, M. A., and Nunley, R. M. (2013). "Why are total knees failing today? Etiology of total knee revision in 2010 and 2011." *J. Arthroplasty*, 28(8 SUPPL), 116–119.

Sellaro, T. L., Hildebrand, D., Lu, Q., Vyavahare, N., Scott, M., and Sacks, M. S. (2007). "Effects of collagen fiber orientation on the response of biologically derived soft tissue biomaterials to cyclic loading." *J. Biomed. Mater. Res. Part A*, 80A(1), 194–205.

Shegaf, A., and Speirs, A. (2020). "Cartilage Biomechanical Response Differs under Physiological Biaxial Loads and Uniaxial Cyclic Compression." *J. Biomech. Eng.*, 142(5), 1–5.

Shepherd, D. E. T., and Seedhom, B. B. (1999). “The ‘instantaneous’ compressive modulus of human articular cartilage in joints of the lower limb.” *Ann. Rheum. Dis.*, 58(1), 27–34.

Shirazi, R., and Shirazi-Adl, A. (2009). “Computational biomechanics of articular cartilage of human knee joint: Effect of osteochondral defects.” *J. Biomech.*, 42(15), 2458–2465.

Shirazi, R., Shirazi-Adl, A., and Hurtig, M. (2008). “Role of cartilage collagen fibrils networks in knee joint biomechanics under compression.” *J. Biomech.*, 41(16), 3340–3348.

Shriram, D., Praveen Kumar, G., Cui, F., Lee, Y. H. D., and Subburaj, K. (2017). “Evaluating the effects of material properties of artificial meniscal implant in the human knee joint using finite element analysis.” *Sci. Rep.*, 7(1), 1–11.

Sibole, S. C., and Erdemir, A. (2012). “Chondrocyte deformations as a function of tibiofemoral joint loading predicted by a generalized high-throughput pipeline of multi-scale simulations.” *PLoS One*, 7(5), 1–13.

Smith, C. R., Vignos, M. F., Lenhart, R. L., Kaiser, J., and Thelen, D. G. (2016). “The influence of component alignment and ligament properties on tibiofemoral contact forces in total knee replacement.” *J. Biomech. Eng.*, 138(2).

Smith, M. (2009). *ABAQUS/Standard User’s Manual, Version 6.9*. Providence, United States: Dassault Systèmes Simulia Corp.

Sophia Fox, A. J., Bedi, A., and Rodeo, S. A. (2009). “The basic science of articular cartilage: Structure, composition, and function.” *Sports Health*, 1(6), 461–468.

Spiegelberg, S., Kozak, A., and Braithwaite, G. (2016). *Characterization of Physical, Chemical, and Mechanical Properties of UHMWPE. UHMWPE Biomater. Handb. Ultra High Mol. Weight Polyethyl. Total Jt. Replace. Med. Devices Third Ed.*, Elsevier Inc.

Suh, J. K., and Disilvestro, M. R. (1999). “Biphasic poroviscoelastic behavior of

hydrated biological soft tissue." *J. Appl. Mech. Trans. ASME*, 66(2), 528–535.

Sylvia, M. K., Czapla, N. A., Lerner, Z. F., Tuttle, D. J., Otto, J., Hazelwood, S. J., and Klisch, S. M. (2015). "Development of a Human Knee Joint Finite Element Model To Investigate Cartilage Stress During Walking in Obese and Normal Weight Adults." 1–2.

Takada, R., Jinno, T., Koga, D., Miyatake, K., Muneta, T., and Okawa, A. (2017). "Comparison of wear rate and osteolysis between second-generation annealed and first-generation remelted highly cross-linked polyethylene in total hip arthroplasty. A case control study at a minimum of five years." *Orthop. Traumatol. Surg. Res.*, 103(4), 537–541.

Tanska, P., Mononen, M. E., and Korhonen, R. K. (2015). "A multi-scale finite element model for investigation of chondrocyte mechanics in normal and medial meniscectomy human knee joint during walking." *J. Biomech.*, 48(8), 1397–1406.

Thambyah, A., Goh, J. C. H., and De, S. Das. (2005). "Contact stresses in the knee joint in deep flexion." *Med. Eng. Phys.*, 27(4), 329–335.

Thordarson, D. B. (1997). "Running biomechanics." *Clin. Sports Med.*, 16(2), 239–247.

Tipper, J. L., Ingham, E., Hailey, J. L., Besong, A. A., Fisher, J., Wroblewski, B. M., and Stone, M. H. (2000). "Quantitative analysis of polyethylene wear debris, wear rate and head damage in retrieved Charnley hip prostheses." *J. Mater. Sci. Mater. Med.*, 11(2), 117–124.

Todd, J. N., Maak, T. G., Ateshian, G. A., Maas, S. A., and Weiss, J. A. (2018). "Hip chondrolabral mechanics during activities of daily living: Role of the labrum and interstitial fluid pressurization." *J. Biomech.*, 69, 113–120.

Tomic, A., Grillo, A., and Federico, S. (2014). "Poroelastic materials reinforced by statistically oriented fibres-numerical implementation and application to articular cartilage." *IMA J. Appl. Math. (Institute Math. Its Appl.*, 79(5), 1027–1059.

Trad, Z., Barkaoui, A., Chafra, M., and Tavares, J. M. R. (2018). “Finite element analysis of the effect of high tibial osteotomy correction angle on articular cartilage loading.” *Proc. Inst. Mech. Eng. Part H J. Eng. Med.*, 232(6), 553–564.

Vaziri, A., Nayeb-Hashemi, H., Singh, A., and Tafti, B. A. (2008). “Influence of meniscectomy and meniscus replacement on the stress distribution in human knee joint.” *Ann. Biomed. Eng.*

Venäläinen, M. S., Mononen, M. E., Salo, J., Räsänen, L. P., Jurvelin, J. S., Töyräs, J., Virén, T., and Korhonen, R. K. (2016). “Quantitative Evaluation of the Mechanical Risks Caused by Focal Cartilage Defects in the Knee.” *Sci. Rep.*, 6(June), 1–12.

Walker, P. S., and Erkman, M. J. (1975). “The role of the menisci in force transmission across the knee.” *Clin.Orthop.*

Wang, A., Essner, A., Polineni, V. K., Stark, C., and Dumbleton, J. H. (1998). “Lubrication and wear of ultra-high molecular weight polyethylene in total joint replacements.” *Tribol. Int.*, 31(1–3), 17–33.

Wang, H., Xu, L., Zhang, M., Li, R., Xing, Z., Hu, J., Wang, M., and Wu, G. (2017). “More wear-resistant and ductile UHMWPE composite prepared by the addition of radiation crosslinked UHMWPE powder.” *J. Appl. Polym. Sci.*, 134(13), 1–11.

Wang, Y., Fan, Y., and Zhang, M. (2014). “Comparison of stress on knee cartilage during kneeling and standing using finite element models.” *Med. Eng. Phys.*, 36(4), 439–447.

Wilson, W., Burken, C. van, Donkelaar, C. C. van, Buma, P., Rietbergen, B. van, and Huiskes, R. (2006). “Causes of mechanically induced collagen damage in articular cartilage.” *J. Orthop. Res.*, 24(2), 220–228.

Wilson, W., Donkelaar, C. C. Van, Rietbergen, B. Van, Ito, K., and Huiskes, R. (2004). “Stresses in the local collagen network of articular cartilage: A poroviscoelastic fibril-reinforced finite element study.” *J. Biomech.*, 37(3), 357–366.

Wilson, W., Rietbergen, B. Van, Donkelaar, C. C. Van, and Huiskes, R. (2003).

"Pathways of load-induced cartilage damage causing cartilage degeneration in the knee after meniscectomy." *J. Biomech.*, 36(6), 845–851.

Yang, N. H., Canavan, P. K., and Nayeb-Hashemi, H. (2010a). "The effect of the frontal plane tibiofemoral angle and varus knee moment on the contact stress and strain at the knee cartilage." *J. Appl. Biomech.*, 26(4), 432–443.

Yang, N. H., Canavan, P. K., Nayeb-Hashemi, H., Najafi, B., and Vaziri, A. (2010b). "Protocol for constructing subject-specific biomechanical models of knee joint." *Comput. Methods Biomech. Biomed. Engin.*, 13(5), 589–603.

Yao, J., Guo, N., Xiao, Y., Li, Z., Li, Y., Pu, F., and Fan, Y. (2019). "Lower limb joint motion and muscle force in treadmill and over-ground exercise." *Biomed. Eng. Online*, 18(1), 1–12.

Zhang, K., Li, L., Yang, L., Shi, J., Zhu, L., Liang, H., Wang, X., Yang, X., and Jiang, Q. (2019). "Effect of degenerative and radial tears of the meniscus and resultant meniscectomy on the knee joint: a finite element analysis." *J. Orthop. Transl.*, 18, 20–31.

Zhao, D., Sakoda, H., Sawyer, W. G., Banks, S. A., and Fregly, B. J. (2008). "Predicting Knee Replacement Damage in a Simulator Machine Using a Computational Model With a Consistent Wear Factor."

PUBLICATIONS

List of Journals

1. **Vaishakh Raju**, Poornesh K. Koorata, and Yogeesh Kamat, (2021), Case study for contact pressure improvisation with graded implant material in articular cartilages of knee joint. Journal of Mechanical Science and Technology, Springer, 35 (3), 1049-1054. [SCIE] https://doi.org/10.1007/s12206-021-0218-8
2. **Vaishakh Raju**, and Poornesh K. Koorata, (2022), Influence of material heterogeneity on the mechanical response of articulated cartilages in a knee joint. Proceedings of the Institution of Mechanical Engineers, Part H: Journal of Engineering in Medicine, SAGE, 236 (9), 1340-1348. [SCIE] https://doi.org/10.1177/09544119221116263
3. **Vaishakh Raju**, and Poornesh K. Koorata, Computational assessment on the impact of collagen fiber orientation in cartilages on healthy and arthritic knee kinetics/kinematics (Minor revision)

List of Conference

1. **Vaishakh Raju**, and Poornesh K. Koorata, 2022, Computational evaluation of the effect of femoral component curvature on the mechanical response of the UHMWPE tibial insert in total knee replacement implants. International Conference on Material Science and Computational Engineering, November 17-18, 2022, Kollam, India.
   (Materials Today: Proceedings, Elsevier, November 2022)
   https://doi.org/10.1016/j.matpr.2022.12.224
2. **Vaishakh Raju**, and Poornesh K. Koorata, 2022, Impact of femoral component curvature in TKR implants on the mechanical response of tibial insert. 20th ISME Conference on Advances in Mechanical Engineering, May 19-21, 2022, IIT Ropar, India.
3. **Vaishakh Raju**, and Poornesh K. Koorata, 2021, Investigation on the influence of soft tissues in knee joint on load transfer mechanism during the gait cycle.

International Conference on Advances in Mechanical Engineering: Transcending Boundaries (ICAMET 2021), June 24-25, 2021, Mangalam College of Engineering, Kottayam, India,

(Accepted for publication in AIP Conference Proceedings [Scopus], AIP Publications, 2565, November 2022)

4. **Vaishakh Raju**, and Poornesh K. Koorata, 2019, Effect of body forces on articulating surface of a knee joint by incorporating the heterogeneous behaviour by using finite element analysis. 7th International Congress on Computational Mechanics and Simulation (ICCMS 2019), December 11-13, 2019, IIT Mandi, India.

BIODATA

VAISHAKH R
Department of Mechanical Engineering
National Institute of Technology Karnataka
Surathkal, Mangalore- 575025, India.
Email ID: vaishakhraju@gmail.com
Mob No: +91-9995292318

EDUCATION

2013–2015	M.Tech, Sardar Vallabhbhai National Institute of Technology (SVNIT), Surat, India. (First class with Distinction)
2006-2010	B. Tech, Mechanical Engineering, Saintgits College of Engineering, Mahatma Gandhi University, Kottayam, Kerala, India. (First class)
2004-2006	12th, St. Berchmans Higher Secondary School, Kottayam, Kerala, (First class)
2003-2004	10th, Sacred Heart High school, Kottayam, Kerala (First class)

COMPUTATIONAL SKILLS

Abaqus CAE, FEBio Studio, CATIA, Solidworks, Autodesk Inventor, Origin, MS Word, MS Excel

ACADEMIC EXPERIENCE

Assistant Professor, College of Engineering Adoor, Kerala

September 2015 - April 2018

Lecturer, St. Joseph's College of Engineering and Technology, Kerala

September 2010 - December 2010

INDUSTRIAL EXPERIENCE

Site Execution Engineer, Bridge and Roof Co. (India) Ltd, MRPL, Karnataka

July 2011-June 2012

I certify that the foregoing information is correct and complete to the best of my knowledge and belief, and nothing has been concealed/distorted.

VAISHAKH R
NITK, SURATHKAL